International Scientific-Technical and Production Journal

The Paton WELDING JOURNAL

June 2003 # 6

English translation of the monthly «Avtomaticheskaya Svarka» (Automatic Welding) journal published in Russian since 1948

Founders: *The E.O. Paton Electric Welding Institute of the NAS of Ukraine International Association «Welding»* *Publisher:* *International Association «Welding»*

Address:
E.O. Paton Electric Welding Institute, International Association «Welding», 11, Bozhenko str., 03680, Kyiv, Ukraine
Tel.: (38044) 227 67 57
Fax: (38044) 268 04 86
E-mail: journal@paton.kiev.ua
http://www.nas.gov.ua/pwj

State Registration Certificate KV 4790 of 09.01.2001

Subscriptions:
$460, 12 issues per year, postage and packaging included. Back issues available.

CONTENTS

MATHEMATICAL MODELLING OF ABSORPTION OF GASES BY ELECTRODE METAL DROP

I.K. POKHODNYA and **O.M. PORTNOV**
E.O. Paton Electric Welding Institute, NASU, Kyiv, Ukraine

The mathematical model is composed from a combined solution of the system of equations of gas mass transfer in metal, in the near-surface Knudsen layer, adjacent to metal, and in the atmosphere of arc discharge. Modelling of metal evaporation and gas absorption is based on a combined solution of Boltzmann kinetic equation for Knudsen layer and system of equations of continuum for the ambient atmosphere using numerical methods. The effect of gas content in atmosphere and drop temperature on the kinetics of the absorption process has been investigated.

Keywords: *arc welding, gas absorption, mathematical modelling, mass transfer equation, kinetics of absoption of gases, Knudsen layer*

Initial gas content in electrode metal is low, but in the period of its location in arc gap the molten drops of electrode metal absorb gases intensively from the arc atmosphere [1]. Due to this, the content of gases in electrode metal drop is increased many times. Almost all gas, absorbed by the drop from the gas atmosphere, enters the welded joint metal.

Absorption of gases by the drop occurs over the entire area of free surface of metal, being in contact with arc discharge atmosphere. The absorption flow depends on metal temperature and arc discharge, partial pressure of gas in atmosphere, drop size and time of its location in the arc gap. Gas evolution occurs simultaneously with absorption. Desorption flow is defined mainly by temperature of metal and concentration of dissolved gas. In Knudsen layer the gas parameters are compared with equilibrium values at the distance of several lengths of a free run of atoms in atmosphere due to collision of atoms of forward and reverse flows.

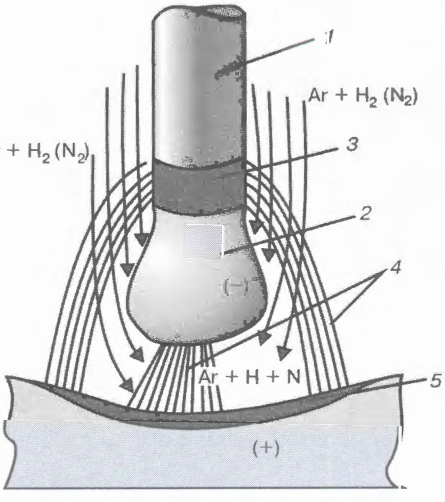

Figure 1. General scheme of metal drop arrangement in arc column in welding at straight polarity current: *1* — consumable electrode; *2* — electrode metal drop; *3* — cathode spot; *4* — arc discharge column; *5* — weld pool

Modelling was performed for the process of absorption of hydrogen or nitrogen by the drop of molten metal locating in arc column. Atmosphere of arc consists of argon with a controllable content of gas being absorbed. Low-carbon steel is selected as a material of electrode metal. General scheme od metal drop arrangement in arc column in welding at straight polarity current is presented in Figure 1. In this mathematical model the results of [2] on study of absorption of gases by weld pool metal were used.

There are some differences in processes of absorption of gases by weld pool and electrode metal. Temperature of weld pool does not exceed 2200 K. Iron evaporation at this temperature is negligible and does not influence the process of absorption of gases. Temperature of electrode metal at drop transfer is approaching the boiling temperature. Due to high heating the electrode metal is evaporated intensively. Concentration of atoms of evaporated metal in plasma atmosphere occurred to be comparable with concentration of atoms of gas absorbed that causes the decrease in absorption of reactive gas by metal. Experimental investigations showed a great effect of the metal evaporation process on content of dissolved gas in it [1–3].

Mathematical model. It is composed of systems of equations of mass transfer in atmosphere and equation of spreading gas dissolved in metal. The first system describes the process of evaporation of metal without allowance for effect of gas absorption process on it, while the second system describes gas absorption with allowance for interaction of gas atoms with atoms of evaporated metal.

It is assumed that electrode metal drop has a spherical shape of radius R_0. The problem is considered in spherical system of coordinates, whose beginning is located in the drop center. Gas concentration in drop is designated $C(r, t)$, where r is the space coordinate directed from the drop center to gas phase; t is the time. The rate of metal surface motion due to evaporation is much lower than the rate of kinetic processes in gas, therefore, the drop size is considered unchanged.

Evaporation of metal. Kinetic analysis of metal evaporation into atmosphere of perfect gas is given in [4]. By making a system of equations on the basis of law of conservation of mass, pulse and energy for vapour flow through the Knudsen layer for plane one-dimensional flow of gas, the author obtained the solution in the form of a shock wave spreading in the space of vapour-gas mixture. As the author noted, the obtained solution is not suitable for the case of diffusion evaporation, typical of welding process. Equations, linking the thermodynamic parameters at the boundaries of Knudsen layer obtained from the solution of system of equations of transfer for moment characters m, mv, mv^2, have the following form [4]:

$$\frac{T_{kn}}{T_s} = \left[\left(1 + \pi\left(\frac{\gamma-1}{\gamma+1}\frac{v_h}{2}\right)^2\right)^{1/2} - \pi^{1/2}\frac{\gamma-1}{\gamma+1}\frac{v_h}{2}\right]^2,$$

$$\frac{n_{kn}}{n_s} = \left(\frac{T_s}{T_{kn}}\right)^{1/2}\left[\left(v_h^2 + \frac{1}{2}\right)\exp(v_h^2)\,\mathrm{erfc}\,(v_h) - \frac{v_h}{\pi^{1/2}}\right] + \quad (1)$$

$$+ \frac{1}{2}\frac{T_s}{T_{kn}}\left[1 - \pi^{1/2} v_h \exp(v_h^2)\,\mathrm{erfc}\,(v_h)\right],$$

where v_h is the ratio of mean flow rate of atoms in radial v_r direction to heat rate of atoms; T_{kn} is the temperature at external boundary of Knudsen layer; T_s is the temperature of metal surface; $\gamma = 1.4$ is the relation between isobaric and isochoric heat contents of gas; n_{kn} is the total density of atoms of vapour and gas at the external boundary of Knudsen layer; n_s is the density of atoms of metal vapour at the metal surface. The latter value is determined by equation of Clapeyron–Clausius [5] $p_s = p_0 \exp \times \times \left(\frac{m_p L_v}{kT_s}\left(1 - \frac{T_b}{T_s}\right)\right)$ and equation of perfect gas condition $p = nkT$. Here, T_b, L_v are the constants of material taken from handbook [5]; p_0 is the standard pressure equal to 0.1 MPa; m_p is the mass of metal (iron) atom; k is the Boltzmann's constant.

System of equations (1) cannot determine the general flow of evaporated atoms of metal and composition of atmosphere at the external boundary of Knudsen layer. Therefore, it should be added by a system of equations, describing the vapour flow beyond the Knudsen layer. Unlike the process, analyzed in [4], let us consider the case of steady evaporation when the shock wave went away for a finite large distance and time derivatives are equal to zero. Taking into account the assumption that vapour-gas mixture is a perfect gas, we shall write the following system of equations consisting of equations of continuity, Navier–Stokes and perfect gas condition [6] in spherical coordinates:

$$\frac{\partial(nv_r)}{\partial r} + \frac{2(nv_r)}{r} = 0,$$

$$v_r\frac{\partial v_r}{\partial r} = -\frac{1}{n}\frac{\partial P}{\partial r}, \quad (2)$$

$$v_r\frac{\partial}{\partial r}\left(\ln\frac{P}{n^\gamma}\right) = 0,$$

where v is the rate of metallic vapour; P is the pressure of vapour-gas mixture; $n = n_g + n_p$ is the density of vapour-gas mixture; n_g and n_p is the density of atoms of gas and metallic vapour, respectively. System (2) describes gas-dynamic processes in the region of hydrodynamic flow in diffusion condition. Combined solution of systems (1) and (2) makes it possible to determine the flow of evaporated atoms.

Absorption of gas. Equation of gas spreading in drop metal by a diffusion mechanism is written in spherical coordinates

$$\frac{\partial C}{\partial t} = \frac{1}{r^2}\frac{\partial}{\partial r}\left(D(T)r^2\frac{\partial C}{\partial r}\right). \quad (3)$$

Initial distribution of gas in drop $C(r, 0) = C_0$. In equation (3) the following designations are used: $D(T)$ is the coefficient of diffusion; $T = T(r, t)$ is the metal temperature. Temperature relationship of coefficient of gas diffusion in molten iron is described by equation $D = D_0 \exp(-T_D/(RT))$, where R is the universal gas constant. Values of constants suggested by different authors are collected in [7]. For calculation the values $D_0 = 0.016$ cm^2/s, $T_D = 22$ kJ/mol are selected as most close to mean values.

Mass of gas entered per unity of drop surface for time unity $j(t)$ is the boundary condition for equation (3):

$$\frac{\partial C(R_0, t)}{\partial r} = -j(t).$$

Flow of gas mass j into metal is associated with gas flow in atmosphere in the direction, normal to metal surface, by the relation given in [2]:

$$j = m_g n_g (2kT_\infty/m_g)^{1/2} S_\infty,$$

where m_g is the gas atom mass; T_∞ is the arc temperature; S_∞ is the mean rate of gas atoms in the direction normal to metal surface which is determined through function of distribution of gas atoms by rates $f(r, v)$:

$$S_\infty = \int_{-\infty}^{\infty} v_r f d\mathbf{v},$$

where $\mathbf{v}$ is the vector of rate of gas atoms.

As the radius of curvature of metal surface is much larger than the length of a free run of particles in gas, the drop shape does not influence the solution of gas dynamic problem. Function of distribution is determined from the solution of gas kinetic equation for Knudsen layer adjacent to metal surface

$$\int Q_L \mathbf{v}\frac{\partial f}{\partial r}d\mathbf{v} = \Delta(Q_L), \quad (4)$$

where $\Delta(Q_L)$ is the integral of collisions between gas atoms.

Equation (4) is solved with allowance for a radial change in density of gas atoms n_g in Knudsen layer caused by metal evaporation.

in [4]. By making a system of equations on the basis of law of conservation of mass, pulse and energy for vapour flow through the Knudsen layer for plane one-dimensional flow of gas, the author obtained the solution in the form of a shock wave spreading in the space of vapour-gas mixture. As the author noted, the obtained solution is not suitable for the case of diffusion evaporation, typical of welding process. Equations, linking the thermodynamic parameters at the boundaries of Knudsen layer obtained from the solution of system of equations of transfer for moment characters m, mv, mv^2, have the following form [4]:

$$\frac{T_{kn}}{T_s} = \left[\left(1 + \pi\left(\frac{\gamma-1}{\gamma+1}\frac{v_h}{2}\right)^2\right)^{1/2} - \pi^{1/2}\frac{\gamma-1}{\gamma+1}\frac{v_h}{2}\right]^2,$$

$$\frac{n_{kn}}{n_s} = \left(\frac{T_s}{T_{kn}}\right)^{1/2}\left[\left(v_h^2 + \frac{1}{2}\right)\exp(v_h^2)\operatorname{erfc}(v_h) - \frac{v_h}{\pi^{1/2}}\right] + \tag{1}$$

$$+\frac{1}{2}\frac{T_s}{T_{kn}}\left[1 - \pi^{1/2}v_h\exp(v_h^2)\operatorname{erfc}(v_h)\right],$$

where v_h is the ratio of mean flow rate of atoms in radial v_r direction to heat rate of atoms; T_{kn} is the temperature at external boundary of Knudsen layer; T_s is the temperature of metal surface; $\gamma = 1.4$ is the relation between isobaric and isochoric heat contents of gas; n_{kn} is the total density of atoms of vapour and gas at the external boundary of Knudsen layer; n_s is the density of atoms of metal vapour at the metal surface. The latter value is determined by equation of Clapeyron–Clausius [5] $p_s = p_0 \exp \times \times \left(\frac{m_p L_v}{kT_s}\left(1 - \frac{T_b}{T_s}\right)\right)$ and equation of perfect gas condition $p = nkT$. Here, T_b, L_v are the constants of material taken from handbook [5]; p_0 is the standard pressure equal to 0.1 MPa; m_p is the mass of metal (iron) atom; k is the Boltzmann's constant.

System of equations (1) cannot determine the general flow of evaporated atoms of metal and composition of atmosphere at the external boundary of Knudsen layer. Therefore, it should be added by a system of equations, describing the vapour flow beyond the Knudsen layer. Unlike the process, analyzed in [4], let us consider the case of steady evaporation when the shock wave went away for a finite large distance and time derivatives are equal to zero. Taking into account the assumption that vapour-gas mixture is a perfect gas, we shall write the following system of equations consisting of equations of continuity, Navier–Stokes and perfect gas condition [6] in spherical coordinates:

$$\frac{\partial(nv_r)}{\partial r} + \frac{2(nv_r)}{r} = 0,$$

$$v_r\frac{\partial v_r}{\partial r} = -\frac{1}{n}\frac{\partial P}{\partial r}, \tag{2}$$

$$v_r\frac{\partial}{\partial r}\left(\ln\frac{P}{n^\gamma}\right) = 0,$$

where v is the rate of metallic vapour; P is the pressure of vapour-gas mixture; $n = n_g + n_p$ is the density of vapour-gas mixture; n_g and n_p is the density of atoms of gas and metallic vapour, respectively. System (2) describes gas-dynamic processes in the region of hydrodynamic flow in diffusion condition. Combined solution of systems (1) and (2) makes it possible to determine the flow of evaporated atoms.

Absorption of gas. Equation of gas spreading in drop metal by a diffusion mechanism is written in spherical coordinates

$$\frac{\partial C}{\partial t} = \frac{1}{r^2}\frac{\partial}{\partial r}\left(D(T)r^2\frac{\partial C}{\partial r}\right). \tag{3}$$

Initial distribution of gas in drop $C(r, 0) = C_0$. In equation (3) the following designations are used: $D(T)$ is the coefficient of diffusion; $T = T(r, t)$ is the metal temperature. Temperature relationship of coefficient of gas diffusion in molten iron is described by equation $D = D_0 \exp(-T_D/(RT))$, where R is the universal gas constant. Values of constants suggested by different authors are collected in [7]. For calculation the values $D_0 = 0.016$ cm^2/s, $T_D = 22$ kJ/mol are selected as most close to mean values.

Mass of gas entered per unity of drop surface for time unity $j(t)$ is the boundary condition for equation (3):

$$\frac{\partial C(R_0, t)}{\partial r} = -j(t).$$

Flow of gas mass j into metal is associated with gas flow in atmosphere in the direction, normal to metal surface, by the relation given in [2]:

$$j = m_g n_g (2kT_\infty/m_g)^{1/2} S_\infty,$$

where m_g is the gas atom mass; T_∞ is the arc temperature; S_∞ is the mean rate of gas atoms in the direction normal to metal surface which is determined through function of distribution of gas atoms by rates $f(r, v)$:

$$S_\infty = \int_{-\infty}^{\infty} v_r f d\mathbf{v},$$

where $\mathbf{v}$ is the vector of rate of gas atoms.

As the radius of curvature of metal surface is much larger than the length of a free run of particles in gas, the drop shape does not influence the solution of gas dynamic problem. Function of distribution is determined from the solution of gas kinetic equation for Knudsen layer adjacent to metal surface

$$\int Q_L \mathbf{v}\frac{\partial f}{\partial r}d\mathbf{v} = \Delta(Q_L), \tag{4}$$

where $\Delta(Q_L)$ is the integral of collisions between gas atoms.

Equation (4) is solved with allowance for a radial change in density of gas atoms n_g in Knudsen layer caused by metal evaporation.

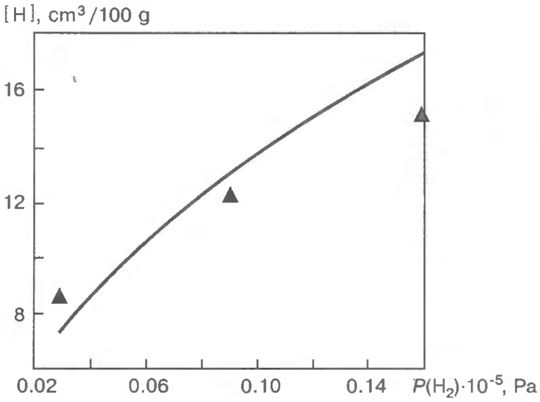

Figure 2. Comparison of calculated dependence of hydrogen content in metal drop on its partial pressure in atmosphere with experimental data (▲) [9]

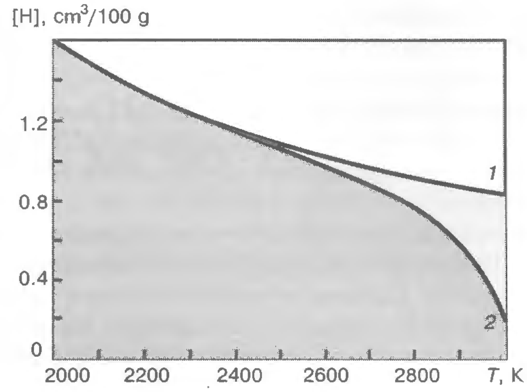

Figure 4. Calculated dependence of hydrogen absoption on iron temperature in case of contact with plasma at 5000 K temperature (atmosphere composition — Ar + 0.1 % H_2)

Mathematical model of solution of system of equations of mass transfer is realized in the form of program in language C^{++}. Algorithm of solution of equations of mass transfer is constructed from functionally independent modules. To solve the equations of diffusion the method of finite differences was used by approximation of a variable symmetrical Crank–Nicholson scheme [8] with a pitch resettable in space and time coordinates.

Results and discussions. The performance of the presented mathematical model was checked by calculation of gas absorption in the conditions for which reliable experimental data are available.

The comparison of results of calculation of dependence of gas concentration in a metal drop on its partial pressure in atmosphere with experimental data for iron sample, subjected to holding in plasma of inert gas and with a controllable content of hydrogen [9], is presented in Figure 2. Experimental data are obtained with allowance for gas loss in sample due to process of desorption in cooling. Calculated time of absorption was 1 s. Results of calculations of hydrogen absorption in the conditions of thermodynamic equilibrium, when iron is in contact with pure gas at atmospheric pressure having a temperature similar to that of metal, are given in Figure 3. The data of experimental investigations of hydrogen absorption made at the same conditions that were described in [3], are also given there. Calculations were made both with and without allowance for metal evaporation. Figure 4 presents results of calculation of hydrogen absorption from the plasma atmosphere.

Mechanism of absorption of hydrogen and nitrogen from atmosphere and arc discharge is similar. Work [7] gives experimental data about absorption of nitrogen from atmosphere of pure gas at 10132.5 Pa pressure in the conditions of thermodynamic equilibrium. Comparison of experimental and calculated results is given in Figure 5. There are reliable experimental data of temperature relation of gas absorption from plasma atmosphere for nitrogen [9], while the calculation of nitrogen absorption from atmosphere of arc discharge was also made to confirm the suggested model. Comparison of experimental and calculated data is shown in Figure 6.

Kind of temperature relation of gas absorption is also important. In contact with usual atmosphere the gas content in iron has maximum in the range of approximately 2600 K. Increase in gas content up to

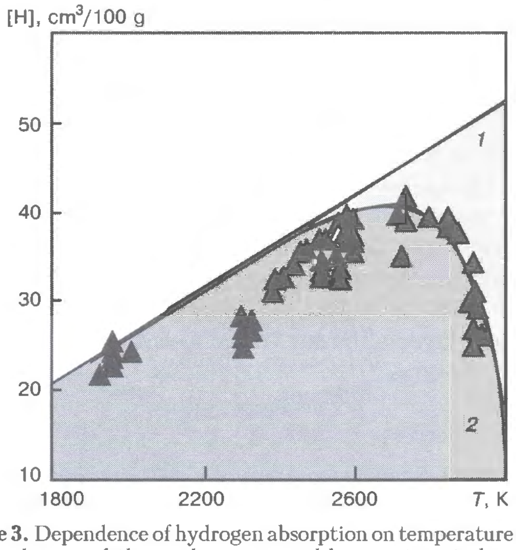

Figure 3. Dependence of hydrogen absorption on temperature under the conditions of thermodynamic equilibrium at partial pressure of gas 0.1 MPa: ▲ — experimental data [3] (here and in Figures 4–6 *1* and *2* — calculated data with and without allowance for metal evaporation, respectively)

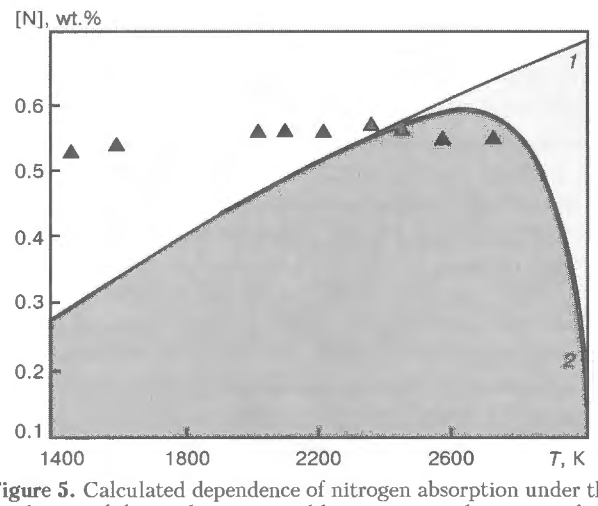

Figure 5. Calculated dependence of nitrogen absorption under the conditions of thermodynamic equilibrium at partial pressure of gas 0.1 MPa: ▲ — experimental data [7]

this temperature is due to increase in degree of gas dissociation with temperature increase. Decrease in gas content in metal after 2600 K depends on the growth of intensity of metal evaporation. In contact with plasma the calculation shows the monotonous decrease in gas content in iron with temperature increase. This is, probably, due to the fact that in absorption of gases from usual atmosphere the dissociation of gas molecules at the metal surface is a limiting link in the absorption process which is increased with the increase in its temperature. The degree of dissociation in the process of absorption from the arc discharge is determined by the arc temperature which depends negligibly on the metal surface temperature.

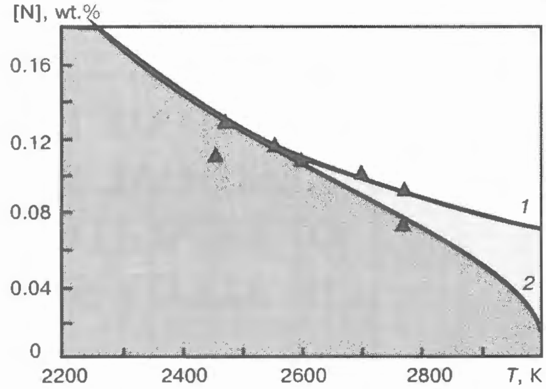

Figure 6. Nitrogen content in metal in welding using wire Sv-08Kh18N9 in flow Ar + 17% N_2: ▲ — experimental data [10]

CONCLUSIONS

1. Mathematical model of absorption of gas by electrode metal drop in the period of its location in arc gap has been developed.

2. Using numerical methods the effect of metal temperature, partial gas pressure in atmosphere and time of drop location in arc gap on amount of gas entered the welded joint metal was investigated by a mechanism of drop transfer.

3. At duration of metal drop in the arc gap region for less than one tenth of second the gas concentration in it is greatly differed from equilibrium concentration. Under these conditions the calculation of gas absorption by drop is possible only using the solution of kinetic equation in gas phase.

4. It is determined that at temperature of metal above 2600 K its evaporation influences greatly the kinetics of gas absorption.

5. It was established that in contact with usual atmosphere under the conditions of thermodynamic equilibrium a maximum in gas content was recorded at temperature of about 2600 K.

6. In contact of metal surface with plasma the gas content decrease in drop occurs at increase in its temperature both with and without allowance for evaporation.

1. Pokhodnya, I.K. (1972) *Gases in welds*. Moscow: Mashinostroenie.
2. Pokhodnya, I.K., Shvachko, V.I., Portnov, O.M. (2000) Mathematical modelling of absorption of gases by metal during welding. *The Paton Welding J.*, **7**, 11–16.
3. Lakomsky, V.I. (1962) Solubility of hydrogen in liquid iron to boiling point. *Doklady AN SSSR*, **3**, 628–629.
4. Knight, C.J. (1979) Theoretical modeling of rapid surface evaporation with back pressure. *AIAA J.*, **17**, 519.
5. (1976) *Tables of physical quantities*. Refer. Book. Ed. by I.K. Kikoin. Moscow: Atomizdat.
6. Landau, L.D., Lifshits, E.M. (1986) *Hydrodynamics*. Moscow: Nauka.
7. Lakomsky, V.I. (1974) *Plasma arc remelting*. Ed. by B.E. Paton. Kyiv: Tekhnika.
8. Samarsky, A.A. (1987) *Introduction to numerical methods*. Moscow: Nauka.
9. Pirch, I.I., Erokhin, A.A., Pugin, A.I. (1980) Some principles of hydrogen absorption by liquid metals in arc heating. *Svarochn. Proizvodstvo*, **9**, 6–8.
10. Pokhodnya, I.K. (1968) Absorption of nitrogen on cathode during consumable electrode welding. *Avtomatich. Svarka*, **12**, 14–18.

METHOD OF EVALUATION OF EFFECT OF RESIDUAL STRESSES ON FORMATION OF LONGITUDINAL COLD CRACKS IN ALLOY STEEL WELDED JOINTS

L.M. LOBANOV, L.I. MIKHODUJ, V.D. POZNYAKOV, O.L. MIKHODUJ, S.B. KASATKIN, A.A. SERGIENKO and **P.A. STRIZHAK**
E.O. Paton Electric Welding Institute, NASU, Kyiv, Ukraine

Technological sample amd procedure of investigations have been developed that makes it possible to evaluate the effect of residual stresses on the resistance of welded joints with multilayer welding to the formation of longitudinal cold cracks. The relationship between the level of residual stresses and resistance to the formation of longitudinal cold cracks of 14KhGN2MDAFB steel welded joints, made using wire Sv-10KhGN2SMFTYu in 75 % Ar + 25 % CO_2 mixture of gases, was established.

Keywords: *high-strength steels, welded joints, cold cracks, method of investigations, shielded-gas welding, mechanical tensometry, holographic interferometry, transverse displacements, residual stresses*

Cold cracks in metal of weld and HAZ are one of most hazardous defects occurring in welded joints of low-carbon alloy high-strength steels with yield strength above 600 MPa. By the location relative to weld axis, the cracks are classified usually into longitudinal and transverse. Numerous investigations and experience in manufacture of welded structures from steels of increased and high strength prove that three main factors influence the initiation and propagation of cold cracks, namely increased concentration of diffusive hydrogen in all the areas of welded joint; unfavourable quenched structures; high level of residual welding stresses. Depending on the definite conditions of effect of each of the above-mentioned factors on the process of initiation and propagation of cracks can be intensified or weakened.

Many works [1–4] are devoted to the analysis of mechanism of effect of hydrogen and structure factors on a delayed fracture of joints made from structural steels of different compositions. In most cases this makes it possible to establish scientifically-grounded principles of the developed technologies of welding hard-to-weld steels. Role and effect of residual stresses on the process of formation of high-level cracks and unfavourable distribution in welded joints are little studied. This is stipulated greatly by the fact that use of many non-destructive methods of evaluation of stress-strain state of welded joints (magneto-elastic, acoustic, ultrasonic, etc.) is difficult due to effect of complex phase-structural transformations in alloy steel on a final result of investigations. At the same time the known methodological approaches of investigations of weldability of steels [5–7] envisage the use of rigid technological samples of small sizes (for example, Tekken, Lehigh, CTS and others) that cannot evaluate the effect of stressed state on the process of formation of cracks in them, or excessively large sizes (for example, shipbuilding sample), which are complicated for analyzing in the laboratory conditions.

The aim of the present work is to search for technological sample which will take into account the role of residual stresses and produce experimental data on this problem.

Welded joints of large-sized structures are located, as a rule, in the condition of complex stressed state in manufacture. Depending on the product design and definite situation both longitudinal and also transverse cold cracks can occur in them. To reproduce these conditions during laboratory tests on one technological sample is difficult. It seems rational from the methodological point of view to divide the analysis of investigations of these two types of cracks. As regards to evaluation of resistance of welded joints to the formation of transverse cracks the investigations were already carried out earlier and the methodological approach was selected [8]. These investigations were performed using multipass welded joints in which high longitudinal stresses were created, opening the lips of artificial cracks. These approaches, and also solutions, used in the development of a rigid sample [4] and samples VMEI-2, VUZ-ERTs [5] served the basis for the creating sample which will be able to evaluate the resistance of welded joints with multilayer welds to the formation of transverse cracks. The same as in samples VMEI-2 and VUZ-ERTs the principle of a variable rigidity was used in it, the degree of which was changed by varying width of elements welded. The length of sample was also changed. In the above-mentioned sample it does not exceed 100 mm that does not make it possible to attain a stable formation of residual transverse stresses which can take place in welding of metal structures in real conditions. To form them it is rational to use the welded joint with a longer weld (not less than 250–300 mm) for tests.

The sample, selected as a base of present investigations (Figure 1), represents a massive plate (400×400 mm size and 50–60 mm thickness), on which butt joints of 15–20 mm thick plates with V-shaped groove, are mounted and welded-on around the entire perimeter (with 10–12 mm leg). These sizes and design of the sample prevented the angular deformation of the sample, and, thus, avoided the effect of other unforeseen factors during investigations. An obligatory gap up to 1.5–2.0 mm is provided in the sample, which serves a stress concentrator in welding joints with blunting n = 3–4 mm (to provide technological lack of penetration). Similar joints with n' = 0.5–1.5 mm were welded in parallel. From the test conditions this allowed producing welds with a complete penetration.

In accordance with the test procedure it is necessary to weld two copies of sample of width B = 100, 200 and 300 mm. One of them should have 0.5–1.5 mm blunting in root weld, the second — 3–4 mm. The first sample was used for determination of residual stresses in it. From the results of testing the second sample the capability of welded joint to resist the formation of cold cracks was evaluated. The change in width of samples allowed adjusting their rigidity and level of residual stresses in welded joints. Conditions of welding should remain unchanged to provide the constancy of effect of hydrogen and structural factors.

It is supposed that this approach will promote the proceeding of thermodeformational processes in welded joints (in a wide range), initiation and propagation of cold cracks in them, their revealing, and also feasibility to establish the limiting values of displacements and tensile stresses experimentally. Criterion of these investigations can be information about the presence (absence) of cracks in weld metal and HAZ during definite variant of welding, and also the levels of transverse displacements or stresses which contribute to this.

During investigations steel of 14KhGN2MDAFB grade of 16 mm thickness was used ($\sigma_{0.2}$ = 752 MPa; δ = 16 %; KCV_{-40} = 75 J/cm^2). Samples were welded using welding wire of Sv-10KhGN2SMFTYu grade of 1.2 mm diameter in mixture of gases on the base of argon (Ar + 25 % CO_2). This combination of welding wire and shielding mixture provide weld metal with a bainitic-martensitic structure and mechanical properties equal to those of steel investigated. Content of diffusive hydrogen in deposited metal in the present investigations was 3.5–4.0 ml/100 g (in determination of its amount by chromotographic method). Welding of samples was realized without preheating using the following conditions: I_w = 130–140 A; U_a = = 24–25 V; v_w = 13–14 m/h. Each layer after root layer was started after cooling the prior layer to 20–30 °C. At such conditions the following parameters of cooling HAZ metal were provided: rate of cooling

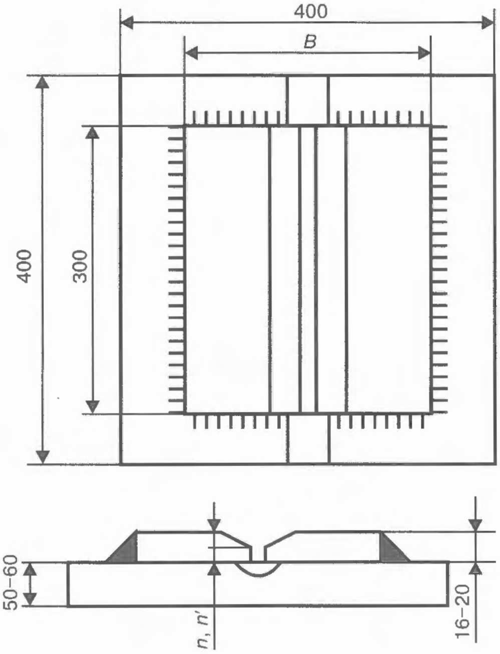

Figure 1. Sample «rigid butt» for evaluation of resistance of high-strength steels to the initiation of longitudinal cracks (for designations see the text)

$w_{6/5}$ = 26–28 °C/s; $\tau_{8/1}$ = 180–200 s (time of cooling from 800 to 100 °C).

The stress-strain state of technological samples was evaluated using two methods: mechanical tensometry and holographic interferometry. Mechanical tensometry was used to evaluate the transverse (relative to weld axis) displacements of welded joints after fulfillment of root and next two layers. For this purpose the path for base holes of 1 mm diameter and 3–4 mm depth were prepared at the face surface of samples in the entire length, then they were counterbored and subjected to grinding. Measurements were made using a three-dimensional deformometer with 0.001 mm accuracy. Measurement base was 25 mm. From difference in measurements of changes in distance between the base holes before (L_0) and after welding (L_i) the full residual deformation (ΔL_w = = $L_i - L_0$) was determined at each examining next regions of the technological sample.

Results of investigations (Figure 2) prove that during the process of deformation of welded joints a significant transverse shrinkage of weld metal and HAZ in the entire length of samples takes place. The most intensive shrinkage was observed after fulfillment of the weld root layer. The second and third layers of the deposited metal promote the developing of this process, however, the shrinkage is greatly reduced and equals 50–65 and 15–40 %, respectively, of the level of displacements which were observed in the fulfillment of a root weld. The highest value of displacements in samples with a complete penetration is observed in rigid samples of 300 mm width ($\Delta L \approx$ $\approx$ 0.71 mm). In the narrower samples (B = 200 and 100 mm) the proceeding of the processes of plastic deformation is difficult and, therefore, the maximum values of transverse shrinkage in them are lower (see

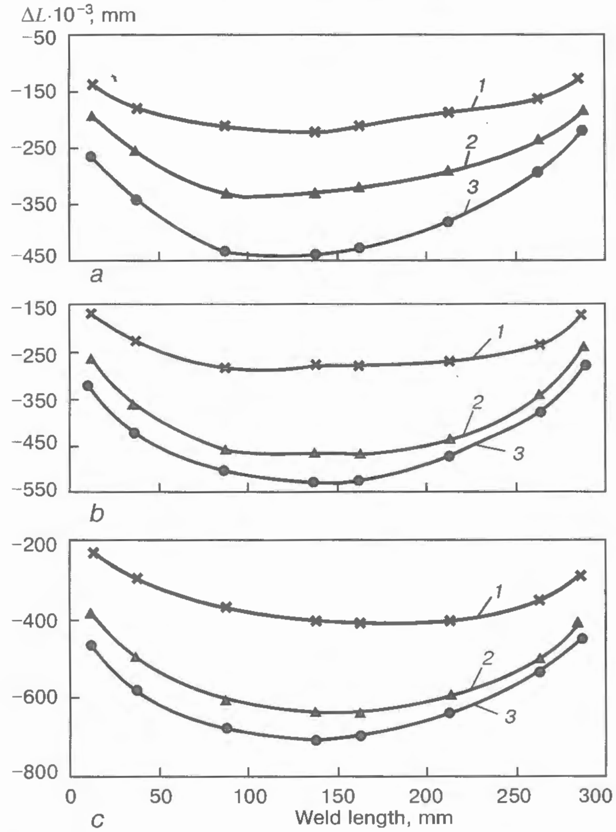

Figure 2. Transverse displacements of rigid butt joints of width 100 (*a*), 200 (*b*) and 300 (*c*) mm after fulfillment of first (root) (*1*), second (*2*) and third (*3*) layers

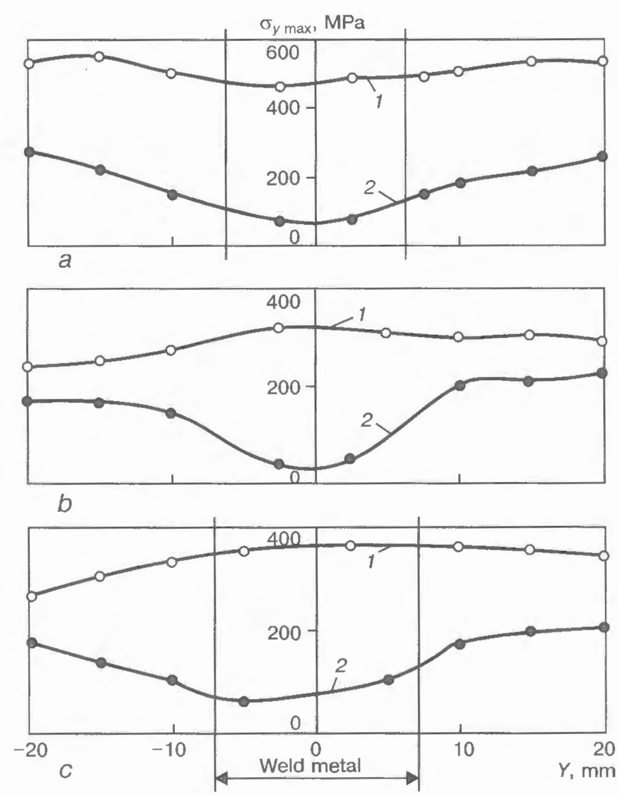

Figure 3. Distribution along axis Y of transverse σ_y stresses in samples of 100 mm width, welded with a complete penetration (*1*) and embedded crack-like defect (*2*), in length of joint investigated 50 (*a*), 150 (*b*) and 250 (*c*) mm

Figure 2, *a, b*) by 24 and 37 %, respectively. This can promote the formation of a high level of residual welding stresses in these samples. The latter were determined using the method of holographic interferometry [9].

The principle of this process is as follows. Holographic device is mounted on the area of the sample, where it is necessary to determine residual stresses. Then, a hologram of initial state of the object region examined is recorded with the help of a thermoplastic camera of instantaneous recording on plates with a coating from amorphous molecular semiconductors. Then, a shallow dosed removal of metal, i.e. drilling a blind hole of 3 mm diameter for 2 mm depth, is made. Further, the field of displacements caused by hole drilling is recorded again on the same plate with coating, where the initial state of object surface was recorded. Plate is visualized twice by the exposed hologram. The interference fringe pattern, obtained here, characterizes the level of stresses in the drilled point.

The investigations showed that in metal of weld and HAZ of technological samples with $B = 100$ mm, made with a complete penetration of root weld, a rather high level of longitudinal σ_x and transverse σ_y tensile stresses is formed (Figures 3 and 4, curves *1*) which can exceed 500 MPa. The presence of lack of penetration and also regions of metal with a low-ductile or brittle structure in these joints can lead to their delayed fracture: in the given case to the formation of longitudinal cracks. This is confirmed by the results of tests of similar sample made with technological lack of penetration. As a result of formation of cracks, the level of tensile stresses decreased by more than 50–60 % in weld metal and adjacent areas of welded joints for a width up to 12–15 mm (Figures 3 and 4, curves *2*). Here, the total level of longitudinal tensile stresses in samples decreased to a lower degree (to 25–30 %).

As regards to test conditions of the given technological sample for initiation and propagation of longitudinal cracks in welded joints of high-strength steel, the presence of maximum high level of tensile transverse stresses in weld metal and adjacent areas of welded joint at the 12–15 mm distance can show the highest effect. Taking into account these approaches the stressed state of technological samples of different width was analyzed (Figure 5). The results obtained prove that the highest level of transverse stresses in all the samples is observed at the beginning and end of the welded joint (in length), that can be caused by specifics of fastening on the plate. In the middle part the values σ_y were much lower. The highest values of tensile stresses ($\sigma_y \approx \approx 570$–$350$ MPa) are recorded in the narrowest technological sample ($B = 100$ mm), that is confirmed indirectly by the results of analysis of displacements of welded joints, and also by the presence of cracks in samples with a technological lack of penetration. In samples of a large width ($B = 200$ and 300 mm) the macrocracks were not revealed.

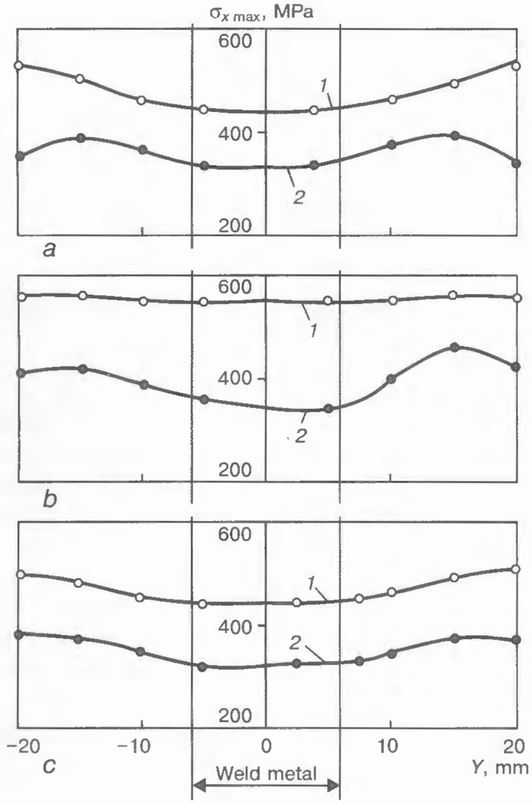

Figure 4. Distribution along axis Y of longitudinal σ_x stresses in samples of 100 mm width, welded with a complete penetration (*1*) and embedded crack-like defect (*2*), in length of joint investigated 50 (*a*), 150 (*b*) and 250 (*c*) mm

Depending on the sizes of technological samples the value of longitudinal stresses in welded joints of steel 14KhGN2MDAFB is also changed. In the narrowest samples (B = 100 mm) the values σ_x can be equal to 350–550 MPa, while in the widest (B = 300 mm) — to 70–250 MPa. Moreover, the highest values are concentrated in the joint central part.

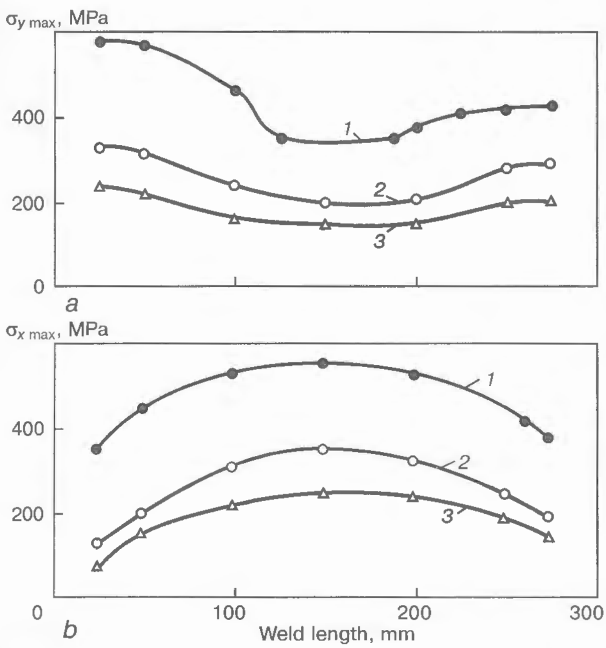

Figure 5. Maximum transverse $\sigma_{y\,max}$ (*a*) and longitudinal $\sigma_{x\,max}$ (*b*) tensile stresses in welded joints of technological samples of width 100 (*1*), 200 (*2*) and 300 (*3*) mm

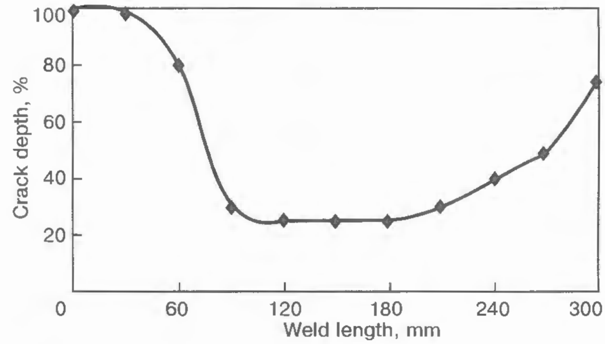

Figure 6. Propagation of longitudinal macrocracks in multilayer butt joints of 100 mm width with a stress concentrator (steel 14KhGN2MDAFB (δ = 15 mm), made with 1.2 mm diameter welding wire Sv-10KhGN2SMFTYu in Ar + 20 % CO_2 mixture of gases

The resistance of welded joints to the formation of cold cracks was evaluated from the results of analysis of sections cut out from technological samples. Results of these investigations prove the presence of longitudinal cracks in welded joints of steels investigated. In most cases the cracks are initiated from stress concentrators which are imperfections of the welded joints: macro- (lack of penetration, lack of fusion, slag inclusions, etc.) and microdefects (nonmetallic inclusions in the fusion zone, places of concentration of coarse and fine grains and others). Nature and sizes of cracks are determined by the peculiarities of formation of joints and level of residual (transverse mainly) stresses. Probably, this explains that fact that the propagation of cracks in length of samples was not uniform (Figure 6). The highest their propagation (70–100 % of weld section height) was observed at the beginning and end of the narrow sample (B = 100 mm) with a technological lack of penetration. On these areas of joints the highest transverse stresses ($\sigma_y \approx$ 450–570 MPa) and relatively low lon-

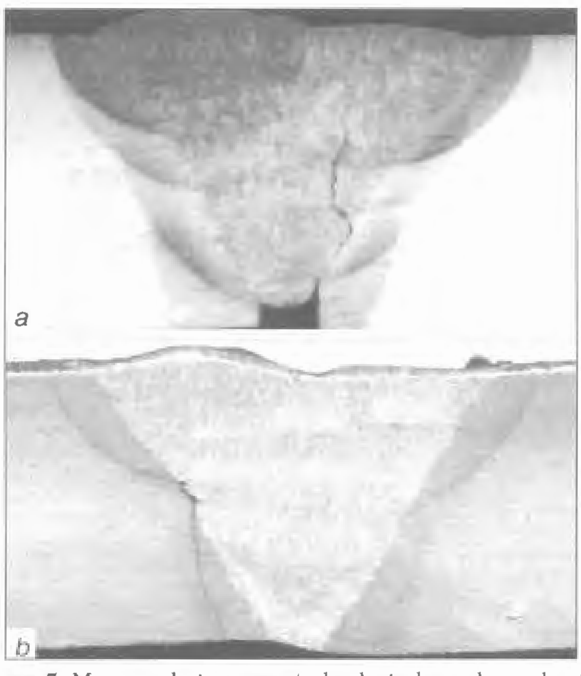

Figure 7. Macrocracks in narrow technological samples made with with a crack-like defect (*a*) and complete penetration (*b*) (×3)

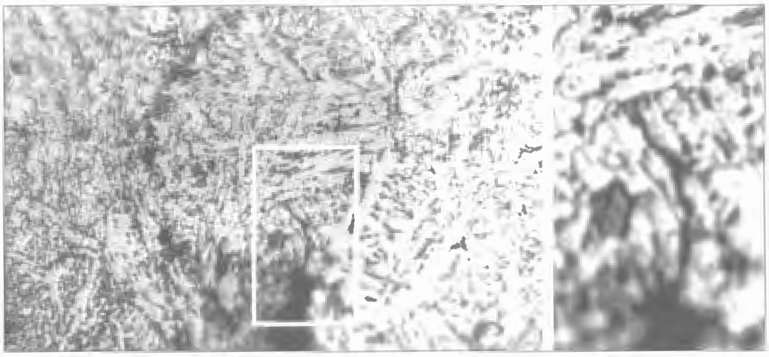

Figure 8. Microcracks in technological sample of 200 mm width (×800) (rectangular fragment of area with microcrack, ×2.3)

gitudinal stresses ($\sigma_x \approx 350$ MPa) were formed. Cracks were initiated from the stress concentrator (lack of penetration). In the middle (in length) part of samples the length of cracks was smallest (up to 25 % of weld height). The level of transverse stresses in this area of the welded joint was $\sigma_y \approx 340$–350 MPa, while the level of longitudinal stresses was $\sigma_x \approx 550$ MPa. This made it possible to conclude that stresses occurred in transverse direction relative to weld have a decisive effect on the process of initiation and propagation of longitudinal cracks in joints of the given technological sample. They are most often initiated and propagated at the initial stage in the fusion zone of joints, and then they propagate to metal of bainitic-martensitic welds (Figure 7, *a*). As the further investigations showed, at this and higher level of residual stresses, other imperfections of welded joints may be the causes of crack occurrence. This is proved by the results of analysis of sections made from rigid welded joints made with a complete penetration (Figure 7, *b*). It showed that in regions of joints where the level of residual transverse stresses is very high ($\sigma_y \approx 550$–580 MPa, that is about 73–77 % of yield strength of steels examined), cracks — spalls were observed. They were initiated in height on average, in weld section near the fusion line in the places of imperfections of microstructure of HAZ metal (non-metallic inclusions) and propagated mainly in HAZ. It should be noted that in these sections of multipass joints the value of transverse residual stresses can be higher than at the surface of samples and is in the range of 580 MPa $\le \sigma_y \le$ 700 MPa. This is proved by investigations of Prof. V. Makhnenko [10] and also results of earlier works with respect to welding of thick-sheet high-strength steels [11]. In that case when the stresses σ_y in welded joints do not exceed 300–350 MPa (that is 40–45 % from steel yield strength), the macrocracks in them are not observed. However, at such level of stresses the microcracks are formed in joints (Figure 8). They are initiated at the boundaries of grains and propagated both along the boundaries and also in body of grains that is typical of a delayed fracture,

Thus, the results of investigations make it possible to widen the conception about the effect of residual stresses on the resistance of welded joints of alloy high-strength steels to the formation of longitudinal cold cracks. The development of these works should be realized in future with allowance for effect of other known factors, first of all, phase-structural composition of welded joints and concentration of hydrogen in them on the delayed fracture.

1. Kasatkin, B.S., Brednev, V.I. (1985) Peculiarities of mechanism of cold crack formation in low-alloy high-strength steel welded joints. *Avtomatich. Svarka*, **8**, 6–18.
2. Pokhodnya, I.K., Shvachko, V.I. (1997) Physical nature of hydrogen-induced cold cracks in structural steel welded joints. *Ibid.*, **5**, 3–10.
3. Sterenbogen, Yu.A., Vasiliev, D.E. (1997) New procedure and energy criteria of evaluation of HAZ metal welded joint resistance to cold cracking. *Ibid.*, **6**, 8–12.
4. Makara, A.M., Gordonny, V.G., Dibets, A.T. et al. (1971) Cold cracks in low-alloy high-strength welds. *Ibid.*, **11**, 1–4.
5. Makarov, E.L. (1981) *Cold cracks in welding of alloyed steels*. Moscow: Mashinostroenie.
6. Hrivnak, I. (1984) *Weldability of steels*. Moscow: Mashinostroenie.
7. Shorshorov, M.Kh., Chernyshova, T.A., Krasovsky, A.I. (1972) *Weldability tests of metals*. Moscow: Metallurgiya.
8. Mikhoduj, L.I., Zhdanov, S.L., Sergienko, A.A. et al. (1997) Peculiarities of delayed fracture of high-strength steel welds. *Avtomatich. Svarka*, **9**, 9–13.
9. Lobanov, L.M., Pivtorak, V.A. (1992) Methods of investigations and control of welding stresses and strains. In: *Improvement of welded metallic structures*. Kyiv: Naukova Dumka.
10. Makhnenko, V.I. (1998) Computer modelling of welding processes. In: *Advanced materials science of the 21st century*. Kyiv: Naukova Dumka.
11. Mikhoduj, L.I., Gonchar, A.K. (1990) Peculiarities of welding of thick structures from low-alloy high-strength steels. *Avtomatich. Svarka*, **10**, 41–45.

INVESTIGATION OF CORROSION FRACTURE OF WELDED JOINTS IN Ni–Cr–Mo ALLOYS IN TITANIA PRODUCTION ENVIRONMENT

K.A. YUSHCHENKO[1], **T.M. STARUSHCHENKO**[1], **A.A. NAKONECHNY**[1], **L.V. CHERVYAKOVA**[1], **T.E. SHEPIL**[2], **V.A. KACHANOV**[2] and **Yu.B. DANILOV**[2]

[1]E.O. Paton Electric Welding Institute, NASU, Kyiv, Ukraine

[2]Open Joint Stock Company «UkrNIIkhimmash», Kharkiv, Ukraine

Susceptibility of ThyssenKrupp VDM nickel-chromium-molybdenum alloys to corrosion cracking was evaluated. Samples with annular welds made by the argon-arc method using filler wire of the AWS A.5.14ERNiCrMo-13 grade were tested in the titania production environment. It is shown that reliable data can be generated from testing experimental models or stressed welded samples with an annular weld simulating residual stresses in a structure.

Keywords: *nickel-chromium-molybdenum alloys, welded joints, titania, general corrosion, corrosion cracking, structural materials, metallography, annular test sample, knife-line corrosion, pitting fracture*

Titania finds wide application in many industries (paint and varnish, production of synthetic fibres, plastics, film-type products, artificial leather, building materials, paper making, printing industry etc.) owing to its high consumer properties. Two methods for production of titania are used in the world practice — sulphate and chloride ones. The former was developed and is widely applied in the European countries, while the latter is used mostly in the USA.

Because of high aggressiveness of the processing media, the basic process equipment was initially made from carbon steel in a protected modification. Later, as a result of investigations conducted at the Company «UkrNIIkhimmash», recommended for this application were stainless steels and alloys, titanium VT1-0 and zirconium E-110 (for the Crimean State Joint Stock Company «Titan» and for upgrading of production at the Sumy Open Joint Stock Company «Khimprom») [1, 2].

New structures and, therefore, new materials are required to increase titania production capacities.

Proceeding from the need to use a new generation of structural materials for titania production, the authors of this study investigated corrosion behaviour of welded joints in alloys Nicrofer 3127hMo (31) and Nicrofer 5923hMo (59) developed lately by ThyssenKrupp VDM.

As shown by the general corrosion tests of alloys Ni–Cr–Mo under conditions of preliminary filtration (H_2SO_4 — 5 %, $TiOSO_4$ — 18 %, $FeSO_4$ — 9 %, Ti^{3+} — 3 g/l, T = 60 °C), a welded joint in alloy 31 exhibits an insignificant general corrosion. The rate of general corrosion of welded joints is less than 0.1 mm/year.

Alloys 31 and 59 supplied in the form of plates by ThyssenKrupp VDM were used to investigate resistance of the alloys to corrosion cracking caused by residual welding stresses. Chemical composition of the alloys is given in the Table.

The annular test samples (Steklov's test) [3] were used to evaluate susceptibility of welded joints in the above alloys to corrosion cracking. Plates measuring 5×130×130 mm with an annular groove for the weld with a diameter of 40 mm were prepared and welded.

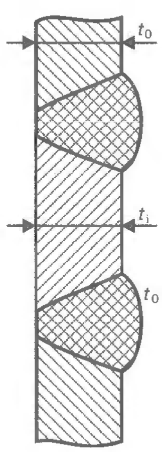

Figure 1. Annular test sample: t_0 — plate thickness; t_i — insert thickness

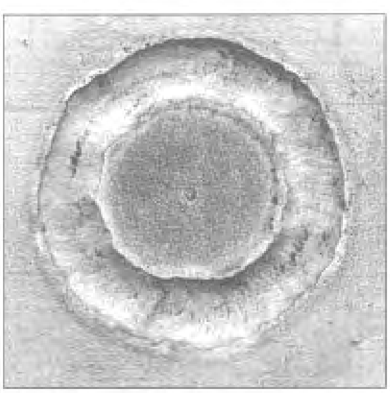

Figure 2. Appearance of the 5 mm thick annular test sample of alloy 59

Chemical composition of materials used

Materials used	Content of elements, wt.%										
	Ni	Cr	Fe	C	Mn	Si	Mo	Co	Al	P	S
59	Base	22–24	1.5	0.010	0.5	0.10	15.0–16.5	0.3	0.1–0.3	0.015	0.005
31*	30–32	26–28	Base	0.015	2.0	0.30	6.0–7.0	–	–	0.02	0.010
Wire Nicrofer S5923-FM59	Base	22–24	1.5	0.010	0.5	0.10	15.0–16.0	0.3	0.1–0.4	N/D	

*Contains additionally 1.0–1.4 % Cu and 0.15–0.25 % N.

Figure 3. Character of corrosion fracture of alloys 31 (*a*) and 59 (*b, c*) after testing at a stage of preliminary filtration at the Company «Titan» (*a, b* — ×120; *c* — ×1500)

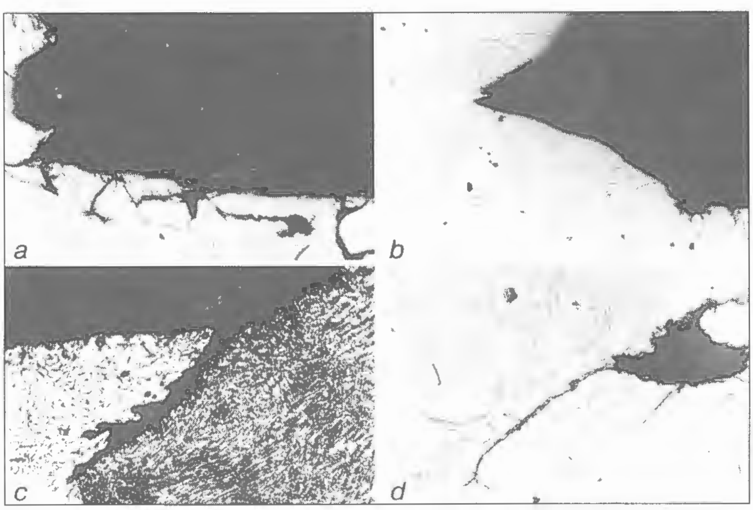

Figure 4. Character of corrosion fractures after testing alloy 31 (*a, b*) in a bleaching reactor at the Company «Titan» and alloy 59 (*c, d*) at the Company «Khimprom» (×125)

Figure 5. Character of fracture of alloy 59 after testing in a peptisation reactor at the Company «Titan» (×120)

The samples were made by manual argon-arc welding using filler wire of the AWS A5.14.ERNiCrMo-13 grade (Nicrofer S5923-FM59) with a diameter of 2.5 mm. Chemical composition of the wire is given in the Table.

Welding was performed in two passes under the following conditions: I_w = 70 A and U_a = 11–12 V for the root weld, and I_w = 85–90 A and U_a = 11–12 V for filling the groove. Appearance of the annular test sample weld in alloy 59 is shown in Figure 2.

The weld was cleaned after each pass. Quality of the annular test samples was evaluated by visual examination of their surfaces, and the presence of defects was detected by the dye penetrant inspection method

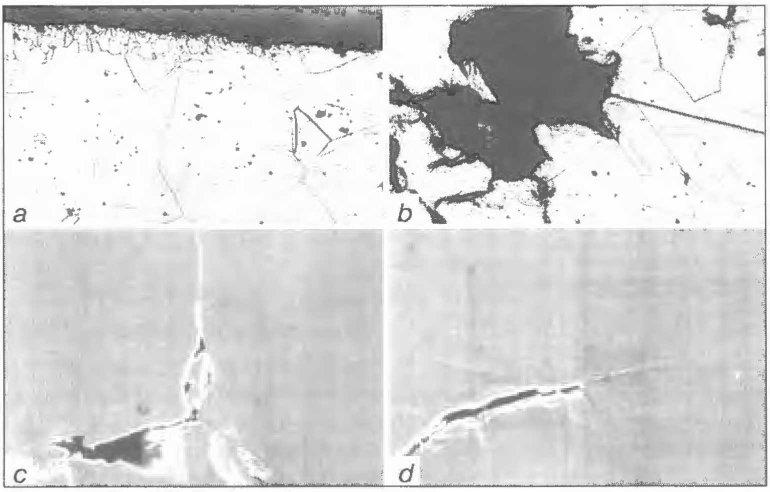

Figure 6. Character of fracture of alloy 31 at the stage of cleaning of waste gases at the Company «Khimprom»: *a* — HAZ metal; *b–d* — base metal

using a set of the penetrants produced by the «Namicon» Company (Italy). At the same time, the welded joints were examined by the metallography method.

Comprehensive testing of quality of welded joints on the annular test samples showed the absence of defects, which made it possible to approve them for the corrosion cracking tests.

Analysis of the tests to corrosion cracking susceptibility under the preliminary filtration conditions showed that a welded joint in alloy 31 was sensitive to corrosion cracking. The crack initiated in the HAZ subjected to knife-line attack and ended with branching in the weld metal (Figure 3, *a*).

Alloy 59 was subjected at this stage to intensive uniform corrosion at a rate of 0.7 mm/year with a considerable etching of the weld metal. Metallography revealed the presence of intercrystalline corrosion (Figure 3, *b*, *c*).

Alloy 31 showed the lack of resistance in a bleaching reactor (94–8 % H_2SO_4, up to 160 g/l TiO_2, hydrogen, zinc metal, $T = 95$ °C). The rate of corrosion in this case was 1.8 mm/year, and a welded joint was prone to knife-line and intercrystalline corrosion (Figure 4).

Having an insignificant general corrosion (the rate of corrosion was 0.002 mm/year), the welded joint in alloy 59 was susceptible to corrosion cracking when testing special samples with an annular weld, corrosion cracking being of an intercrystalline character (Figure 4).

Welded joint in alloy 59 in a peptisation reactor (4–10 % HCl, zinc metal, hydrogen, T = 100 °C) exhibited intensive intercrystalline and knife-line corrosion down to 0.5 mm deep (Figure 5).

The alloy in the vapour-gas phase was susceptible to pitting fracture, the corrosion rate being higher than 0.12 mm/year.

Waste gases of the baking furnace contain SO_3 and SO_2. Therefore, before ejection into the atmosphere, the gases are washed with water in a scrubber at a temperature of up to 70 °C. Investigation of corrosion resistance of alloys 31 and 59 showed that welded joints in alloy 31 were susceptible to intensive intercrystalline corrosion (Figure 6). The rate of uniform corrosion ranged from 0.2 to 0.68 mm/year.

Alloy 59 exhibited insignificant uniform corrosion at a rate of up to 0.03 mm/year.

Therefore, as shown by the conducted corrosion and metallographic investigations, the data on resistance of welded joints to uniform corrosion cannot serve as the basis to give recommendations whe ther structural materials can be used for development of the equipment. For this it is necessary to conduct tests on stressed welded samples with an annular weld simulating residual welding stresses in a structure, and on experimental models.

1. Kachanov, V.A., Gvozdikova, E.K., Nikitin, D.G. (1985) Corrosion-electrochemical behaviour of structural materials in sulphuric acid solutions in the presence of reducing agents. *Zashchita Metallov*, **4**, 24–25.
2. Kachanov, V.A., Nikitin, D.G., Gvozdikova, E.K. (1978) Examination of corrosion and electrochemical behaviour of 06Kh28MDT alloy in titania process media. *Khim. i Neft. Mashinostroenie*, **6**, 18–21.
3. (1976) *Strength of welded structures in aggressive media*. Moscow.

PECULIARITIES OF EXPLOSION TREATMENT OF THE CIRCUMFERENTIAL WELD ON PIPE FILLED WITH LIQUID

V.G. PETUSHKOV
E.O. Paton Electric Welding Institute, NASU, Kyiv, Ukraine

The problem is considered for a case of filling a pipe with water in an assumption of axial symmetry of geometric and force parameters of loading, using a stiff-plastic model of a medium and a known method of reflected shock adiabats. It is shown that the presence of liquid in the pipe leads to a substantial decrease in its explosion reduction, thus preventing the use of a traditional method of treatment with external explosive charges placed at a distance from the weld to relieve residual stresses. The effect of liquid is such that it becomes possible to load the pipe directly on the weld, the liquid acting as a kind of support.

Keywords: *circumferential welds, pipelines, explosion treatment, shock adiabat, shock wave, reduction, residual stress relief*

In application of explosion treatment to relieve residual stresses (RS) in circumferential welds on pipes, there may be situations where the above process has to be performed on pipelines filled with liquid (oil, condensate etc.). In this case it is necessary to estimate to which circumferential strains this treatment may lead and to what extent the liquid medium may diminish these strains and, hence, the efficiency of decreasing RS. Consider in general the method for estimation of the degree of reduction of a pipe filled with water. Suppose that width of the zone treated by explosion is sufficiently large, and shock waves formed in the pipe and its shape retain cylindrical symmetry during reduction. However, width of the reduction zone is much smaller than radius of the pipe, and waves reflected from the pipe axis do not lead to substantial secondary strains.

Analysis of disintegration of discontinuity at the metal–water interface within the framework of the elasto-plastic model of metal. Assume that the state of metal before interaction of shock waves at the metal–water interface corresponds to point A in the shock adiabat of metal (Figure 1). Here $0B$ is the shock adiabat of water, which in the first approximation in a range of low pressures can be approximated to straight line $0G$, the inclination of which to the axis of abscissas is determined by the velocity of sound in water under normal pressure of detonation wave D_w. As follows from [1], the state of water and metal after interaction of the shock waves can be determined by the method of a reflected adiabat. In this case it corresponds to point G. At a sufficiently high pressure the energy of a shock wave is distributed in equal parts between the kinetic and potential components [1]. This allows estimation of the energy absorbed by the wave during a period of the first interaction of the shock waves:

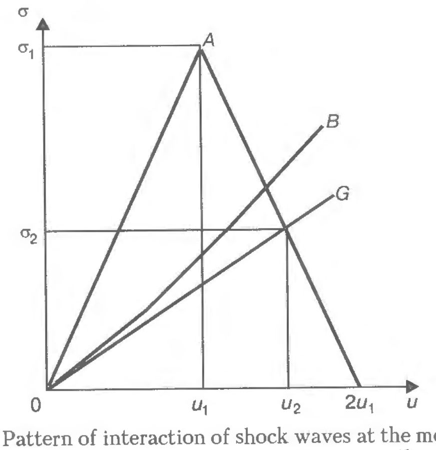

Figure 1. Pattern of interaction of shock waves at the metal–water interface (u — radial displacement of the pipe wall; see the rest of the designations in the text)

$$E_w = \rho_{water} \Delta x_w u_2, \qquad (1)$$

where ρ_{water} is the water density; Δx_w is the thickness of the compression wave, and u_2 is the mass velocity of water. On the one hand,

$$\frac{\Delta x_w}{\Delta x} = \frac{D_w}{D}, \qquad (2)$$

where Δx is the thickness of the shock wave front in metal; D is the velocity of propagation of the plastic compression wave before interaction of the shock waves, which is equal to

$$D = \sqrt{\frac{K}{\rho}};$$

K is the bulk elasticity modulus, and ρ is the density of the pipe metal.

Using (1) and (2), and given that $E_1 = \rho \Delta x u_1^2$ (here E_1 and u_1 are the energy and mass velocity of shock waves in metal before their interaction, respectively), we find that

$$\frac{E_w}{E_1} = \frac{\rho_{water} D_w u_2^2}{\rho D u_1^2}. \qquad (3)$$

It can also be concluded from Figure 1 that

$$\frac{u_2}{u_1} = \frac{2\rho D}{\rho D + \rho_{\text{water}} D_{\text{w}}}. \tag{4}$$

Formulae (3) and (4) yield

$$\alpha = \frac{E_{\text{w}}}{E_1}. \tag{5}$$

It follows from equation (5) that α does not depend upon the amplitude of a wave in metal (or upon energy E_1) in interaction of the shock waves. This fact allows consideration of the set of such discontinuities at the metal–water interface for a series of waves reflected from the external surface of the pipe. It should be noted here that energy αE_n (here E_n is the energy transferred to the pipe) is transferred to water at the n^{th} interaction.

Displacement of a hollow pipe after explosion loading within the framework of the stiff-plastic model of metal. Assuming that specific pulse I_0 (per unit surface) is transferred to the pipe at time moment $T = 0$, and further deformation causes stresses in it equal to dynamic yield stress σ_d, we find that

$$E_{\text{c}} = E_0 - \frac{\sigma_d h}{R} u, \tag{6}$$

where E_{c} and E_0 are the current and initial energies, respectively, absorbed by the pipe; h is the wall thickness; and R is the pipe radius.

Dependence $E(u)$ at different values of E_0 is schematically shown in Figure 2. Maximum reduction of the hollow pipe can be determined from the following formula:

$$u_m = \frac{I_0^2 R}{2\rho h^3 \sigma_d}. \tag{7}$$

Displacement of a pipe filled with water. The first interaction of shock compression waves at the metal–water interface occurs at time moment $T = t/2$, where $t = 2h/D_0$ (here D_0 is the velocity of detonation of an explosive). Let the initial energy be equal to $E\frac{t}{2} - E_1$ (Figure 2, point k). Then, after the first interaction, the pipe energy will become equal to $E_1(1-\alpha)$ (Figure 2, point l).

The second interaction will take place in a period of time t after the first one. Here energy E_2 absorbed by the pipe, which is lower than $E_1(1-\alpha)$ (Figure 2, point m), will decrease to $E_2(1-\alpha)$, (Figure 2, point n), and so on. Thus, it is necessary to find the radial displacement of the pipe, u_{n^*}, corresponding to a zero final energy:

$$u_{n^*} = \sum_{n=1}^{n^*} u_n, \tag{8}$$

where n^* can be determined from the following condition:

$$v_{n^*} = 0, \tag{9}$$

where v is the radial velocity of the pipe wall.

The situation illustrated in Figure 2 allows the following recurrent formula to be derived for u_n:

$$u_n = \beta u_{n-1}, \tag{10}$$

where $\beta = \sqrt{1-\alpha}$; $s = \frac{1}{2}t^2(1-\beta)\frac{\sigma_d}{\rho R}$.

Simple transformations of formula (10) yield the following expression:

$$\begin{aligned} u_n &= \beta^{n-1}u_1 - s(1+\beta+\ldots+\beta^{n-2}) = \\ &= \beta^{n-1}\left(u_1 - \frac{s}{1-\beta}\right) - \frac{s}{1-\beta}. \end{aligned} \tag{11}$$

This expression is valid for $n > 1$. Hence, it follows from equation (8) that

$$u_{n^*} = u_0 + \sum_{n=1}^{n^*} u_n = u_0 \frac{sn^*}{1-\beta} + \left(u_1 + \frac{s}{1-\beta}\right)\frac{1-\beta^{n^*}}{1-\beta}. \tag{12}$$

Here $u_0 = \frac{1}{2\rho}\left(\frac{I_0}{h} - \frac{t^2\sigma_d}{R}\right)$; $u_1 = \frac{\beta t I_0}{\rho h} - s$.

Then it is necessary to determine n^* from expression (9). One can easily see that the recurrent formula similar to equation (10) is valid for v_n:

$$v_n = \beta v_{n-1} - b, \tag{13}$$

where $b = \beta t \sigma_d / \rho R$.

Transforming expression (13) in a way similar to formula (10) yields

$$\begin{aligned} v_n &= \beta^{n-1}v_1 - b(1+\beta+\ldots+\beta^{n-2}) = \\ &= \beta^{n-1}\left(v_1 - \frac{b}{1-\beta}\right) - \frac{v}{1-\beta}, \end{aligned} \tag{14}$$

where $v_1 = \frac{\beta}{\rho}\left(\frac{I_0}{h} - \frac{t\sigma_d}{2R}\right)$.

Using expressions (9) and (14), we find that

$$\beta^{n^*} = \frac{\beta b}{b - v_1(1-\beta)}. \tag{15}$$

u_{n^*} can be determined from relationships (12) and (15).

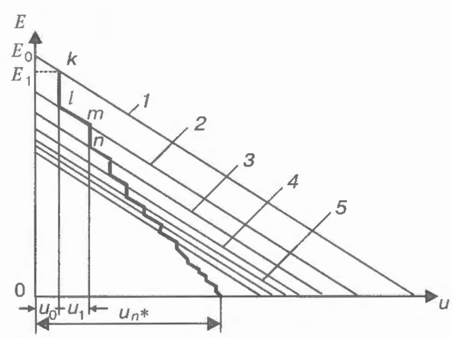

Figure 2. Paths of deformation of pipe on coordinates E–u (see designations in the text)

Example. Let $R = 0.5$ m; $h = 10^{-2}$ m; $\sigma_d = 7.5$ N/m^2; $\rho = 7.8$ kg/m^3; $\rho_{water} = 1 \cdot 10^3$ kg/m^3; $D_w = 1.5$ m/s; $E = 2.1 \cdot 10^{11}$ N/m^2 (elasticity modulus of steel); $\nu = 0.28$ (Poisson's ratio); and $I_0 = 5 \cdot 10^3$ N·s/m^2. Using these parameters we find that $\alpha = 0.15$; $t = 4.4$ ms; $n^* = 23$ and $u_{n^*} = 2.3$ mm. To compare, consider the value of u_{n^*} for the hollow pipe:

$$u_{n^*} = \frac{RI_0^2}{2\sigma_d \rho h^2} = 10 \text{ [mm]}.$$

Therefore, it can be concluded that despite a low acoustic stiffness, compared with steel, the liquid that fills in the pipe hinders substantially its explosion reduction. It follows therefrom that the captive external explosive charges can be used to relieve welding stresses in circumferential welds on pipelines filled with liquid products. In this case the charges can be located directly within the weld zone, as opposed to the method described in [2], meaning that the effect of reliving RS can be achieved only as a result of the basic effective factor of explosion treatment, i.e. the stress-strain trace with compressive RS formed within the above zone due to explosion [3].

1. (1975) *Explosion physics*. Ed. by K.P. Stanyukovich. Moscow: Nauka.
2. Makhnenko, V.I., Kudinov, V.M., Petushkov, V.G. et al. (1975) Calculation of the efficiency of decreasing residual stresses in circumferential welds by explosion treatment. *Avtomatich. Svarka*, **12**, 6–8.
3. Petushkov, V.G., Fadeenko, Yu.I. (1999) *Welding stress relief be explosion treatment*. New York: Backbone.

TRIBOLOGICAL PROPERTIES OF THE Fe–Cr–Si–Mn–P SYSTEM DEPOSITED METAL

I.I. RYABTSEV[1], **Yu.M. KUSKOV**[1], **V.F. GRABIN**[1], **G.N. GORDAN**[1], **T.G. SOLOMIJCHUK**[1] and **V.V. POLOTAJ**[2]

[1]E.O. Paton Electric Welding Institute, NASU, Kyiv, Ukraine

[2]I.N. Frantsevich Institute for Materials Science Problems, NASU, Kyiv, Ukraine

Studies of assimilation of phosphorus in open-arc and submerged-arc (with fluxes AN-26 and AN-348) surfacing using flux-cored wires containing up to 2.5 % P, as well as tribological properties (sliding friction coefficient and wear resistance) and structure of deposited metal of the Fe–Cr–Si–Mn–P alloying system, were conducted. Almost all phosphorus was found to be assimilated by the deposited metal in surfacing by the flux-cored wire open-arc and submerged-arc (with fluxes AN-26 and AN-348) methods. It is shown that samples of the deposited metal alloyed with 0.9–1.2 % P have a minimum sliding friction coefficient, and a minimum wear of the sample and mating body is provided at a phosphorus content of 2.0 %.

Keywords: *electric arc surfacing, deposited metal, flux-cored wires, phosphorus in steel, phosphide eutectic, sliding friction, wear resistance*

The use of phosphorus as an alloying element of surfacing consumables for repair and hardening of parts operating under conditions of friction of metal on metal was suggested in [1]. According to some data [2–4], phosphorus raises wear resistance and lowers the sliding friction coefficient of Fe-base alloys containing about 10 % Cu, 0.3–1.6 % P, 0.42–1.36 % S and ≈ 1 % C. The phosphide eutectic phases acting as a grease are formed in structure of such alloys. However, surfacing and welding consumables do not contain phosphorus as an alloying element. Therefore, the task was to estimate assimilation of phosphorus in surfacing by the open-arc method and submerged-arc method with fluxes AN-26 and AN-348 using flux-cored wires containing up to 2.5 % P, study tribological characteristics (sliding friction coefficient and wear resistance) and examine structure of the deposited metal of a matching composition. A flux-cored wire which provides deposited metal of the type of steel 20KhGS was selected as the baseline one. Wires of this type are applied now in different industries for repair and hardening of parts operating under conditions of friction of metal on metal.

Experimental procedure. Seven experimental wires providing deposited metal of the 20KhGS type with a design phosphorus content of 0.3–2.5 % (Table 1) were made to conduct experimental studies. Alloying ranges were selected on the basis of preliminary investigations of crack resistance of these materials. The investigations showed that the first cracks initiated at a phosphorus content of the deposited metal equal to 2.0–2.5 % in five- and six-layer surfacing of plates of steel St.3 measuring 40×100×250 mm. Samples for estimation of friction coefficient and wear resistance, metallography and X-ray microanalysis were taken from the upper layer of the deposited metal. Wear resistance and anti-friction properties of the deposited metal were evaluated using the friction testing machine [5] additionally equipped with a system for positioning of the samples with respect to the rotating shaft used as the mating body. The tests were conducted by the method of

Table 1. Chemical composition of the deposited metal samples

Wire grade	*Sample No.*	*Surfacing method*	*Content of elements, wt.%*				
			C	*Mn*	*Si*	*Cr*	*P*
PP-0	1	Open arc	$\frac{0.23}{0.22}$	$\frac{1.30}{1.15}$	$\frac{1.30}{0.88}$	$\frac{1.50}{1.10}$	–
	1a	Flux AN-26	$\frac{0.23}{0.16}$	$\frac{1.30}{1.29}$	$\frac{1.30}{1.72}$	$\frac{1.50}{1.04}$	–
	1b	Flux AN-348	$\frac{0.23}{0.10}$	$\frac{1.30}{2.00}$	$\frac{1.30}{1.45}$	$\frac{1.50}{0.72}$	–
PP-0.3	2	Open arc	$\frac{0.23}{0.22}$	$\frac{1.30}{1.20}$	$\frac{1.30}{0.92}$	$\frac{1.50}{1.23}$	$\frac{0.30}{0.31}$
	2a	Flux AN-26	$\frac{0.23}{0.16}$	$\frac{1.30}{1.21}$	$\frac{1.30}{1.84}$	$\frac{1.50}{1.10}$	$\frac{0.30}{0.30}$
	2b	Flux AN-348	$\frac{0.23}{0.11}$	$\frac{1.30}{1.95}$	$\frac{1.30}{1.38}$	$\frac{1.50}{0.91}$	$\frac{0.30}{0.35}$
PP-0.6	3	Open arc	$\frac{0.23}{0.21}$	$\frac{1.30}{1.17}$	$\frac{1.30}{0.95}$	$\frac{1.50}{1.13}$	$\frac{0.60}{0.57}$
	3a	Flux AN-26	$\frac{0.23}{0.19}$	$\frac{1.30}{1.27}$	$\frac{1.30}{1.83}$	$\frac{1.50}{1.06}$	$\frac{0.60}{0.60}$
	3b	Flux AN-348	$\frac{0.23}{0.12}$	$\frac{1.30}{2.10}$	$\frac{1.30}{1.73}$	$\frac{1.50}{1.03}$	$\frac{0.60}{0.61}$
PP-0.9	4	Open arc	$\frac{0.23}{0.24}$	$\frac{1.30}{1.10}$	$\frac{1.30}{0.96}$	$\frac{1.50}{1.33}$	$\frac{0.90}{1.00}$
	4a	Flux AN-26	$\frac{0.23}{0.18}$	$\frac{1.30}{1.33}$	$\frac{1.30}{1.63}$	$\frac{1.50}{1.14}$	$\frac{0.90}{1.00}$
	4b	Flux AN-348	$\frac{0.23}{0.10}$	$\frac{1.30}{2.05}$	$\frac{1.30}{1.65}$	$\frac{1.50}{1.09}$	$\frac{0.90}{1.05}$
PP-1.2	5	Open arc	$\frac{0.23}{0.23}$	$\frac{1.30}{1.13}$	$\frac{1.30}{1.02}$	$\frac{1.50}{1.28}$	$\frac{1.20}{1.28}$
	5a	Flux AN-26	$\frac{0.23}{0.17}$	$\frac{1.30}{1.23}$	$\frac{1.30}{1.56}$	$\frac{1.50}{1.13}$	$\frac{1.20}{1.36}$
	5b	Flux AN-348	$\frac{0.23}{0.14}$	$\frac{1.30}{1.98}$	$\frac{1.30}{1.72}$	$\frac{1.50}{1.12}$	$\frac{1.20}{1.26}$
PP-2.0	6	Open arc	$\frac{0.23}{0.21}$	$\frac{1.30}{1.01}$	$\frac{1.30}{0.92}$	$\frac{1.50}{1.35}$	$\frac{2.00}{1.98}$
	6a	Flux AN-26	$\frac{0.23}{0.17}$	$\frac{1.30}{1.34}$	$\frac{1.30}{1.68}$	$\frac{1.50}{1.22}$	$\frac{2.00}{1.94}$
	6b	Flux AN-348	$\frac{0.23}{0.13}$	$\frac{1.30}{2.03}$	$\frac{1.30}{1.81}$	$\frac{1.50}{1.12}$	$\frac{2.00}{1.96}$
PP-2.5	7	Open arc	$\frac{0.23}{0.21}$	$\frac{1.30}{1.14}$	$\frac{1.30}{0.89}$	$\frac{1.50}{1.23}$	$\frac{2.50}{2.38}$
	7a	Flux AN-26	$\frac{0.23}{0.18}$	$\frac{1.30}{1.48}$	$\frac{1.30}{1.67}$	$\frac{1.50}{1.25}$	$\frac{2.50}{2.34}$
	7b	Flux AN-348	$\frac{0.23}{0.12}$	$\frac{1.30}{2.00}$	$\frac{1.30}{1.78}$	$\frac{1.50}{1.19}$	$\frac{2.50}{2.26}$

*Numerator gives the calculated and denominator — actual content of a corresponding alloying element.

rubbing off hollows by the shaft against plane method without any additional grease fed to the friction zone. The samples for tribological tests had plan sizes of 3×20 mm. The shaft used as the mating body was 40 mm in diameter and 12 mm high. It was made from hardened steel of the 45 grade and had hardness HRC_e 42. The following values were estimated by testing the deposited metal samples: friction force, wear of a coating on the basis of volume of the hollow, and wear of the mating body on the basis of differences in its weight before and after the tests. The friction coefficient was calculated as a quotient of the friction force by load, the calculation error being not more than 5 %. The volume of the hollow was calculated from the known formulae on the basis of the mean value of its width using a toolmaker's microscope with an error of not more than 0.01 mm. Weight of the mating body was determined using the analytical ba-

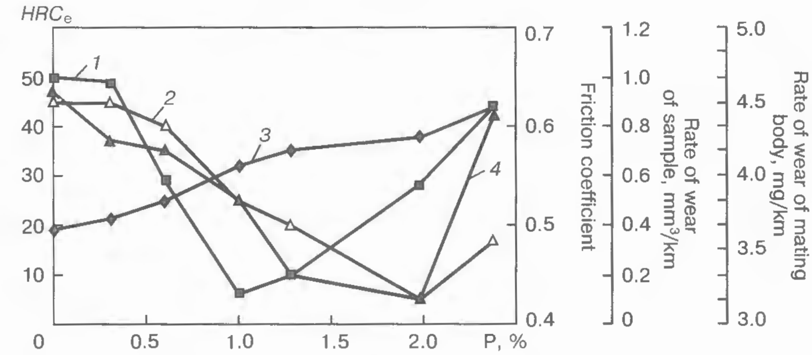

Figure 1. Effect of phosphorus on hardness and tribological characteristics of deposited metal of the 20KhGS type: *1* — friction coefficient; *2* — rate of wear of experimental samples of the deposited metal; *3* — hardness of the deposited metal; *4* — rate of wear of the mating body

lance with an error of not more than 0.0005 g. The total error of estimation of wear of the sample and mating body was not in excess of 1 %. The following testing parameters were selected from the preliminary test results: sliding speed 1 m/s, load 30 N and test time 600 s. These parameters provided stabilisation of tribological characteristics of all the samples. The use of the positioning system allowed testing of each sample to be repeated not less than three times in a new region of the sample friction surface and in a new friction strip of the mating body. Metallography of the deposited metal was carried out using the optical microscope «Neophot 22», analysis of fracture surface of the deposited metal samples was conducted using the scanning microscope JSM-840, and distribution of alloying elements in the deposited metal was examined using the X-ray microanalyser «Camebax».

Results and discussion. As shown by chemical analysis, almost all phosphorus is assimilated by the deposited metal (Table 1). In the case of submerged-arc surfacing with fluxes AN-26 and AN-348 the carbon content of the deposited metal decreases because of the Si- and Mn-reduction reactions, the manganese and silicon contents changing accordingly. Considering almost the same assimilation of phosphorus with all the surfacing methods under consideration, further studies were conducted on the deposited metal samples produced by using flux AN-26.

Results of investigations of tribological characteristics of the deposited metal samples containing differing amounts of phosphorus are shown in Figure 1. Increase in the phosphorus content is accompanied by a uniform increase in hardness from HRC_e 20 (at a phosphorus content of 0.3 %) to HRC_e 44 (at a phosphorus content of 2.5 %). Other properties change following more complicated principles. The friction coefficient (Figure 1, curve *1*) decreases with increase in the phosphorus content and reaches minimum at a phosphorus content of about 1 %. Increase in the phosphorus content to more than 1 % leads to increase in the friction coefficient, and it becomes almost equal to that of steel 20KhGS at a phosphorus content of 2.5 %. Curves describing the rate of wear

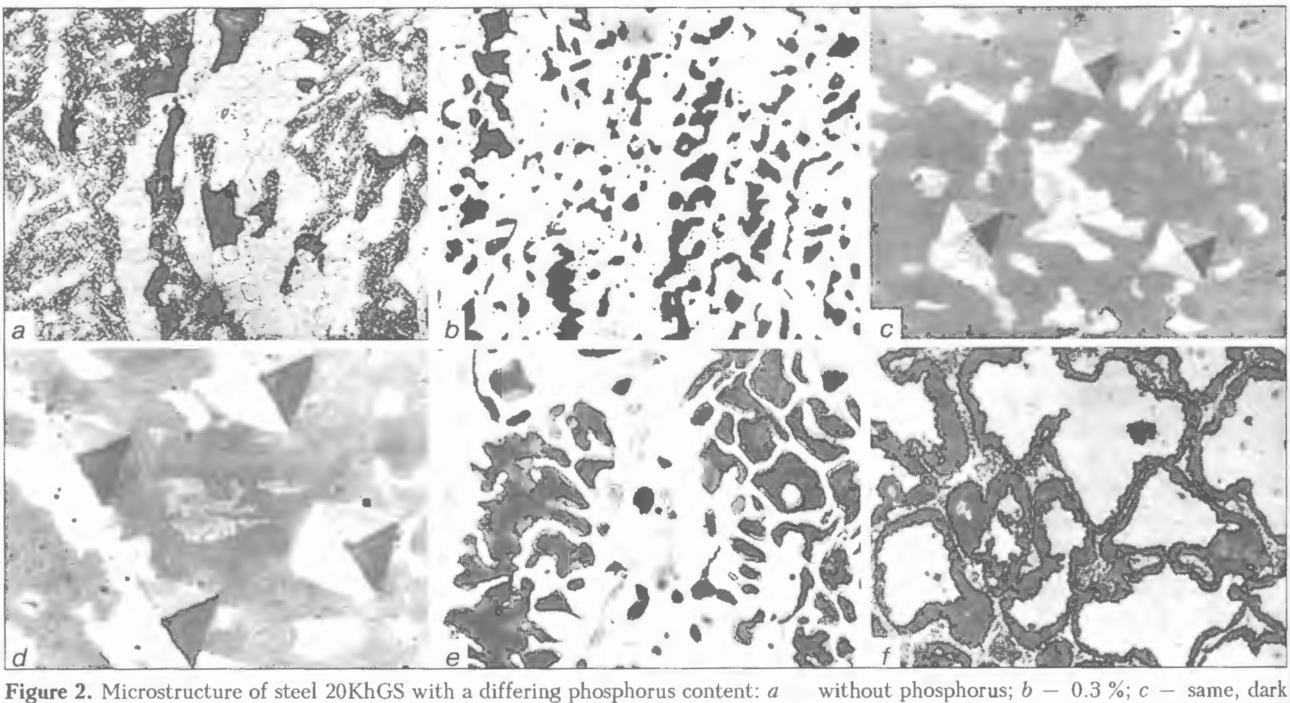

Figure 2. Microstructure of steel 20KhGS with a differing phosphorus content: *a* — without phosphorus; *b* — 0.3 %; *c* — same, dark phase inclusion; *d* — same, light phase inclusion; *e* — 1.2 %; *f* — 1.98 %. Electrolytic etching in 20 % solution of chromic acid (*a*, *b*, *e*, *f* — ×500; *c*, *d* — ×800)

Table 2. Results of analysis of fracture surfaces of deposited metal samples of the 20KhGS type using the scanning microscope JSM-840

Sample No.	*Point of analysis*	*Content of elements, wt.%*				
		Fe	*Mn*	*Si*	*Cr*	*P*
2a	Dark phase	95.77	0.60	1.27	1.00	0.41
	Light phase	94.98	1.27	1.30	1.10	0.25
	Matrix	94.03	0.80	1.32	1.22	0.58
3a	Dark phase	94.25	1.14	1.22	1.24	0.70
	Light phase	95.54	0.84	1.03	1.21	0.53
	Matrix	93.90	1.45	1.27	1.02	0.71
4a	Dark phase	93.62	1.19	1.20	0.98	0.60
	Light phase	95.24	1.17	1.33	1.01	0.62
	Matrix	94.40	1.25	1.44	1.11	0.88
	Phosphide inclusion	85.53	2.40	0.58	2.24	8.46
5a	Dark phase	92.95	0.76	1.53	1.10	0.71
	Light phase	93.00	1.16	1.30	1.20	0.85
	Matrix	93.46	1.82	0.71	1.05	1.45
	Phosphide inclusion	90.78	1.96	0.85	1.74	12.53
6a	Matrix	94.75	1.09	1.18	1.12	0.98
	Phosphide inclusion	81.53	3.68	0.17	2.45	11.59
7a	Matrix	90.94	1.66	1.45	1.08	1.23
	Phosphide inclusion	80.92	3.24	0.01	2.46	12.47

of the sample and mating body (Figure 1, curves *2* and *4*) are of a similar character. First the rate of wear of the sample and mating body decreases with increase in the phosphorus content. Then it begins to grow, starting from a phosphorus content of about 2 %.

Examinations of microstructure of samples of steel 20KhGS with a differing phosphorus content were carried out to reveal causes of an ambiguous effect of phosphorus on tribological characteristics of the deposited metal of the type of the above steel. The deposited metal containing no phosphorus has a pearlitic structure with a small amount of polyhedral and acicular ferrite (Figure 2, *a*). Addition of 0.3 % P (as a ferritising element) increases the amount of ferrite (Figure 2, *b*). Isolated dark and light inclusions identified as phosphide ones by metallography were fixed at a phosphorus content as low as 0.3 % (Figure 2, *c, d*). Increase in the phosphorus content leads to further increase in the amount of ferrite and phosphides (Figure 2, *e*). At a phosphorus content of about 2 % a continuous grid of the phosphide eutectic is formed in structure of steel 20KhGS, enclosing the alloy matrix grains (Figure 2, *f*). The amount of the phosphide eutectic grows with increase in the phosphorus content.

Analysis of fracture surfaces of the deposited metal samples of the 20KhGS type was conducted using the

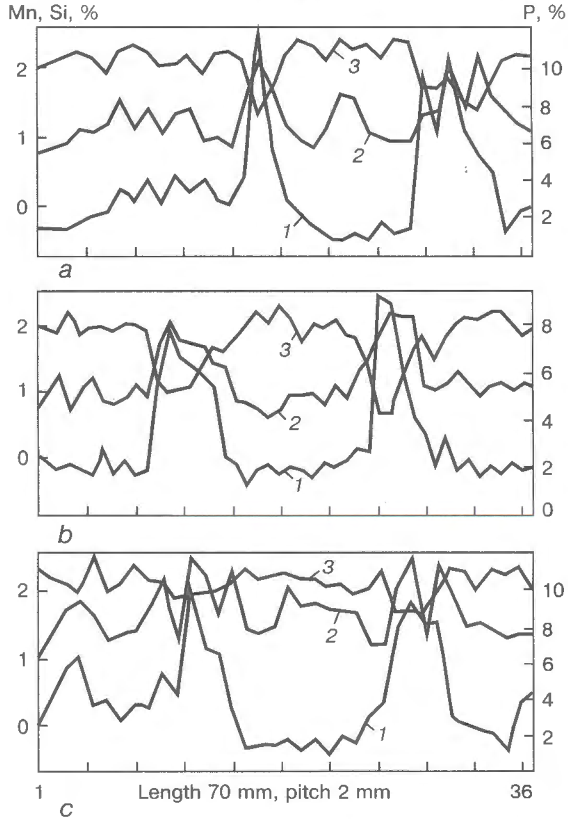

Figure 3. Distribution of phosphorus (*1*), manganese (*2*) and silicon (*3*) in structure of deposited metal of the 20KhGS type: *a* — 0.3; *b* — 1.2; *c* — 2.5 % P

scanning microscope JSM-840 (Table 2). This method failed to fix an increased phosphorus content of isolated inclusions of the light and dark phases in samples No.2a and 3a, the boundaries of which were marked by pins in corresponding sections (see Figure 2, *c, d*, and Table 2). It is likely to be attributed to the fact that size of a spot being analysed was in excess of sizes of the inclusions and covered the alloy matrix. Inclusions identified as the phosphide ones were fixed at a phosphorus content of more than 0.6 % (alloy sample No.4a). Considerable amounts of the phosphide eutectic were fixed at a phosphorus content of about 2 % (alloy sample No.6a). The phosphide eutectic was found to contain iron, chromium and manganese. In addition, it featured a decreased silicon content. Increase in the total phosphorus content was accompanied by increase in the phosphorus content of the alloy matrix (maximum value is 1.45 %, which disagrees with the available literature data on solubility of phosphorus in pure iron). According to [6] the solubility limit of phosphorus in pure iron is 0.6, and according to [2] it is 1.2 %. Therefore, this issue requires further investigations.

Examinations of the deposited metal samples of the 20KhGS type with a differing phosphorus content were conducted using the X-ray microanalyser «Camebax». Samples for the examinations were cut from the upper (fifth) deposited layer. Figure 3, *a–c* shows results of these examinations. This method revealed phosphide inclusions at a phosphorus content as low as 0.3 %. It was proved that phosphides contained manganese and chromium, in addition to iron, and that they had a decreased silicon content. Increase in the total phosphorus content was accompanied by increase in the phosphorus content of the steel matrix and increase in the amount of phosphides.

Analysis of the data given in Table 2 and shown in Figure 3, *a–c*, indicates to the fact that chemical composition of phosphides hardly changes with increase in the phosphorus content: they contain 2–3 % Mn and 2.0–2.5 % Cr, in addition to iron, i.e. chemical composition of phosphides cannot have a substantial effect on tribological properties of steel. The total content of phosphides in steel exerts a higher effect. The data of tribological tests and metallographic examinations are indicative of the fact that phosphorus stops to have a favourable effect on the friction coefficient of steel 20KhGS after the phosphide inclusions form a continuous grid in the steel structure. Most likely that this has the following causes.

The friction coefficient and wear decrease in the presence of isolated phosphide inclusions with a higher hardness than the ductile matrix. Under contact loading, in this case [7] the load is distributed over hard inclusions which provide a low friction coefficient and high resistance to adhesion. A relatively ductile base allows the system to acquire the optimal geometry of contact within a very short period of time, thus reducing the probability of formation of local centres of high pressure leading to formation of cleavage or adhesion. Increase in the amount of the eutectic and formation of a continuous phosphide grid characterised by increased hardness and brittleness dramatically decrease ductility of the working layer and lead to formation of spalls during wear, which act as an abrasive and enhance wear of the sample and mating body.

CONCLUSIONS

1. In arc surfacing using flux-cored wires containing up to 2.5 % P by the open-arc and submerged-arc methods with fluxes AN-26 and AN-348 almost all phosphorus is assimilated by the deposited metal. In this case isolated inclusions of phosphides in the low-alloy deposited metal 20KhGS are formed at a phosphorus content of more than 0.3 %. The content of phosphorus dissolved in the steel matrix increases in proportion to its total content and may amount to 1.45 %.

2. Samples of the deposited metal alloyed with phosphorus in an amount of 0.9–1.2 %, i.e. until phosphides remain in the steel structure in the form of isolated hard inclusions, providing a low friction coefficient and high adhesion resistance, have the minimum sliding friction coefficient.

3. Minimum wear of the sample and mating body is provided at a phosphorus content of the 20KhGS type deposited metal equal to about 2 %. Further increase in the phosphorus content leads to dramatic decrease in ductility of the working layer, thus leading to fracture of the brittle and hard eutectic component and increase in wear.

1. Kuskov, Yu.M., Ryabtsev, I.I., Doroshenko, L.K. et al. (2002) Peculiarities of melting and solidification of the 20KhGS type deposited metal alloyed with phosphorus. *The Paton Welding J.*, **8**, 21–24.
2. Markovsky, E.A., Kachko, N.A., Mashinetsky, N.Ya. (1993) Formation of surface structure of the Fe–Cu alloy system alloyed with sulphur and phosphorus. *Protsessy Litia*, **4**, 15–18.
3. Kachko, M.O., Markovsky, E.A., Ilchenko, V.D. (1998) Anti-friction iron alloys with grease phases. *Metaloznavstvo ta Obrobka Metaliv*, **3**, 17–21.
4. Markovsky, E.A., Ilchenko, V.D., Butenko, L.I. et al. (1999) Effect of composition and structure of anti-friction iron alloy on its wear resistance. *Protsessy Litia*, **2**, 60–64.
5. Polotaj, V.V. (1970) Friction and wear testing machine. *Tekhn. i Organiz. Proizvodstva*, **6**.
6. Goudremont, E. (1966) *Special steels*. Moscow: Metallurgiya.
7. Kolesnichenko, L.F., Polotaj, V.V. (1970) Directed solidification of alloys as a method of production of high wear-resistant structures. *Poroshk. Metallurgiya*, **7**, 62–67.

ON THE INFLUENCE OF THE SPEED OF VARIATION OF ELECTRODE EXTENSION AND ARC LENGTH ON ARC SENSOR SIGNAL

G.A. TSYBULKIN
E.O. Paton Electric Welding Institute, NASU, Kyiv, Ukraine

Physical principles are considered, which underlie the action of arc sensors. Analytical dependencies are given of welding current on the current distance between the torch edge and weld pool surface, as well as the speed of variation of this distance.

Keywords: *arc welding, consumable electrode, welding operations, arc sensors*

In connection with arc welding robotisation quite extensive experience of practical application of the so-called arc sensors has been gained in many industrialized countries. These sensors provide to the control systems of welding robots current information on the spatial position of the consumable electrode end relative to the line of the welded joint. Some interesting results have been obtained. On the other hand, analysis of published sources indicates that some issues of conceptual nature, arising in design of arc sensors, are still unsolved. In particular, an integral concept of the physical principles, underlying their action, has still not been established. In keeping with the approach, accepted in the majority of recent publications [1–4], measurements, performed with the arc sensors, are based on the dependence of welding current on the current distance between the torch edge and weld pool surface. This is true, but only in part. In reality, the most significant (and sometimes even the determinant) is the functional dependence between the welding current and speed of variation of this distance. The nature of this connection, judging by numerous publications, is still unstudied.

In this paper the extent of the influence of each of the above two factors on welding current is studied, namely current distance from the torch edge to the weld pool surface and speeds of variation of this distance.

Analytical model of the arc sensor. Let us consider equations [5, 6]

$$v_n T_w \frac{di}{d\xi} + i = \frac{1}{M} g, \tag{1}$$

$$g = v_e + F'(v_n + N\xi) + F''\xi v_n, \tag{2}$$

describing the reaction of welding current i on the setting and disturbing actions during gas-shielded consumable electrode arc welding of metal items.

In equations (1), (2) $v_n = dn_p/dt$ is the speed of the torch motion along axis n (Figure 1); $\xi = n_p - n_0$ is the current deviation of electrode extension from the initial position n_0; T_w is the time constant of the welding process; v_e is the speed of motion (feed) of the electrode relative to the torch edge; $v_m = v_m(i, h)$ is the speed of electrode melting; $M \equiv \partial v_m/\partial i$ and $N \equiv \partial v_m/\partial h$ is the slope of speed characteristics of the electrode melting by current i and electrode stick-out h, respectively, at nominal values of i_0 and h_0; $F' \equiv dF/dn$, $F'' \equiv d^2F/dn^2$, where $F = F(n)$ is the function, characterizing the shape and position of the axial line of the joint being welded in plane bn.

When equations (1) and (2) were derived, it was assumed that distance H between torch edge and axis n is unchanged, i.e. H = const, and speeds v_e and v_n were also taken to be equal.

From equations (1) and (2) it is immediately seen that welding current i at fixed values of T_w, M and N is determined not only by the rate of electrode wire feed v_e, but also by the speed of variation of function $F(n)$ at the change of coordinate n. From the same equations it follows that welding current i at $F' \neq 0$ depends also on the speed of motion of torch v_n along axis n. This is a highly significant moment, so we will consider it in greater detail.

Let us consider a very characteristic case, when line $F(n)$ is in an inclined position relative to the specified line of the torch motion. Let initial section $F(n)$ up to point n_0 coincide with axis n (Figure 2), directed parallel to the above line of the torch motion,

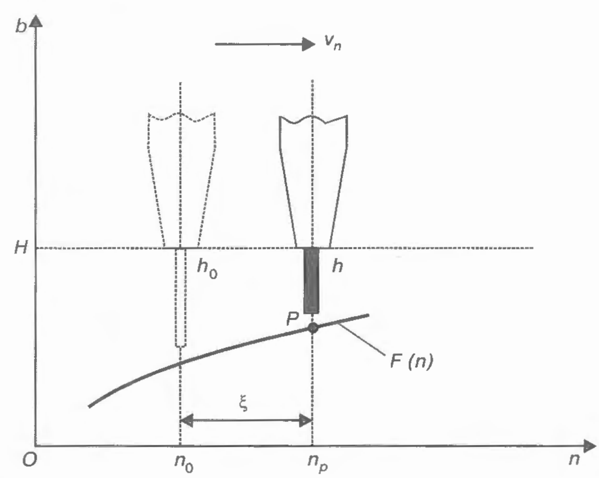

Figure 1. Schematic of movement of the welding torch

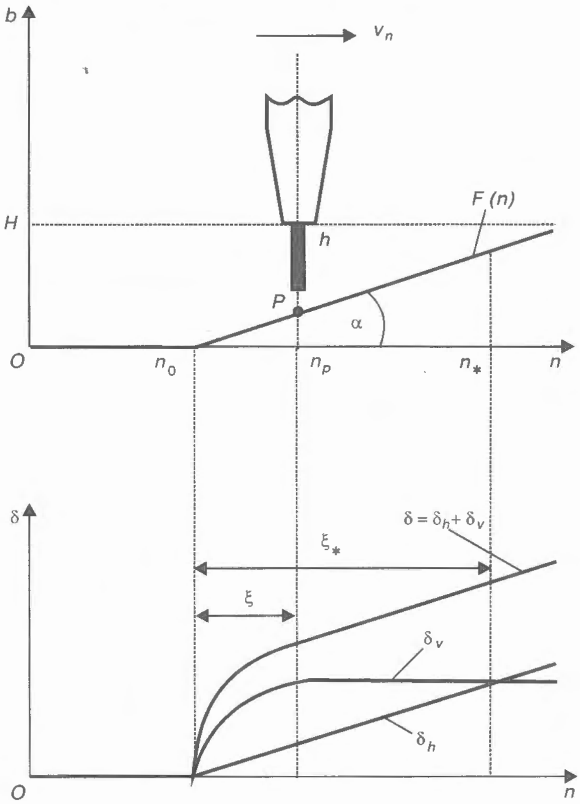

Figure 2. Reaction of welding current to change of distance H–F

and starting from point n_0 let line $F(n)$ pass at angle α to axis n, i.e. function $F(n)$ is described as follows:

$$F(n) = \begin{cases} 0 & [n \le n_0]; \\ K\xi & [n > n_0]. \end{cases} \qquad (3)$$

Here $K = \mathrm{tg}(\alpha)$, and point n_0 on axis n is selected so, that by the moment of time $t_0 = n_0/v_n$ the transient processes in the welding circuit were practically completely over.

From Figure 2 it is seen that at displacement of the welding torch in the positive direction of axis n distance $H - F(n_p)$ between the torch edge and current point of welding P decreases by a linear law, starting from point n_0. We will see, how welding current i changes in this case. In this connection let us study the solution of equation (1), which, taking into account (2), (3), becomes

$$i = \frac{v_e}{M} + \frac{KN}{M}\xi + \frac{Kv_n}{M}(1 - NT_w)(1 - e^{-a\xi}), \qquad (4)$$

where $a = 1/v_nT_w$.

Let us consider deviation $\delta = i - v_e/M$ of welding current i from nominal value $i_{\mathrm{nom}} = v_e/M$. Since in expression (4) $NT_w << 1$, we will present the relationship for δ in a simpler form:

$$\delta = \frac{K}{M}[N\xi + v_n(1 - e^{-a\xi})]. \qquad (5)$$

Let us plot in Figure 2 the graphs of two functions

$$\delta_h = \frac{KN}{M}\xi; \qquad (6)$$

$$\delta_v = \frac{Kv_n}{M}(1 - e^{-a\xi}) \qquad (7)$$

and their sums $\delta = \delta_h + \delta_v$ and fix on axis n point n_*, where $\delta_v = \delta_h$.

Thorough consideration of expressions (5)–(7) and Figure 2 demonstrates that at a small deviation of the electrode from point n_0, when $\xi < \xi_*$, the main contribution to δ formation is made by deviation of welding current δ_v, caused by a jump-like variation in point n_0 of the speed of electrode movement $\Delta v_e = Kv_n$ relative to the current point of welding P. This contribution is the greater, the higher the speed of displacement of the torch v_n. Deviation δ_h, related to decrease of electrode extension h, is small. And only at $\xi = \xi_*$, both the components are equal, i.e. $\delta_v = \delta_h$.

Practical value of establishing this fact is determined by that how effectively it can be used to build arc sensors to solve the problems of adaptive control of the spatial position of the welding torch. This issue can be best clarified by specific examples.

Examples. Let us first consider a numerical example, indicating how the actual «weights» of both components δ_v and δ_h are distributed at torch motion at a constant speed v_n along slanting line $F = K\xi$. Such a situation may arise, in particular, as a result of thermal deformations during robotic arc welding of extended elements of a thin material or in case of their inaccurate set up for welding.

Let in the given example $K = 0.1$ (angle of inclination $\alpha \approx 6°$), $v_n = 10$ mm/s, $H = 17$ mm, $i = 130$ A, electrode wire diameter $d = 1.2$ mm. Here $M = 0.5$ mm/(s·A), $N = 0.8\ \mathrm{s}^{-1}$, $T_w = 0.1$ s. Let us select measurement step s of current deviation δ, proceeding from such a compromise: step s should be small enough to provide minimum deviation δ over the entire length of the joint being welded due to periodical correction of the torch motion by the results of δ measurement, and, on the other hand, according to (4), it should be not less than $3v_nT_w$, so that the transient process from the corrective action were practically over by the time of the next measurement of δ.

So, let us assume $s = 10$ mm. Then, in view of (6) and (7) at $\xi = s$, we will have

$$\delta_h = \frac{KN}{M}s = \frac{0.1 \cdot 0.8}{0.5}10 = 1.6\ \mathrm{A};$$
$$\delta_v = \frac{Kv_n}{M}(1 - e^{-a\xi}) = \frac{0.1 \cdot 10}{0.5}(1 - e^{-10}) = 2\ \mathrm{A}. \qquad (8)$$

As was anticipated, deviation of welding current δ at $s = 10$ mm is almost equally due both to the change of this distance K_s and rate of change of this distance Kv_n. It should be noted right away that values of δ_h and δ_v, calculated by formulas (8), agree well with the experimental data.

Considering formulas (8) it is easy to see that at $v_n = 0$, i.e. when current point P (Figure 2) is stationary relative to the initial point n_0, the steady-state value of welding current differs from its nominal value by $\delta_h = 1.6$ A. Such a very slight deviation is not so easy to measure under the real conditions of arc welding, i.e. under the conditions of a rather high level of random noise, accompanying the welding process. Therefore, the idea, expressed in [3] about using for arc welding a pair of electrodes, located parallel to each other at small distance (5–10 mm), in order to obtain information about shifting of the center of this pair relative to the axis of the joint being welded by the calculated difference of currents, flowing through the above electrodes, is ineffective.

This way, we come to the natural conclusion, that in order to obtain a noticeable (measurable) deviation of welding current from its nominal value, it is necessary to perform torch motions relative to point n_0 at high enough speed v_n.

Let us consider another example. Let the longitudinal axis of electrode extension, passing in parallel to coordinate axis n, make the following harmonic oscillations in plane bn (Figure 3) relative to a fixed point n_0:

$$\xi = A \sin \omega t; \quad \omega = 2\pi f \tag{9}$$

with a small amplitude A and fixed frequency f. Now line $F = K\xi$ is still located at a certain angle $\alpha =$ = arctg K to axis n.

Such a situation arises in arc welding of butt or fillet (with edge preparation) joints with transverse oscillations of the torch, when for some reason the middle position of the oscillating torch turns out to be shifted by distance On_0 from the axial line of the joint being welded (passing in Figure 3 through point O, normal to plane bn).

Let us assume, that $A < On_0$. Then, function g, according to expression (2), becomes

$$g = v_e + AK\,(\omega \cos \omega t + N \sin \omega t). \tag{10}$$

Considering expression (10), it is easy to see that at $f \geq 1$Hz relationship $\omega >> N$ is valid, and the second addend in parenthesis, characterizing the change of electrode extension, is negligible. Function g can be represented in a simpler form:

$$g = v_e + AK\,\omega \cos \omega t. \tag{11}$$

Therefore, speed component $v_n = A\omega \cos \omega t$ of harmonic oscillation (9) at $f \geq 1$Hz has a dominant impact, which actually is what generates periodical deviations of welding current:

$$\delta_v(t) = \frac{AK}{MT_w} \frac{\omega T_w}{\sqrt{1 + (\omega T_w)^2}} \cos(\omega t - \mathrm{arctg}\, \omega T_w). \tag{12}$$

Function (12) is a partial solution of equation (1), obtained taking into account expression (11), as well as relationships $d\xi = v_n dt$ and $\delta_v = i - v_e / M$. Analysis of the above function shows that as frequency ω increases, amplitude of set oscillations of welding current

$$\Delta = \frac{AK}{MT_w} \frac{\omega T_w}{\sqrt{1 + (\omega T_w)^2}} \tag{13}$$

increases (Figure 4), becoming asymptotically close to maximum value

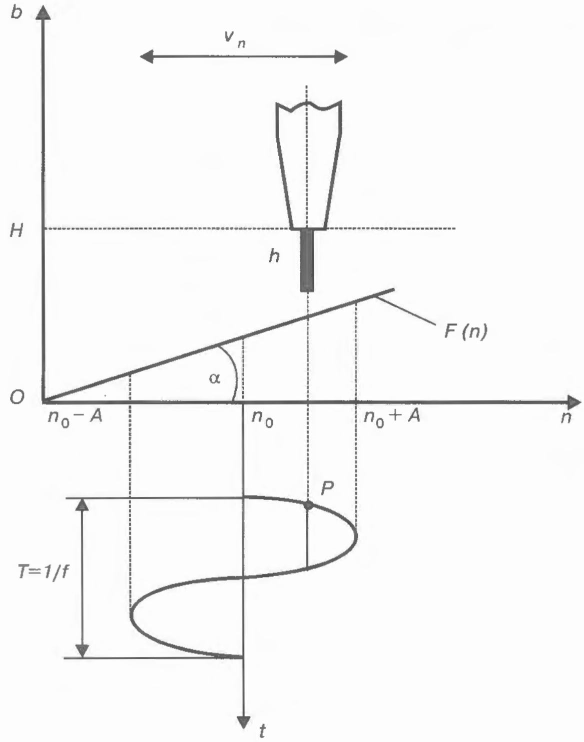

Figure 3. Schematic of oscillatory motion of the torch

$$\Delta_* = \max_{\omega} \Delta = \frac{AK}{MT_w}.$$

This fact has a precise physical explanation: with the increase of the frequency of electrode oscillations the effect of self-restoration of the arc becomes smaller. At high frequencies ω arc length does not have enough time to restore its previous value in the case of a fast change of the distance between the torch end and free surface of weld pool, as the time, required for it, determined by value T_w, is much greater than oscillation period $T = 2\pi/\omega$.

Selection of electrode oscillation frequency. As follows from expression (13) and Figure 4, already at $\omega T_w = 4$ amplitude Δ comes so closely to its limit value Δ_*, that further increase of ω is practically not needed. Therefore, a quite acceptable value of frequency f of electrode oscillations can be calculated by a simple formula

$$f \approx \frac{2}{\pi T_w}. \tag{14}$$

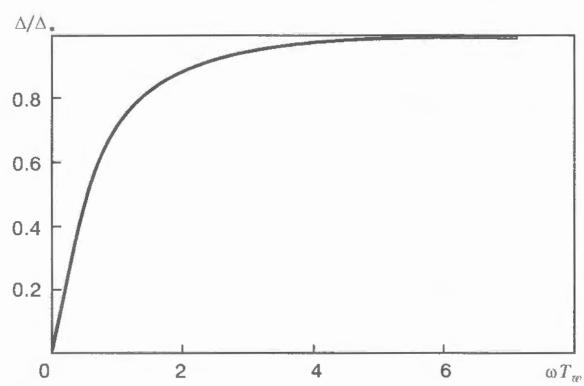

Figure 4. Dependence of Δ/Δ_* on ωT_w

In particular, at $T_w = 0.1$ s frequency f, according to expression (14), is approximately equal to 6 Hz. Substitution of the numerical values of parameters $A = 2$ mm, $K = 1$, $M = 0.5$ mm/(s·A), $T_w = 0.1$ s and $\omega T_w = 4$ in formula (13) yields $\Delta = 38.8$ A. Maximum possible value Δ_* (i.e. value Δ at $f = \infty$), according to equation (13), is equal to 40 A. Thus, simple calculation confirms the conclusion made: there is no sense in increasing the frequency of oscillations (or rotation) of the electrode above 6 Hz to increase the amplitude of welding current.

Work (7) also gives other arguments in favour of low frequencies of electrode oscillations. In particular, notable is the fact that in usually used in practice modes of consumable electrode CO_2 welding the molten metal drops, depending on the nature of their transfer through the arc gap, periodically close this gap or change its length without a complete short-circuit. The frequency of welding current fluctuations, determined by the frequency of the above quasi-periodic changes of the arc gap, depends on a multitude of factors, including amplitude A of transverse oscillations of the welding tool, and according to [8–11], it takes up a quite broad band (20–150 Hz). These fluctuations of welding current are external disturbances (noise) for arc sensors, preventing correct assessment of side deviations of the welding tool from the axis of the joint being welded. It is much easier to filter the above noise, if the working frequency of electrode oscillations is much lower than the frequency bands, taken up by the noise.

On the other hand, at selection of the frequency of electrode oscillations, it is necessary to take into account also the technological side of the issue, in particular, dependence of frequency f on welding speed v_w. It is easy to find the nature of this dependence, if we use the notion of spatial period λ, equal by definition to the distance between closest points, in which transverse oscillations of the electrode proceed in the same phase. Hence, the known in mechanics relationship $\lambda = v_w/f$. As welding speed v_w is pre-set in each concrete case, then, using the above relationship, it is always possible to determine the frequency of electrode oscillation or rotation by a very simple formula:

$$f = \frac{v_w}{\lambda}. \qquad (15)$$

Period λ, apparently, should not be greater than the diameter of the arc column. This is exactly the case, when a uniform melting of the base metal is guaranteed. In robotic arc welding with electrode wire of 0.8–1.6 mm diameter an experimentally established value $\lambda = 2$ mm can be recommended. If $v_w <$ < 20 mm/s, then frequency f, according to expression (15), is below 10 Hz.

However, attention should be given to the fact that spatial period λ is a minimum distance, at which it is possible to determine electrode deviation from the line of the joint being welded, based on measurement of welding current in extreme points of oscillating electrode. Simple calculation shows that distance $\lambda = 2$ mm is quite acceptable at one-time count, i.e. when instant values of amplitude Δ are measured in extreme points just once per period λ. To improve the validity of evaluation of electrode deviation from the axis of the joint being welded, the incremental method is sometimes used, which, essentially, consists in that during λ the above counts are taken not once, but several times (η times). Then the accumulated counts are averaged. The influence of uncontrolled noise on measurement results is reduced. It is obvious that frequency f, when using the above method of evaluation of the deviation, should be selected not from formula (14), but from the following relationship:

$$f = \eta\frac{v_w}{\lambda}.$$

Thus, the price to be paid for greater validity of evaluation of the measured deviation in this case is increase of the frequency of transverse oscillations of the electrode η times, i.e. more complicated kinematic of the arc sensor and introduction of an additional computing device with sufficiently quick response and required storage capacity. There exist, however, other methods to improve the validity of evaluation of the deviation, unrelated to the above complications of the arc sensor, for instance, methods of synchronous detection, considered in [12].

Thus, when the issue of selection of the frequency of transverse oscillations of the electrode is considered, it may be stated, that in case of the actually used speeds of consumable electrode arc welding, there is no basic need to increase frequency f above 10 Hz.

CONCLUSIONS

1. It is established that the action of arc sensors is based on functional dependencies of welding current on the current distance between the torch edge and weld pool surface, as well as on the speed of variation of this distance.

2. It is determined that dependence of welding current on the speed of variation of the above distance predominates at transverse oscillations of the electrode in arc welding of fillet (and grooved butt) joints.

1. Sugitani, Y. (2000) Making best use of the arc sensor. *J. JWS*, **2**, 46–50.
2. Dilthey, U., Stein, L., Oster, M. (1996) Through-the-arc sensing — an universal and multipurpose sensor for arc welding automation. *Int. J. Joining of Materials*, **1**, 6–12.
3. Inoue, K., Zhang, J., Kang, M. (1991) Analysis of detection sensitivity of arc sensor in welding process. *Transact. of JWRI*, **2**, 53–56.
4. Ushio, M. (1991) Sensors in welding. *Ibid.*, 157–163.
5. Tsybulkin, G.A. (1994) Mathematical model construction in problems of adaptive control of arc welding. *Avtomatich. Svarka*, **1**, 24–28.
6. Tsybulkin, G.A (1999) On evaluation of current electrode deviation from welded joint line. *Ibid.*, **12**, 53–54.
7. Tsybulkin, G.A. (1994) On problem of selection of the frequency of welding tool oscillation across axial line of welded joints. *Ibid.*, **11**, 24–26.
8. Paton, B.E., Lebedev, V.K. (1966) *Electric equipment for arc and slag welding*. Moscow: Mashinostroenie.
9. Zaruba, I.I. (1966) *CO_2 welding*. Kyiv: Tekhnika.
10. Potapievsky, A.G. (1974) *Consumable-electrode gas-shielded welding*. Moscow: Mashinostroenie.
11. Lenivkin, V.A., Dyurgerov, N.G., Sagirov, Kh.N. (1989) *Technological properties of welding arc in shielded gases*. Moscow: Mashinostroenie.
12. Tsybulkin, G.A. (1994) Side correction of welding tool current position based on the continuous measurement of welding current. *Avtomatich. Svarka*, **7/8**, 28–31.

APPLICATION OF AGGLOMERATED FLUXES FOR WELDING OF LOW-ALLOY STEELS (REVIEW)

V.V. GOLOVKO
E.O. Paton Electric Welding Institute, NASU, Kyiv, Ukraine

It is shown that agglomerated fluxes are characterised by higher metallurgical activity, compared with the fused ones. Their application fields in fabrication of facilities from structural low-alloy steels are given. It is noted that development of these type of welding consumables holds high promise.

Keywords: *welding, low-alloy steels, agglomerated flux, metallurgical properties, welded joints, performance*

Growth of volumes of application of low-alloy steels during the last quarter of the 20th century was accompanied by a continuous increase in requirements to the level of their specified properties and manufacture technologies. In the 1960–1970s the required mechanical properties of low-alloy steel rolled stock were achieved mostly by thermomechanical treatment, the 1980s were characterised by increase in output of plates with precipitation hardening and controlled rolling, whereas the second half of the 1990s featured a commercial manufacture of steels subjected to metallurgical and thermomechanical treatments based on nano-technologies.

Improvement of the manufacture technologies allowed the level of performance of low-alloy steel rolled products, and primarily their cold crack resistance, to be substantially increased. Such steels provide safe operation of large-size constructions, bridge structures, ship hulls and main pipelines [1].

The field of welding consumables used for the fabrication of structures from high-strength low-alloy (HSLA) steels experienced similar transformations. Analysis of catalogues and expositions of the leading world manufacturers of welding consumables at such a respectable forum as the Essen fair, Germany [2, 3] shows that automatic arc welding of HSLA steels is performed using exclusively agglomerated fluxes. This situation is attributable to the fact that fluxes of this type are not melted during manufacture. As a result they have a high metallurgical activity. Combined with low-alloy low-pearlite welding wires, the agglomerated fluxes make it possible to refine the weld metal as to oxygen, hydrogen and other adverse impurities, control composition and distribution of non-metallic inclusions, microalloy and modify metal in the weld pool, and provide its more reliable shielding from the ambient atmosphere owing to affecting the gas phase within the welding arc zone. Wide metallurgical capabilities combined with excellent welding-operational properties led to an extensive use of the agglomerated fluxes (7–9 % of the total amount of metal melted by the arc welding methods) [4].

The basic application fields of the agglomerated fluxes include manufacture of large-diameter pipes used for construction of main pipelines, ship building and fabrication of bridge and truss structures.

Low-alloy steels applied in each of the above industries differ in composition, manufacture technology, service conditions and levels of requirements to mechanical properties. Thus, welding of specific grades of steels requires as a rule specific fluxes combined with specific grades of welding wires. For example, welding of large-diameter pipes under factory conditions requires a special combination of welding consumables, ensuring not only a certain level of mechanical properties of the weld metal and welded joints but also the appropriate welding-operational characteristics [5]. The use of the agglomerated fluxes for these purposes guarantees the specified characteristics at a level of standard API 5L [6] in welding of pipes from steels of grades X-70 and X-80, manufacture of pipes used for the underwater part of pipelines in the North Sea [7] and construction of drilling platforms for production of mineral resources in the Arctic shelf [8].

Analysis of progress in the world ship building performed by foreign specialists [9] showed the necessity to replace the tanker and bulk-carrier fleets may lead to increase in the number of orders in this field. High rates of growth of the ship building industry are noted in China [10]. The need to replace old ships and steady growth of requirements to freight turnover of the sea transport led to a marked enhancement of the activity of ship yards in the CIS countries [11, 12]. Given that in the fabrication of ship structures the volume of welding operations amounts to 95 %, and the level of mechanical properties of hull steels and requirements to performance of the weld metal and welded joints continuously grow, we can understand that increased attention which is traditionally given to the choice of welding consumables in ship building.

Investigations into weldability of modern HSLA steels [13] for the fabrication of hull and underwater structures show that the agglomerated fluxes, combined with low-alloy welding wires, are capable of meeting the entire set of requirements imposed on the weld metal and welded joints by the Lloyd's and Det Norske Veritas registers. Excellent welding operational properties of the high-bacisity agglomerated fluxes which, when combined with the appropriate grades of welding wires, can provide not only the required level of mechanical properties of the weld metal, but also its super low hydrogen content, as well as an increased resistance of welded joints to corrosion in sea water, determined the choice of this combination of welding consumables for the fabrication of multi-purpose ice breakers, off-shore ice-resistant stationary platforms and floating drilling rigs made from HSLA steels with a yield point of up to 690 MPa [11, 14].

The use of the agglomerated fluxes makes it possible to solve many problems arising both in factory fabrication of bridge metal structures and in field welding of span structures of highway and railway bridges. Low-alloy steel welded joints in bridge structures operate under conditions of cyclic alternating loading within a wide range of climatic temperatures, and are subjected to intensive atmospheric corrosion impact. Such joints are susceptible to low-temperature embrittlement [15]. Therefore, they require development of a special welding technology and a proper choice of welding consumables. The use of the increased-basicity agglomerated fluxes for the factory fabrication of bridge metal structures [16, 17], as well as for welding under field conditions [18], provides a high level of specified properties of the weld metal and welded joints.

Wide application of the agglomerated fluxes for the fabrication of structures, equipment and constructions of low-alloy steels is attributable to the possibility of ensuring the high level of mechanical properties of the weld metal and welded joints, which is favoured by the excellent welding-operational characteristics of the fluxes. The latter are provided by the peculiarities of the technology used for their manufacture, which does not include the charge melting process. This technology forms two basic advantages of the agglomerated fluxes — high technological flexibility and decreased level of power consumption during manufacture.

Relatively low (650–750 °C) temperature of heat treatment of the fluxes allows ferroalloys, master alloys and pure metals to be introduced into their composition. The above materials can get from the flux to the weld pool in a non-oxidised state during welding, and enter there into corresponding metallurgical reactions. In addition, carbonates, complex fluorides, higher oxides of metals and other materials which, when heated during welding, evolve gaseous products can be added to the charge of the non-fused flux, thus controlling the welding arc burning conditions and development of reactions occurring in the gas phase. Both of these factors determine the technological flexibility of the agglomerated fluxes, enable the processes of microalloying, modifying and refining of the weld pool metal to be controlled with a high accuracy and reliability, and conditions of the reactions of oxidation and deoxidation of molten metal at the drop stage, as well as the gas content of the weld metal, to be affected.

Power consumption in the manufacture of agglomerated fluxes is 5 times as low as that in the manufacture of fluxes produced by melting in electric furnaces. In addition to a substantial reduction in power consumption, the agglomeration technology allows a decrease in wastes (not more than 5 % of the entire output) causing pollution of the environment.

Large amount of information has been accumulated up to now concerning the effect of alloying on structure and mechanical properties of the weld metal in low-alloy steels. This makes it possible to develop mathematical models and use them to predict composition of welding consumables to ensure the required level of properties of the weld metal [19, 20]. The use of such models for the agglomerated fluxes allows prediction of the level of alloying and modifying of the weld metal, and control of composition, amount and distribution of non-metallic inclusions in the weld metal [21], thus providing high mechanical properties of metal of the welded joints [22].

The most pressing problem in submerged-arc welding of low-alloy steels is the risk of formation of cold cracks in a welded joint. It was established that one of the basic causes of cold fracture of welded joints is the presence of diffusible hydrogen in the weld metal. The nature of its effect on conditions of formation and propagation of this type of defects has been studied for many years, and by now it has been described in detail [23–25]. Basic methods for eliminating this phenomenon have been developed. They include the use of the welding technology with preheating and concurrent heating, and the application of austenitic welding consumables.

In submerged-arc welding the flux is the main source of hydrogen entering into the weld pool. Moisture can be contained both in granules of the flux and in air contained in gaps between the flux granules. Whereas it was believed in the middle of the 1970s that the main amount of moisture is concentrated in air [26], later studies proved that not more than 20 % of air concentrated between the flux grains takes part in saturation of molten metal with hydrogen [27].

One of the main methods for decreasing hydrogen in submerged-arc welding using fused fluxes is to raise the baking temperature [28–30]. Baking of the agglomerated fluxes also favours decrease in the hydrogen content of the weld metal [31]. Moreover, in the case of using this type of the flux the option of means for controlling the behaviour of hydrogen in welding joints is much wider. Firstly, if in the case of using the fused fluxes the role of fluorine is limited to its effect on the arc stability [32], in the case of the agglomerated fluxes the arc stability can be substantially increased through adding the appropriate compounds (e.g. alkali metal oxides) to the flux composition, while the reactivity of fluorides may be very high [33]. Secondly, complex fluorides having a more intensive effect on the composition of the gas phase, compared with calcium fluoride [34], then carbonates which dissociate to evolve carbon dioxide to the arc atmosphere, thus affecting the hydrogen content of the deposited metal [27], and metallic components promoting formation of the «traps» and arresting hydrogen during its diffusion in the weld metal [23], can be added to the flux. Owing to such a wide spectrum of metallurgical capabilities for controlling the behaviour of hydrogen, the agglomerated fluxes are widely applied in such cases where it is necessary to ensure the minimum hydrogen content of the weld metal [35, 36].

Combination of an increased diffusible hydrogen content of the weld metal and a high level of residual stresses in a welded joint is especially dangerous in terms of formation of cold cracks. Stresses in welded joints are determined by the level of thermal deformation of metal welded as a result of thermal effect exerted by the arc, as well as by deformation of metal overheated to temperatures above A_{c_3} during refining. In the first case it is recommended for decreasing stresses that submerged-arc welding of low-alloy steels be performed with a limited heat input ($q_w \leq$ $\leq$ 18 kJ/cm), combined with preheating to 130 °C [37], which leads to a substantial decrease in productivity of the process and increase in power consumed for performing it. Stresses formed in the second case are caused by changes in the amount of structural components during the γ–α transformation occurring in the overheated metal. Therefore, to decrease the level of these stresses, it is necessary to limit the content of alloying elements which determine the intensity of such reactions in the weld metal [38].

The agglomerated fluxes make it possible to considerably diminish the risk of brittle fracture of welded joints under the effect of residual stresses. Interaction of thermocapillary and capillary-concentration convection of molten metal results in the mode of auto-oscillatory flow established in the weld pool. This leads to concentration oscillations and, hence, to a layered heterogeneity of the weld metal [39]. A high level of stabilising properties of the agglomerated fluxes enables conditions of the submerged-pulsed-arc welding (SPAW) process to be varied over wide ranges. As a result, it is possible to form the weld with a smaller thickness of the solidification layers and interlayer gaps. This provides improvement in mechanical properties of the weld metal without the need to decrease welding heat input or use preheating [40].

Thermal cycle of the SPAW process is such that it is possible to markedly reduce the time of heating and cooling of the HAZ of a welded joint in a range of temperature above 1000 °C, and the time of cooling in a range from 800 to 500 °C [41–43]. Results of modelling and experimental studies of structure of the HAZ metal of low-alloy steel welded joints made by the SPAW technology showed the possibility of varying both width of individual regions and entire HAZ of a welded joint and its metallurgical characteristics [44, 45]. The above peculiarities of the SPAW process make it possible to increase resistance of low-alloy steel welded joints to brittle fracture and avoid the need of using preheating of workpieces [46, 47].

Of high importance in the case of multi-pass welding of thick plate products is the set of welding-operational properties of the flux, allowing formation of the weld metal without surface defects, as well as easy and full removal of slag from the surface of root passes. The ability of the flux to form the weld surface of a regular shape with smooth transition to the base metal and having no scales is determined by its such physical-chemical properties as melting point, viscosity and interface tension [48, 49]. Given that the length of the weld pool zone in which slag may affect formation of the weld surface is very limited [50], viscosity of welding slags changes by two orders of magnitude in a narrow temperature range [51], and that the slag layer should be non-uniform through thickness to provide good slag crust detachability [52], it becomes clear how important is the possibility of varying the chemistry of slag, synthetic and metallic compositions making up the base of the flux.

Several studies were carried out to solve this problem by using fused fluxes. The improved technology of melting the fluxes in double-bath furnaces [53] was developed and introduced into production, the technology for the manufacture of synthetic sintered fluxes [54] was elaborated, and it was suggested that the system of the fused flux plus electrode wire with a filler [55] should be used for this purpose. Each of the above technologies has its capabilities and advantages. However, as shown by practice, none of them can replace the agglomerated fluxes in terms of flexibility and economic efficiency. As proved by the experience of application of the agglomerated fluxes for welding low-alloy steels, they are capable of ensuring a combination of good welding-operational properties and a high level of specified characteristics of the weld metal and welded joints [56, 57]. That is why they receive wide acceptance in welding fabrication of industrialised [58] and CIS countries. It is planned to upgrade the available facilities for the manufacture of welding consumables in order to substantially increase the output of the agglomerated fluxes [59, 60].

1. Ishikawa, T. (1997) Ultra-high crack-arresting steel plate (HI-ARST) with super-refined grains in surface layers. *Nippon Steel Techn. Report*, **75**, 31–42.
2. Christoph, H. (1997) Schweiβzusätze. *Bänder-Bleche-Rohre*, **12**, 51.
3. (2002) Welding and related technologies at the Essen Fair. *The Paton Welding J.*, **1**, 27–41.
4. Aichele, G. (1995) Ein altbekanntes Verfahren im Schaffen der Publizitaet. Arbeitspferd Unterpulverschweiβen. *Schweiz. Maschinenmarkt*, **41**, 52–54.
5. Nies, H., Keville, B., Schlafter, B. (1996) Schweiβen von Groβrohren mit dem Unterpulver-Mehrdrahtverfahren. *Oerlikon Schweiβmitt.*, **131**, 4–13, 25.

6. Bosela, M., Bernasovsky, P., Simon, A. (1997) Production and properties of spirally welded pipes of grade X-70 steels. In: *Proc. of ASM Int. Eur. Conf. on Weld. and Join. Sci. and Technol.*, Madrid, March 10–12, 1997. Brussels.
7. Sigeru, E., Moriyasu, N., Sakae, F. et al. (1996) High strength UOE pipe with excellent preferential corrosion resistance of welded joint. *NKK Techn. Rev.*, **74**, 26–32.
8. Lukkari, J. (1996) Jauhekaarihitsausta raskaassa metallissa Sento Oy. *Hinsausuutiset*, **1**, 17–19.
9. (1998) World shipbuilding demand forecast. *Hansa*, **9**, 57–58, 60.
10. Lu, X. (1998) Shipbuilding in China. *Metal Bull. Mon.*, **2**, 81.
11. Gorynin, I.V., Baranov, A.V. (1998) Prospects of welding in shipbuilding. In: *Proc. of Int. Conf. on Welding and Related Technologies for the 21st Century, Kyiv, November, 1998.*
12. Olkhovoj, Yu.G., Evchenko, V.M., Ganich, S.I. (1996) Experience of «Azovskaya Sudoverf» in solving technical problems to conclude contract with a foreign firm in the welding fabrication area. In: *Welded structures and technology of their fabrication.*
13. Buglacki, H. (1996) Technology of welding high strength low alloy quenched and tempered steel plates for offshore technology and shipbuilding. In: *Proc. of 6th Int. Offshore and Polar Eng. Conf.*, Los Angeles, May 26–31, 1996.
14. Lukkari, J. (1996) Welding multipurpose icebreakers. *Anti-Corros. Met. and Mater.*, **1**, 9–12.
15. Cheprasov, D.P., Ivanajsky, E.A., Platonov, A.S. et al. (1998) Properties of field welded joints in 10KhSND and 15KhSND steel bridge structures. *Svarochn. Proizvodstvo*, **6**, 16–19.
16. Golovko, V.V., Grebenchuk, V.G. (1991) Weldability of 14KhGNDTs steel at different flux-wire combinations. *Ibid.*, **5**, 13–15.
17. Golovko, V.V., Grebenchuk, V.G. (1992) Cold resistance of submerged-arc welded joints in steel 14KhGNDTs. *Ibid.*, **3**, 11–12.
18. Varga, T. (1996) Safety of welded modern high strength steel constructions in particulate bridges. *Welding in the World*, **38**, 1–22.
19. Badianov, B.N. (1997) Thermodynamic computational method in development of welding consumables. *Svarochn. Proizvodstvo*, **11**, 30–33.
20. Zinigrad, M., Zalomov, N., Mazurovsky, V. et al. (1997) Creating new welding materials on the basis of metallurgical processes modeling. *NIST Spec. Publ.*, **923**, 291–297.
21. Golovko, V.V. (2001) Modelling of composition of non-metallic inclusions in weld metal of high-strength low-alloyed steels. *The Paton Welding J.*, **5**, 2–5.
22. Fox, A.G., Brothers, D.G. (1995) The role of titanium in the non-metallic inclusions which nucleate acicular ferrite in the submerged-arc weld (SAW) fusion zones of NAVY HY-100 steel. *Scr. Met. et Mater.*, **7**, 1061–1066.
23. Pokhodnya, I.K., Shvachko, V.I. (1995) Influence of hydrogen on structure of welds of structural steels. In: *Proc. of 1st VOM'95 Int. Conf.*, Donetsk, Sept. 20–22, 1995.
24. Pokhodnya, I.K., Shvachko, V.I. (1997) Physical nature of hydrogen-induced cold cracks in structural steel welded joints. *Avtomatich. Svarka*, **5**, 3–12.
25. Maroef, I., Olson, D.L.Yu., Edvards, G.R. (1998) Hydrogen-induced cracking of high-strength steel welded items, In: *Proc. of Int. Conf. on Welding and Related Technologies for the 21st Century*, Kyiv, November, 1998.
26. Aristov, V.S., Badasen, P.P., Dzhansyz, E.G. et al. (1975) Reduction of hydrogen content in weld metal during automatic submerged-arc welding. *Svarochn. Proizvodstvo*, **12**, 27–28.
27. Tsuboi, J., Terashima, H. (1973) Hydrogen behavior during submerged-arc welding. Hydrogen solution in SAW weld metal. *J. JWS*, **6**, 12–17.
28. Kovach, Ya., Petrov, G.L. (1974) Investigation of hydration and dehydration of acid fluxes for automatic arc welding of steels. In: *Abstr. of pap. of Int. Conf. on Welding Fluxes and Slags*, Nikopol, September, 1974.
29. Ruge, J. Schrode, G. (1982) Zusammenhang zwischen dem Feuchtigkeitsgehalt basischer Schweiβpulver und dem Gehalt an diffusiblem Wasserstoff im Schweiβgut. *Arch. Eisenhuttenw.*, **5**, 199–208.
30. Kasatkin, B.S., Vakhnin, Yu.N., Tsaryuk, A.K. et al. (1988) Influence of the total hydrogen content of flux AN-17M on the concentration of diffusible hydrogen in deposited metal. *Avtomatich. Svarka*, **2**, 14–16.
31. Barzaune, L., Panaitescu, R. (1983) Influenta temeperaturii de calcinare asupra calitatii fluxurilor ceramice pentru sudare. *Sudura si Incerc. Mater.*, **3**, 41–44.
32. Podgaetsky, V.V. (1970) Role of fluorine in submerged-arc welding. In: *Transact. of Scientific Problems of Welding and Special Electrometallurgy*. Kyiv: Naukova Dumka.
33. Ito, Y., Nakanishi, M., Katsumoto, N. (1976) Effect of CaF_2 in flux on toughness of weld metal. Relation between CaF_2 content in welding flux and in pure gas content in weld metal. *Sumitomo Search*, **16**, 78–86.
34. Pokhodnya, I.K., Shvachko, V.I., Ustinov, V.G. et al. (1971) Mass-spectrometry examination of gaseous fluorides evolved during arc welding. *Avtomatich. Svarka*, **6**, 10–11.
35. Matsushita, M., Liu, S. (2000) Hydrogen control in steel weld metal by means of fluoride additions in welding flux. *Welding J.*, **10**, 295–303.
36. Low-hydrogen speed challenge large-part fabricator. *Ibid.*, **6**, 57–60.
37. Lobanov, L.M., Mikhoduj, L.I., Pivtorak, V.A. et al. (1995) Influence of peculiarities of submerged-arc welding on stressed state of high-strength steel welded joints. *Avtomatich. Svarka*, **9**, 21–23.
38. Tozuka, N., Chiga, C., Yamaguchi, T. et al. (1995) Toughness degradation mechanism for reheated Mo–Ti–B bearing weld metal. *ISIJ Int.*, **10**, 1232–1238.
39. Dubovenko, I.P. (1998) Modelling of processes of formation of chemical heterogeneity in solidification of the weld. In: *Abstr. of pap. of 2nd All-Union Sci.-Techn. Conf. on Computer Technologies in Joining of Materials*, Tula, September, 1998.
40. Grabin, V.F., Golovko, V.V., Novikova, D.P. (1995) Peculiarities of weld metal structure in submerged pulsed arc welding. *Avtomatich. Svarka*, **8**, 3–10.
41. Pokhodnya, I.K., Golovko, V.V., Grabin, V.F. et al. (1997) Peculiarities of thermal cycle of submerged pulsed arc welding. *Ibid.*, **9**, 3–8.
42. Karkhin, B.A., Akatsnevich, V.A. (1998) Modelling of thermal processes in welding using the periodic power source. In: *Abstr. of pap. of 2nd All-Union Sci.-Techn. Conf. on Computer Technologies in Joining of Materials*, Tula, September, 1998.
43. Hrivnak, I. (1998) Physical metallurgy of pulsed current submerged arc welding of steels. *ISIJ Int.*, **10**, 1100–1106.
44. Pokhodnya, I.K., Grabin, V.F., Golovko, V.V. et al. (1997) Mechanism and kinetics of austenite decomposition in the HAZ of low-alloy steels in submerged pulsed arc welding. *Avtomatich. Svarka*, **4**, 3–13.
45. Dudko, D.A., Savitsky, A.M., Savitsky, M.M. et al. (1998) Peculiarities of thermal processes in welding with thermal cycling. *Ibid.*, **5**, 8–12.
46. Golovko, V.V. (1995) Submerged pulsed arc welding (Review). *Ibid.*, **12**, 14–18.
47. Vishnu, P. (1995) Modelling microstructural changes in pulsed weldments. *Welding in the World*, **4**, 214–222.
48. Malin, V. (2001) Root weld formation in modified refractory flux one-side welding. Part 1. Effect of welding variables. *Welding J.*, **9**, 217–226.
49. Sudnik, V.A., Erofeev, V.A., Ivanov, A.V. (1997) Development and application of computer technologies for weld formation prediction in arc welding. *Svarochn. Proizvodstvo*, **11**, 40–45.
50. Petrov, S.Yu., Timakova, E.A. (1998) Classification of welding slags in conformity with toughness variation depending on temperature. *Ibid.*, **8**, 21–23.
51. Kuzmenko, V.G., Galinich, V.I., Tokarev, V.S. (1997) Typical zones of the weld pool in submerged-arc welding. *Avtomatich. Svarka*, **5**, 24–27.
52. Kuzmenko, V.G., Goncharov, I.A. (1997) Peculiarities of slag crust in submerged-arc welding. *Ibid.*, **12**, 7–13.
53. Mednikov, B.A., Plyasunov, V.A., Zhuchaev, V.A. et al. (1997) Mastering of a new technology for melting of welding fluxes. *Stal*, **9**, 42–43.
54. Tsaryuk, A.K. (1998) Synthetic fluxes for mechanized welding and surfacing. *Svarshchik*, **1**, 15.
55. Paton, B.E., Voropaj, N.M., Slivinsky, A.M. et al. (1998) Set of environmentally clean welding consumables: fused flux–electrode wire with a filler. *Avtomatich. Svarka*, **5**, 43–48.
56. Pokhodnya, I.K., Golovko, V.V. (1999) Fluxes for welding of high-strength low-alloy steels developed by the E.O. Paton Electric Welding Institute. *Svarshchik*, **1**, 8–9.
57. Pokhodnya, I.K., Kushneryov, D.M., Ustinov, S.D. et al. (1987) Results of comparative tests of fused and ceramic fluxes used in welding of steel 12KhN2MDF. *Avtomatich. Svarka*, **11**, 61–64.
58. Maison, B. (1998) Consumables for next century. *Welding and Joining*, Dec.-June, 18–19.
59. Zubchenko, A.S., Potapov, N.N., Starchenko, E.G. et al. (1995) New welding consumables. *Tyazh. Mashinostroenie*, **10/11**, 14–17.
60. Potapov, N.N. (1997) State-of-the-art and prospects of development of flux manufacturing in Russia. *Svarochn. Proizvodstvo*, **9**, 34–36.

DIFFUSION BONDING OF TITANIUM STRUCTURES (REVIEW)

L.S. KIREEV[1], **V.V. SHURUPOV**[2], **V.V. PESHKOV**[2] and **A.A. BATISHCHEV**[2]
[1]E.O. Paton Electric Welding Institute, NASU, Kyiv, Ukraine
[2]Voronezh State Technical University, Voronezh, Russia

Analysis of modern concepts of the mechanism of formation of the welded joint, produced by diffusion bonding, was used demonstrate that this welding process is a promising technology to produce titanium structures with developed surfaces in terms of geometry, which permits making high-quality precision joints.

Keywords: *diffusion bonding, thin-walled laminated structures, titanium, mechanical properties, microstructure*

Diffusion bonding is a promising technology in modern mechanical engineering [1–3]. It is currently widely used to produce joints of dissimilar difficult-to-weld materials [4–7 etc.] However, the possibilities of diffusion bonding are not limited by it. As described in the work of local, as well as foreign researchers [8–18 etc.] it may be effectively used also to produce titanium structures and semi-finished products. The latter should be considered as a separate class. These are hollow thin-walled laminated structures, characterized by a developed surface, great length and small cross-section of the welded elements. Thin-walled laminated structures in most cases have considerable overall dimensions. They are a combination of load-carrying shells with a filler, which acts as a stiffener. Such structures may have one- or two-sided shells, may be two- or multi-layered, flat, or with a large radius of curvature. Used fillers can be honeycomb, square, tubular, finned, forming tee-joints with the shell, or box-type corrugated, forming overlap joints with shell (Figure 1). The main requirement, made of the technology of making these structures, is provision of a high strength of the joint of load-carrying shells with a filler without loss of stability of the latter.

Thin-walled laminated structures of titanium are effectively used in the engines of flying vehicles and gliders, in order to lower their weight [19].

In the opinion of foreign authors [20], in economic terms even 10 to 20 times higher initial cost of titanium products, compared to those of other materials, is justified in aircraft-making.

A great number of local and foreign publications are devoted to studying both the process proper of diffusion bonded joint formation, and the possibility of its actual application. However, despite the higher interest to this process actual application of diffusion bonding in titanium structure fabrication is still quite limited. This is due to a whole number of objective causes: availability of other more versatile and well-studied conventional processes and technologies (machining, fusion welding, resistance welding, brazing); relatively high labour consumption and complexity of the technological process of diffusion bonding; absence of specialized equipment for this welding process and quality control of the joints; absence of any actual experience of producing and performance of welded joints, made by this process. In this connection the designers quite often do not take into account the potential possibilities of this welding process and do not specify its application even, when it is advantageous.

The aim of this review consists in demonstration of the capabilities of diffusion bonding in fabrication of titanium structures and attracting the attention of technologists and designers to this process.

The problem of producing sound diffusion bonding of titanium alloys on the level of samples for mechanical testing can be regarded as solved [18, 21, 22], although complete clarity and scientifically-grounded common opinion have been reached by far not on all the issues (including those, related to welded joint formation). The need to use compressive pressure in welding, on the one hand, and existing limits on the values of residual deformation of the elements being welded, on the other, make the task of producing a sound welded joint not at all simple. In the case of precision thin-walled laminated structures it becomes a problem.

Depending on stresses, causing metal deformation in the contact zone and determining the conditions of joint formation, it is rational to make a distinction between high- (P = 20–100 MPa) and low-intensity ($P \leq 2$ MPa) force action.

In welding with highly intensive force action, the welding pressure in most cases is applied using a press, fitted with a vacuum chamber and heating device. Batch-produced units of UDS-2 type are also designed along this principle. The working space of the vacuum chamber allows welding only small parts. The same schematic can be used to develop units, which allow welding large-sized parts. In a number of cases «open» processes can be used. Before placing the parts to be welded into the press, they are assembled in air-tight containers (retorts), which are degassed and heated up to the welding temperature. Other equipment is also in place (gasostats, rolling mills, etc.), which allows performing the process of diffusion bonding.

In order to prevent the possible loss of stability of the elements being welded, transferring the pressure to the welding zone and creating the conditions for locally directed deformation of the material being

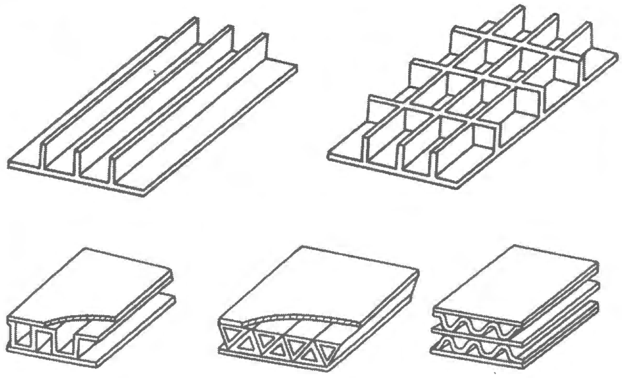

Figure 1. View of thin-walled laminated structures

welded in the butt zone, diffusion bonding is performed in special devices, using process steel inserts and blocks to fill the cavities (inter-stiffener spaces) (Figure 2) [23, 24], which are dismantled or removed by chemical etching after welding.

In welding with highly intensive force action the local deformation of metal in the butt zone, as a rule, reaches several tens of percent [6], and exceeds minimal deformation, required to implement the processes of joint formation. For this reason, welding with highly intensive force action provides a stable quality of the welded joint. The problem of making titanium structures by this technology is related not so much to the conditions of implementation of physical-chemical processes, influencing the formation of a diffusion bond, as to development of unique specialized equipment and fixtures. Application of diffusion bonding with highly intensive force action allows producing semi-finished products and finished items with tee and overlap joints (beams, panels of turbocompressor wheels, etc.).

According to the data, given in a number of works [14, 15, 25–27], some US companies, for instance Rockwell International, Whitney Aircraft, etc. apply diffusion bonding, using presses for making batch and pilot samples of specialized large-sized titanium structures for aircraft engineering. There are currently more than 60 types of such structures: elements of the system of airing the windshield of strategic bomber B-1B; middle part of the fuselage, including the wing middle-section of 1016×4190×(254–710) mm size; single-module structure of the rear part of the fuselage; stabilizer support frame; landing gear beams for Boeing-747; helicopter rotor hubs; engine cryogenic impeller; hollow hubs of a fan, etc.

Works [10, 12, 13, 17, 18 etc.] report that diffusion bonding may be applied for fabrication of three-layer structures with honeycomb filler. When making flat panels (or those with a large curvature radius), the compressive force can be provided using atmospheric pressure, applied to the external surface of process fixtures at lower gas pressure in the joint zone (Figure 3).

Availability of auxiliary elements, for instance, process gaskets etc., located on the external part of the elements being welded, prevents loss of stability of the shell in the form of sagging of unsupported sections, and values of working pressure P are limited by limit stresses of the loss of stability of the filler [28, 29]. In this case it is possible to produce a sound joint of structural elements (Figure 4).

In fabrication of structures of a complex curvilinear profile a technological sequence is used (Figure 5), where the pressure of a neutral gas is applied directly to the external elements of the structure proper, for instance, load-carrying shells. During welding the shells deform in unsupported sections and loose stability. In this case pressure P is limited by stresses of the loss of stability in unsupported sections of the shell. In should be noted that since welding is

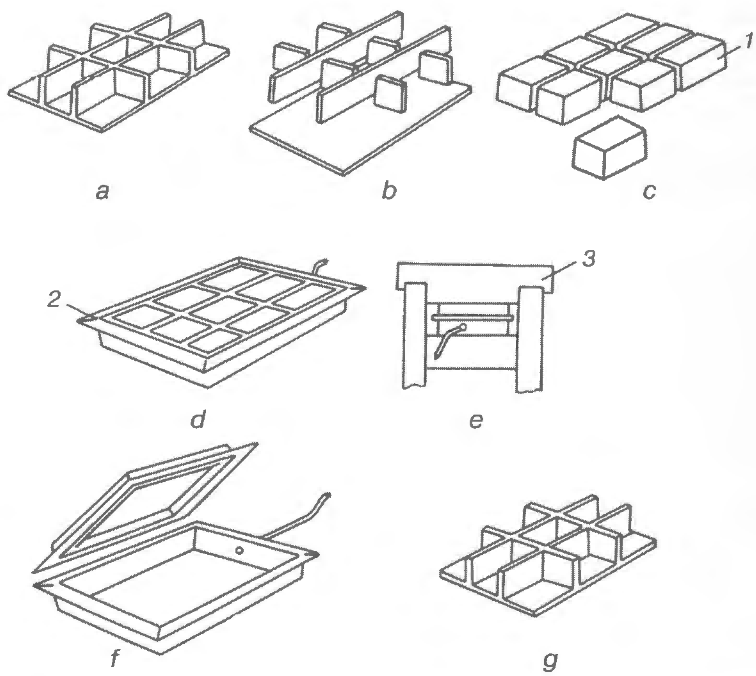

Figure 2. Process sequence of diffusion bonding with highly intensive force action: a — required structure; b — blanks for welding; c — technological elements-inserts; d — assembly; e — welding process; f — dismantling; g — finished structure; 1 — technological inserts; 2 — process container; 3 — press

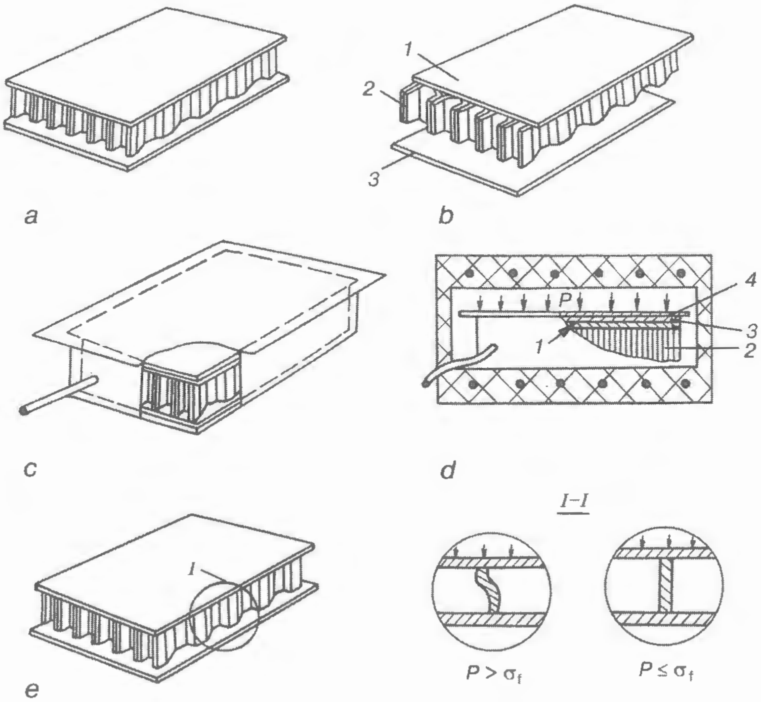

Figure 3. Process sequence of diffusion bonding with a low-intensity force action: *a* — required structure; *b* — blanks for welding; *c* — assembly; *d* — welding process; *e* — finished structure; *1* — load-carrying shell; *2* — honeycomb filler; *3* — process sheets; *4* — membrane (P — pressure; σ_f — loss of stability of the filler)

performed at a low specific compressive pressure, when solving the problem of fabrication of precision thin-walled structures, one of the prominent positions is taken up by the problems of a systematic study and analysis of physical-chemical processes, proceeding in welding and affecting the interaction of the titanium sample surfaces being welded, for optimization of the technological process.

Analysis of the data derived on the mechanism of welded joint formation, obtained by other authors [2, 4, 8, 10, 18, 30–38 etc.] gives an idea of this welding process as a complex physical-chemical process, in which formation of such a bond depends on the thermally activated diffusion processes, such as creep, metal interaction with gases, and recrystallization.

As-delivered titanium alloys feature diverse microstructural conditions. Mechanical properties of α'- and $(\alpha' + \alpha)$-alloys depend on the produced microstructure of the joint [34–40]. While the difference in the values of ductility characteristics, due to the microstructure, may be in the range of several percent or several tens of percent, the difference in the rate of high-temperature creep, underlying development of physical contact, is equal to several orders of magnitude [41, 42].

The lowest resistance to high-temperature deformation is characteristic of alloys with an equiaxed fine-grained microstructure, and the highest is found in those with coarse-grained plate-like microstructure. Thus, microstructural state of the elements being welded may be regarded as a factor, which allows controlling the process of making the welded joint [43, 44], as well as its quality.

In annealing of titanium alloys in the temperature range of polymorphous transformations, a local deformation of the welded surfaces of the titanium sam-

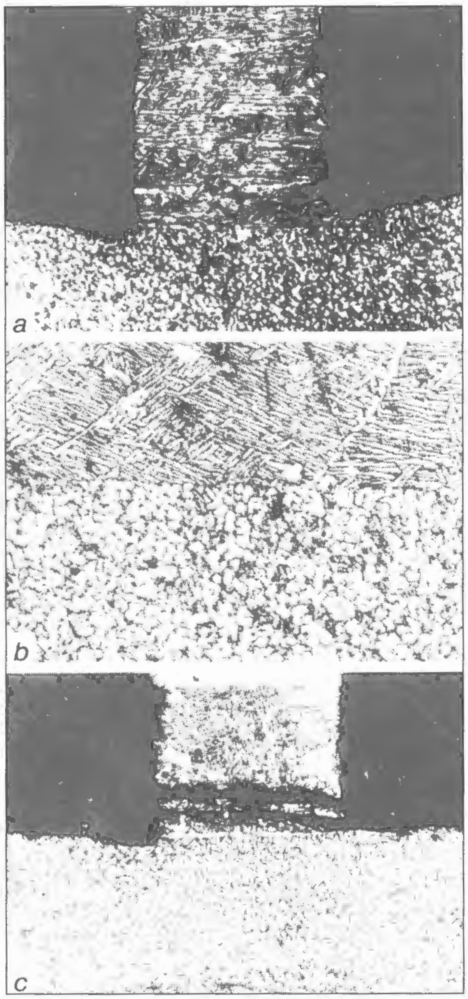

Figure 4. Microstructure of the zone of the joint of the shell with honeycomb filler (*a* — ×200; *b* — ×500) and nature of fracture of the joint in testing for fracture in the filler (*c* — ×200)

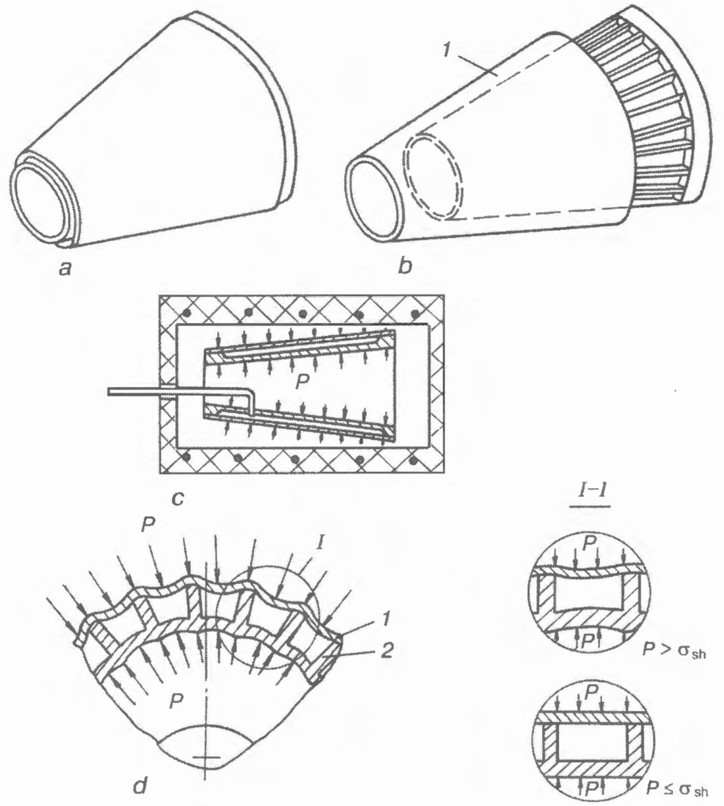

Figure 5. Process sequence of diffusion bonding with low-intensity force action of complex-shaped structures: *a* — required structure; *b* — blanks for welding; *c* — welding process; *d* — nature of deformation of structural elements in welding; *1*, *2* — outer and inner shells, respectively (σ_{sh} — residual stress of shell deformation in unsupported sections of the structure)

ple is found, which is accompanied by formation of a substructural relief in the form of parallel slip lines. The latter are the points of escape of dislocations, which form under the impact of inherent (internal) stresses and under the conditions of welding act as active zones with a high reactivity [18, 45 etc.]. Internal stresses, due to restructuring of the hexagonal α'-phase into a cubic α'-phase during polymorphous transformation, should be regarded as a source of activation of the welded surfaces of a titanium sample, which does not lead to macrodeformation of the welded elements.

Another important feature of titanium is its ability to dissolve most of the oxygen, and, as a result, quickly clean the surface from oxides, thus lowering oxygen concentration in the surface layers. Titanium, however, is a thermodynamically unstable element, and oxidizes readily even in deep vacuum [18, 46, 47], i.e. two competing processes proceed simultaneously in welding, namely those of growth and dissolution of the oxides. Therefore, the physical-chemical condition of the contacting surfaces of the titanium sample, and, therefore, their reaction ability, will be determined by the kinetics of growth and dissolution of gas-saturated oxides.

Analysis of the processes, proceeding in welding in the contact zone, demonstrated that the composition of the gas phase between the surfaces being welded, significantly differs from that in the welding chamber. Partial pressure of oxygen drops in the direction from the peripheral zone of welding to the central zone. Therefore, oxidation processes, which are accompanied by increase of the thickness of oxidized metal, may proceed in the zone of the elements being welded, and conditions for surface cleaning from oxides are created in the central zone [48].

Deformation ε of contact surfaces in diffusion bonding is a mandatory condition of formation of a sound joint, and its required magnitude depends on a multitude of factors.

In the presence of oxidized metal on the surfaces being welded, which is revealed as an embrittled layer [49], ε value, required for realization of the processes of development of physical contact and activation of the surfaces being welded, rises abruptly and may reach 15–20 %.

A significant influence on ε values is produced by the sequence of implementation of the stage of the process of joint formation. If the stage of development of physical contact goes ahead of activation of the surfaces being welded, then $\varepsilon > 10$ % [50], and if the physical contact develops between the already activated surfaces, then $\varepsilon < 1$–3 %.

Elements of precision thin-walled structures (filler, load-carrying shells) are manufactured, as a rule, of sheet material, having a fine-grained microstructure in as-delivered condition, which is characterized by a low resistance to high-temperature deformation.

In welding panels with honeycomb filler of OT4-1 alloy the admissible limit compressivle pressure drops from 4.0 to 0.1 MPa at temperature increase from 800 to 925 °C. Strength of the joint, produced by diffusion bonding at such a pressure, is not more than half of that of the base metal. This is due to the fact that the process, limiting the formation of a joint, in this case is activation of the surfaces being welded, which is realized only on part of the surface, because of insufficient deformation of the metal in the contact zone under the impact of external stresses.

Process of joint formation in diffusion bonding can be intensified either by additional annealing at temperature above that of the end of polymorphous transformation (which leads to a certain deterioration of ductility characteristics of the material proper), or by soaking before pressure application at the temperature of polymorphous transformation of titanium sample surfaces, welded with a small gap. This, on the one hand, promotes a more intensive cleaning of the surfaces from oxides formed during heating, which leads to smaller deformation required for activation, and on the other hand, provides activation of the surfaces under the impact of internal stresses. It should be noted that because of low *P* values such a technological procedure does not ensure stable mechanical characteristics of the joint. When going over from the laboratory samples to production structures a number of difficulties are encountered, which are related to separation of the surfaces being welded.

Proceeding from even such a short review, it can be seen that diffusion bonding is a complex physical-chemical process, despite its great potential capabilities. Its use for fabrication of titanium structures requires additional research in each concrete case.

1. Kazakov, N.F. *Method of joining ceramic and metal parts, for example, cutting plates to holders*. USSR author's cert. 112460. Int. Cl. B 23 K 1/00. Publ. 02.07.58.
2. Kazakov, N.F. (1976) *Diffusion bonding of materials*. Moscow: Mashinostroenie.
3. Belov, A.F. (1983) New metallurgical processes based on high-speed solidification and diffusion of metals. *Izv. AN SSSR, Metally*, **6**, 11–20.
4. Charukhina, K.E., Golovanenko, S.A., Masterov, V.A. et al. (1970) *Bimetallic joints*. Moscow: Metallurgiya.
5. Bordakov, P.A., Grishin, I.S., Demichev, S.F. (1984) Experience of application of diffusion bonding in repair of gas turbine engine. In: *Improvement of repair technologies for aircraft systems in civil aviation plants*. Moscow: Aviaremont.
6. Bordakov, P.A., Samorodov, D.V., Grishin, I.S. (1979) Selection of welding conditions of EI 961 steel shaft with gas turbine engine rotor of VZhL 12U alloy. *Avtomatich. Svarka*, **7**, 54–56.
7. (1999) Vacuum diffusion bonding of bimetallic attachments and boring tool billets. In: *Transact. of VNTK*. Samara: SGAU.
8. Karakozov, E.S., Vigdorchik, S.A., Petrosyan, V.A et al. (1975) Validation of a variant of honeycomb sandwich structure fabrication by the pressure welding. *Svarochn. Proizvodstvo*, **12**, 21–25.
9. Gelman, A.A., Kolodkin, N.I., Pavlov, V.M. et al. (1978) Diffusion bonding of T-joints of VT6s titanium alloy. *Ibid*., 5, 15-17.
10. Peshkov, V.V., Kudashov, O.G., Grigorievsky, V.I. et al. (1980) Peculiarities of titanium laminated structures production by diffusion bonding. *Ibid*., **5**, 17–19.
11. Matyushkin, B.A., Kotelnikov, A.A., Majdanov, A.P. (1980) Diffusion bonding of finned panels of titanium alloys. *Ibid*., **7**, 43–45.
12. Peshkov, V.V., Kudashov, A.O. (1982) Influence of initial microstructure on joint formation in diffusion welding of OT4-1 titanium alloy honeycomb sandwich structures. *Ibid*., **6**, 27–31.
13. Peshkov, V.V., Gusev, S.I. (1984) On selection of process parameters of diffusion bonding of titanium alloy honeycomb sandwich structures. *Ibid*., **10**, 12–14.
14. Owczarski, W.A., Paulonis, D.F. (1981) Application of diffusion welding in the USA. *Welding J*., **2**, 20–33.
15. Vaccari, J.A. (1983) Form-bonding titanium in one-shot. *American Machinist*, **10**, 91–94.
16. Sheldon, E.F. (1979) Diffusion bonding: aerospace application. In: *Diffus. Bonding Prod. Process*. Abington.
17. Salikov, V.A., Shushpanov, M.N., Kolomensky, A.B. et al. (2001) *Welding in aircraft construction*. Voronezh: VGTU.
18. Bondar, A.V., Peshkov, V.V., Kireev, L.S. et al. (1998) *Diffusion bonding of titanium and its alloys*. Voronezh: VGTU.
19. Hertel, G. (1965) *Thin-walled structures*. Moscow: Mashinostroenie.
20. Du Mond, T.C. (1973) Titanium arrives: Now in short supply. *Iron Age*, **212**, 49–50.
21. Karakozov, E.S., Orlova, L.M., Peshkov, V.V. et al. (1977) *Diffusion bonding of titanium*. Moscow: Metallurgiya.
22. Gelman, A.A., Kolodkin, N.I., Kotelnikov, A.A. et al. (1983) Optimal parameters of diffusion bonding of titanium alloys with different phase composition. *Avtomatich. Svarka*, **4**, 53–57.
23. Grin, E.D. *Diffusion bonding method*. Pat. 3497945 USA. Int. Cl. B 23 K 31/02. Publ. 03.03.70.
24. (1967) Diffusion bonding of formable structural panels by composite rolling. *Industrial Heating*, **8**, 1432–1434.
25. (1975) New fabrication method stimulate titanium use. *Iron Age*, **26**, 28–31.
26. Weisert, E.D., Staiher, G.W. (1977) Fabrication of titanium parts with SPF/DB process. *Metal Progress*, **3**, 33–37.
27. (1983) Testing in USA of structures of future airplane (Review). *Zarub. Voen. Obozrenie*, **2**, 90–91.
28. Peshkov, V.V., Rodionov, V.N., Podoprikhin, M.N. et al. (1981) On methods to decrease distortion of thin-walled titanium structures in diffusion bonding. *Avtomatich. Svarka*, **9**, 24–27.
29. Peshkov, V.V., Rodionov, V.N. (1984) Structure as a factor of control of diffusion bonding process of titanium thin-walled laminated structures. *Svarochn. Proizvodstvo*, **4**, 9–11.
30. Krasulin, Yu.L. (1971) *Interaction of metal with a semiconductor in the solid phase*. Moscow: Nauka.
31. Karakozov, E.S. (1976) *Solid phase bonding of metals*. Moscow: Metallurgiya.
32. Gelman, A.S. (1970) *Principles of pressure welding*. Moscow: Mashinostroenie.
33. Karakozov, E.S. (1986) *Pressure welding of metals*. Moscow: Mashinostroenie.
34. Kolachev, B.A., Livanov, V.A., Bukhanova, A.A. (1974) *Mechanical properties of titanium and its alloys*. Moscow: Metallurgiya.
35. Glazunov, S.G., Moiseev, V.N. (1974) *Structural titanium alloys*. Moscow: Metallurgiya.
36. Solonina, O.P., Glazunov, S.G. (1978) *Heat-resistant titanium alloys*. Moscow: Metallurgiya.
37. Kaganovich, I.N., Zvereva, E.F., Beloborodova, A.I. (1971) Influence of heating on structure and mechanical properties of titanium alloys. *Tsvet. Metally*, **11**, 61–64.
38. Shakhanova, G.V., Brun, M.Ya. (1982) Structure of titanium alloys and methods of its control. *Metallovedenie i Term. Obrab. Metallov*, **7**, 19–22.
39. Kolachev, B.A., Malkov, L.V. (1983) *Physical principles of fracture of titanium*. Moscow: Metallurgiya.
40. Moroz, L.S., Khesin, Yu.D., Belova, O.S. (1963) Structure and mechanical properties of low-alloyed titanium alloys. *Metallovedenie i Term. Obrab. Metallov*, **2**, 17–23.
41. Peshkov, V.V., Rodionov, V.N., Vorontsov, E.S. (1977) Creep of OT4 titanium alloy. *Izv. AN SSSR, Metally*, **2**, 188–192.
42. Peshkov, V.V., Rodionov, V.N., Podoprikhin, M.N. (1980) Creep of OT4 titanium alloy with coarse-grained structure. *Izv. Vuzov, Tsvet. Metallurgiya*, **5**, 95–97.
43. Peshkov, V.V., Rodionov, V.N., Grigorievsky, V.I. (1977) Joint quality control in diffusion welding of titanium alloys due to control of the initial structure. *Svarochn. Proizvodstvo*, **10**, 18–20.
44. Peshkov, V.V., Rodionov, V.N. (1984) Methods to increase the stability level of mechanical characteristics of OT4 titanium alloy welded joints, produced by diffusion bonding. *Avtomatich. Svarka*, **11**, 39–43.
45. Musin, R.A., Antsiferov, V.N., Kvasnitsky, V.F. (1979) *Diffusion bonding of heat-resistant alloys*. Moscow: Metallurgiya.
46. Baj, A.S., Lajner, D.I., Slyusaryova, E.N. et al. (1970) *Oxidation of titanium and its alloys*. Moscow: Metallurgiya.
47. Peshkov, V.V., Vorontsov, E.S. (1973) Investigation of the process of oxide film dissolution in titanium. *Izv. AN SSSR, Metally*, **4**, 99–102.
48. Peshkov, V.V., Milyutin, V.N., Podoprikhin, M.N. (1984) On interaction between titanium and vacuum space residual gases in the conditions of diffusion bonding. *Svarochn. Proizvodstvo*, **2**, 14–16.
49. Peshkov, V.V., Milyutin, V.N., Rodionov, V.N. (1985) Influence of diffusion bonding thermal cycle on the condition of the surface and surface layers of OT4 titanium alloy. *Avtomatich. Svarka*, **1**, 15–18.
50. Peshkov, V.V., Milyutin, V.N., Rodionov, V.N. et al. (1984) Kinetics of joint formation in diffusion bonding of VT5 titanium alloy. *Ibid*., **7**, 27–31.

WELDING OF TITANIUM INGOTS USING DISPERSED MELT

G.V. ZHUK, N.P. TRIGUB and **V.N. ZAMKOV**
E.O. Paton Electric Welding Institute, NASU, Kyiv, Ukraine

It was established that it is possible to weld titanium alloys using a flow of dispersed melt. In this case the welded joint possesses mechanical properties at the level of appropriate properties of joints made by fusion welding. It is shown that this method of joining can be applied for enlargement of titanium ingots. After deformation of welded ingots the structure and properties of weld metal do not differ from similar characteristics of the rolled ingot.

Keywords: *dispersed melt, welded joint, titanium alloys, enlargement of ingots, rapid crystallization, electron beam installation, prospects*

Increase in mass and sizes of ingots is one of the actual problems of metallurgy of titanium [1]. To solve it the high-capacity melting furnaces are created, specifics of formation of ingots is investigated and technology of melting ingots of large sizes is developed. All this requires significant expenses and does not always provide the necessary quality of metal of ingots, produced, in particular, from medium- and high-alloy titanium alloys. However, another way of solution of this problem is possible. Using welding it is possible to produce large-sized titanium ingots of comparatively small-sized ingots. However, in this case one more specific requirement should be specified to the quality of welded joints, except absence of cracks, pores, lack of fusion and other defects in welds. As the ingot is an initial link in the technological chain of manufacture of semi-products, so it is necessary that as-deformed metal in the zone of the former weld had the same crystalline structure, chemical composition and properties as the metal of the ingot itself. After analyzing the known methods of welding titanium, it is possible to state that none of them can provide fulfillment of these requirements.

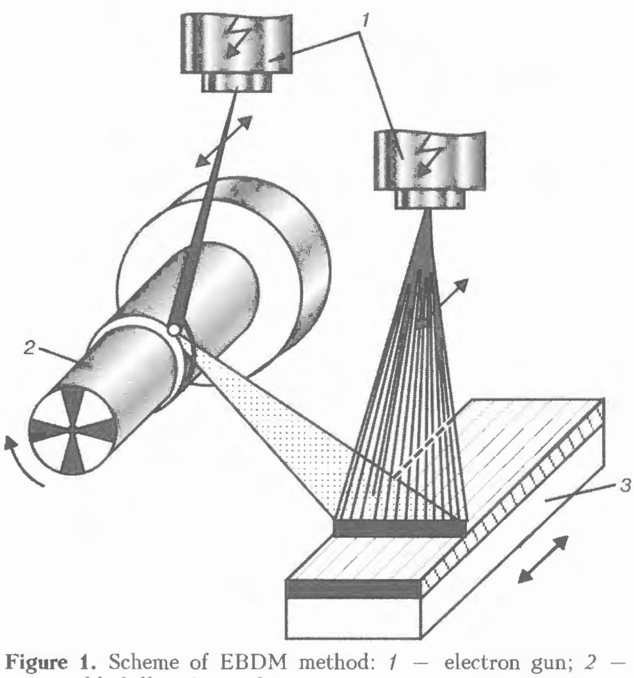

Figure 1. Scheme of EBDM method: *1* — electron gun; *2* — consumable billet; *3* — substrate

The present work is devoted to the evaluation of feasibility of use of a flow of dispersed melt for welding and to the development of fundamental technology of enlargement of titanium ingots on the basis of this process.

At the E.O. Paton Electric Welding Institute the method of producing ingots (including those of titanium) and coatings using electron beam dispersion of melt (EBDM) has been developed [2, 3]. It combines advantages of refining electron beam melting and high-speed solidification of molten metal (rate of cooling is $1\cdot10^4$ K/s). The principle of this process is as follows. A layer of molten metal is formed under the action of electron beam at the surface of a cylindrical billet. At definite technological parameters, the flow of dispersed melt as a result of centrifugal spraying from a rotating billet is directed to a substrate (Figure 1). Its fine drops, colliding the substrate, are spread along its surface, solidified and form a thin layer of metal. Using this layer-by-layer spraying it is possible to form ingot of preset sizes or to deposit coating of the required thickness on the part. First of all, it is necessary to establish a principal feasibility of joining parts by filling the gap between them (or groove of appropriate shape) with a dispersed melt for welding ingots.

Plates of 300×100×10 mm size, made from commercial titanium of VT1-0 grade and PT3V alloy, were used for investigations. From them the butt joints with V-shaped edge preparation were assembled (Figure 2). Cylindrical billets of 200 mm diameter, made from the same alloys, were used to produce the flows of dispersed melt. To provide the interaction of drops of dispersed melt with the surface of plates and formation of a metal bond coat between them before welding beginning, the metal at groove site and adjacent regions of plates was preheated by a defocused electron beam. Parameters of electron beam, directed to the rotating billet to create molten metal pool at its surface, had the following values: beam current

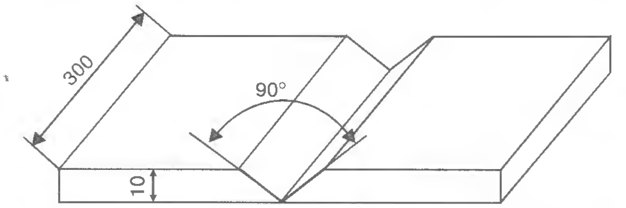

Figure 2. Scheme of groove preparation for welding with dispersed melt

I = 2.6 A; accelerating voltage U_{acc} = 20 kV; j = = $1.04 \cdot 10^8$ W/m^2. At selected rate of billet rotation a flow of dispersed melt in the form of drops of about 0.8 mm diameter was created. The rate of their flight was ≈ 15 m/s. Here, the efficiency of the process of melt dispersion reached 16 kg/h, and the time of groove filling (time of welding) was 20 s.

In examination of macrosections of joints produced by filling grooves with a dispersed melt, no visible defects in weld metal, and also at weld–parent metal interface were revealed. However, the macrostructure of welded joint produced by this procedure had a number of peculiar features (Figure 3): the absence of a visible zone of fusion and presence of an abrupt interface between the weld metal and parent metal, clearly repeating the shape of groove (see Figure 2). The weld metal grain is finer than that in parent metal. Crystalline structure of weld metal is not associated with advantageous heat removal to the parent metal, that takes place in welds made by fusion welding. In the HAZ, adjacent to weld, the presence of overheating zone, typical of fusion welding, was not revealed on macrosections. All the visible part of HAZ metal structure consisted of relatively coarse recrystallized grains.

The examination of microstructure of welded joint confirmed that the interface between HAZ and parent metal is the transition from structure of the recrystallized metal to the structure of the deformed metal (Figure 4, *a, b*). At the same time in the region located

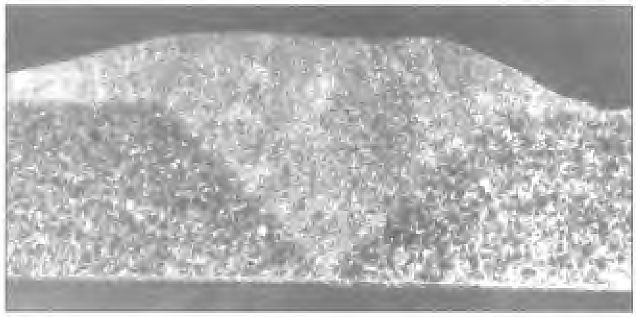

Figure 3. Macrostructure of welded joint produced by EBDM method

in HAZ near weld a microstructure of metal, typical of overheating zone in commercial titanium, is formed (Figure 4, *c, d*). Width of this zone does not exceed two-three diameters of grain and therefore, probably, it is not possible to reveal it on macrosection at small magnifications. It should be also noted that the fusion zone, typical of welded joints made by fusion welding, is absent (Figure 4, *d*). Joining of parent metal with weld metal in this case has a form of clear lines separating two regions of welded joint with microstructures quite different one from another. This proves that in filling groove by a flow of dispersed melt the parent metal is not prefused. Microstructure of weld metal, presented in Figure 4, *e*, is typical of welds made on commercial titanium by fusion welding.

It is necessary to note the high strength of welded joints. At static tensile test the samples, cut out across the weld, were fractured, as a rule, along the fusion line of weld and parent metal. Ultimate strength of joints was 470 and 723 MPa for alloys VT1-0 and PT3B, respectively, from results of testing five samples of each alloy.

To clarify the mechanism of joint formation, further special investigations will be required. It can be only stated that the preheating of edges is an obligatory element of the technological process, as in weld-

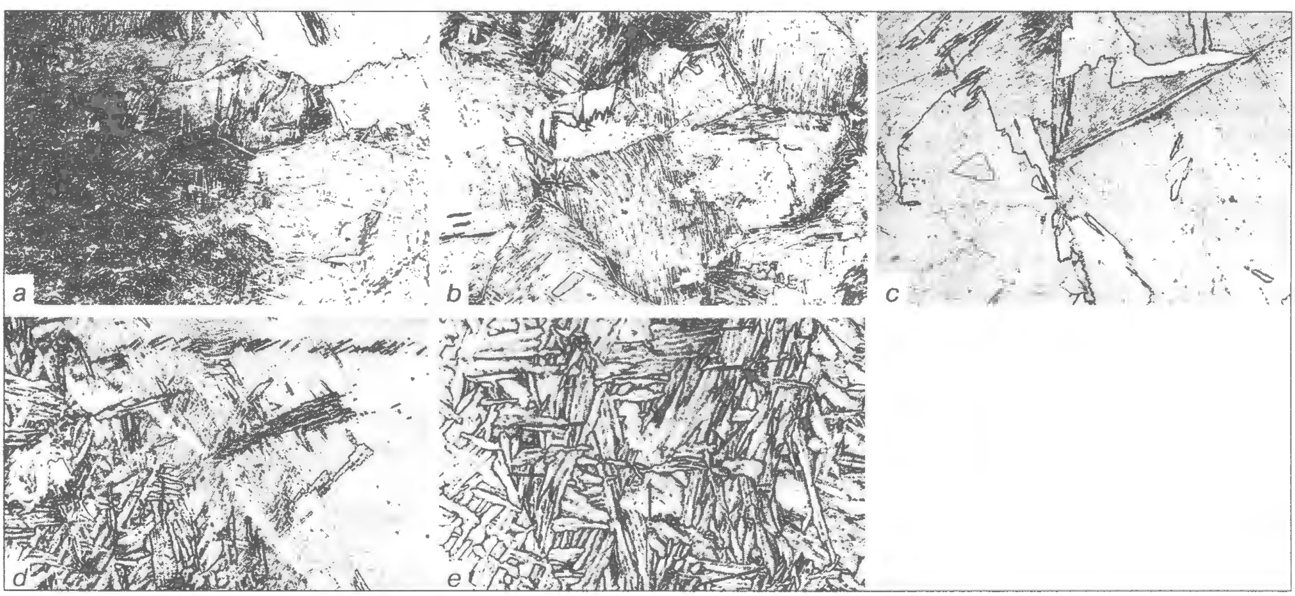

Figure 4. Typical regions of microstructure of welded joint produced by EBDM: *a* — parent metal–HAZ interface; *b* — HAZ; *c* HAZ area near weld; *d* — weld boundary; *e* — weld metal (×100)

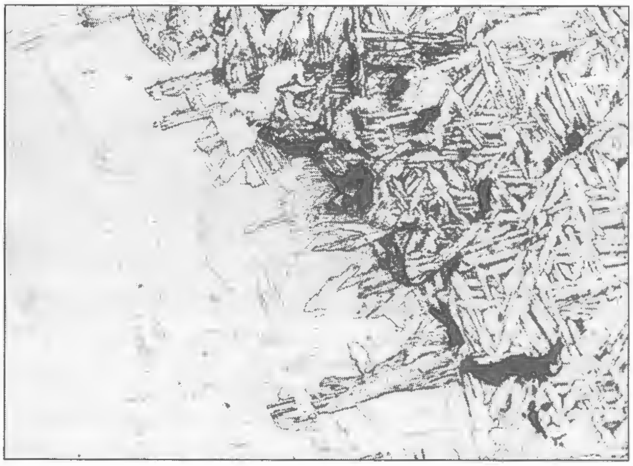

Figure 5. Pores at weld–parent metal interface in welding without preheating of edges (×100)

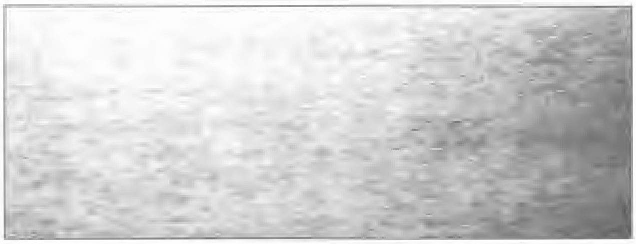

Figure 6. Macrostructure of as-rolled plates

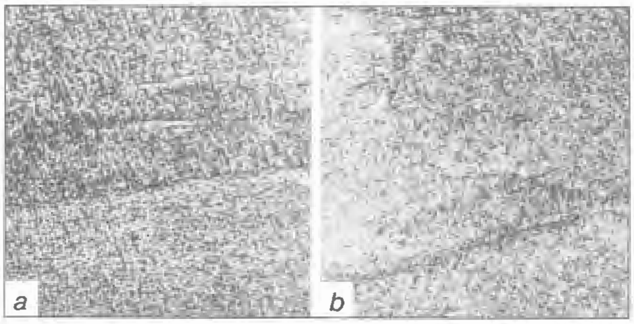

Figure 7. Microstructure of as-rolled ingot-slab, welded with dispersed metal: *a* — parent metal; *b* — welded joint zone (×100)

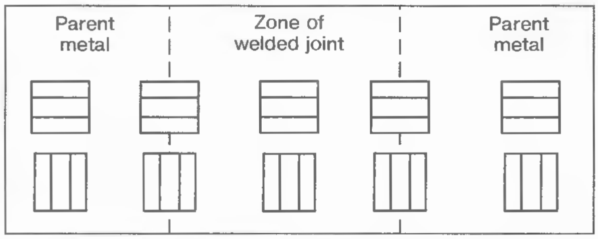

Figure 8. Scheme of samples cut out for mechanical tests

ing without preheating of the parent metal the defects are appeared in welded joint (Figure 5).

To evaluate the suitability of welding with dispersed melt for enlargement ingots by this method, samples (100×100×70 mm) were cut out from ingots-slabs of alloy VT1-0. Welded joints were subjected to rolling first at temperature 950–920 °C (reduction degree 40 %), and then at 850–800 °C (reduction degree 75 %). Final thickness of plates after rolling (Figure 6) was 10 mm.

Comparative examination of microstructure of metal shows its homogeneity in the plate length. After rolling of welded ingot the microstructure of the deformed metal of weld and HAZ had no differences in microstructure of metal of slab-ingot itself (Figure 7). In all the regions of plate the microstructure of metal represented primary β-grains elongated along the rolling direction, inside of which the decay products are seen: fine acicular α′-phase. Mechanical properties of metal were characterized by uniformity in the plate length. Results of static tensile tests of samples cut out from different plate regions (Figure 8) are presented in the Table. They indicate that welding with the directed flow of dispersed melt is challenging for enlargement of ingots. The further investigations are necessary to use this method for enlargement of ingots of medium- and high-alloy titanium alloys.

Mechanical properties of as-rolled ingot-slab welded by dispersed melt

Direction of sample cut out	*Ultimate strength σ_t, MPa*	*Yield strength σ_y, MPa*	*Elongation δ, %*	*Reduction in area ψ, %*
Along rolling	$\frac{479–486}{483}$	$\frac{435–441}{438}$	$\frac{22–28}{24}$	$\frac{53–68}{59}$
Across rolling	$\frac{495–512}{505}$	$\frac{459–483}{472}$	$\frac{19–23}{21}$	$\frac{48–57}{52}$

Note. In numerator the maximum and minimum values are given, while in dominator the mean values from results of testing 15 samples are given.

1. Eylon, D., Seagle, S.R. (2000) Advances in titanium technology — an overview. *JILM*, **50**, 359–370.
2. Tikhonovsky, A.L., Pap, P.A., Kozlitin, D.A. et al. (1993) Electron beam casting method from dispersed melt. *Problemy Spets. Elektrometallurgii*, **3**, 35–39.
3. Zhuk, G.V., Trigub, N.P. (2002) New method for dispersing the melt in electron beam units and equipment for its realisation. *Advances in Electrometallurgy*, **4**, 15–16.

IMPROVEMENT OF THE GUIDE CHANNEL AND ROLLER FEED ASSEMBLY OF SEMI-AUTOMATIC MACHINES FOR WELDING ALUMINIUM AND ITS ALLOYS*

V.A. LEBEDEV
E.O. Paton Electric Welding Institute, NASU, Kyiv, Ukraine

A new approach is proposed to design of elements of the system of electrode wire feed, which is practically completely based on selection of materials, which perform in the most effective manner in the specific assemblies of this system, or on a combination of these materials with the design solutions for the mechanism of transfer of motion from the rollers to the wire. The above technical solutions and the above approach on the whole can be widely applied both in the currently used equipment for mechanized welding of aluminium and in the semi-automatic machines being developed.

Keywords: *arc welding, aluminium alloys, semi-automatic machine, wire feed, pulsed feed, rollers, guide channel, electric drive*

Improvement of the technology of welding aluminium and its alloys involves difficulties, which are due to the physico-chemical properties of the materials being welded, as well as the degree of functional perfection, reliability and fatigue life of processing equipment.

Several types of semi-automatic machines for welding aluminium and its alloys are batch-produced in Ukraine. These are PDI-304 with VDGI-302 power source and PDGO-509 with VDU-506S and VDU-601S power sources. The only manufacturer of these semi-automatic machines in Ukraine is SELMA Company (Simferopol). PDI-304 semi-automatic machine is designed for pulsed-arc welding with aluminium electrode wires of 1.2–2.0 mm diameter, and PDGO-509 for welding with steel solid wires of 0.6–1.6 mm diameter, as well as aluminium and flux-cored wires of 1.0–3.2 mm diameter. The above semi-automatic machines are usually fitted with hose holders of Binzel Company (Germany) with steel or brass replaceable guide channels.

In order to obtain sound welds in welding aluminium and its alloys semi-automatic machines with synergetic principle of controlling the electrode metal transfer of Fronius (Austria) and KEMPPI (Finland) are used in Ukraine. However, they have a limited application, because of their high cost and problems with repair (which, as rule, is not possible outside special service centers).

Ukraine does not yet have its own production of hose holders for welding aluminium alloys. And this is so, despite the fact that similar products, namely hose holders for feeding steel solid and flux-cored wires are manufactured by Ilnitsky Plant of Mechanical Welding Equipment.

Analysis of the problems, which can be solved in the most effective manner only with application of semi-automatic machines for welding aluminium and its alloys, as well as a number of effective engineering and technological solutions for different systems of the semi-automatic machine at optimal cost are given in [1–4].

The aim of this paper was determination of the most perfect designs of the semi-automatic machines for welding aluminium and its alloys (in particular, guide channels and electrode wire feed system). All the design solutions, used in the semi-automatic machines, were considered only in terms of implementation of the arc process, using batch-produced smoothly adjusted or step-switched rectifiers (as the simplest and least expensive) for two types of electrode wire feed systems: undisturbed (smooth) motion and disturbed pulsed motion (changed by a certain law).

In the first case all the disturbances in electrode wire motion are introduced via the feed line and affect the technological process of welding and to a certain extent also the indices of reliability of the semi-automatic machine as whole. In the second case the influence of disturbances in the feed line is much less pronounced [5]. It is obvious, that disturbances of a lower level (if these are not emergency situations, related to jamming of electrode wire) are absorbed or compensated by specially introduced mechanical disturbances of a higher level. Influence of external disturbances with two kinds of electrode wire feed on the technological process of arc welding of aluminium and its alloys may be evaluated by analyzing oscillograms of arc current, shown in Figure 1. They were obtained at maximum identical conditions (one dismantable hose holder, same modes, etc.). Evaluation of process stability was performed by measurement of arc current I_a during time periods t_i. In this case in order to facilitate calculations for undisturbed wire feed, time t_i was selected to be equal to the time of

---
* Engineers I.S. Kuzmin and V.G. Novgorodsky took part in performance of the work.

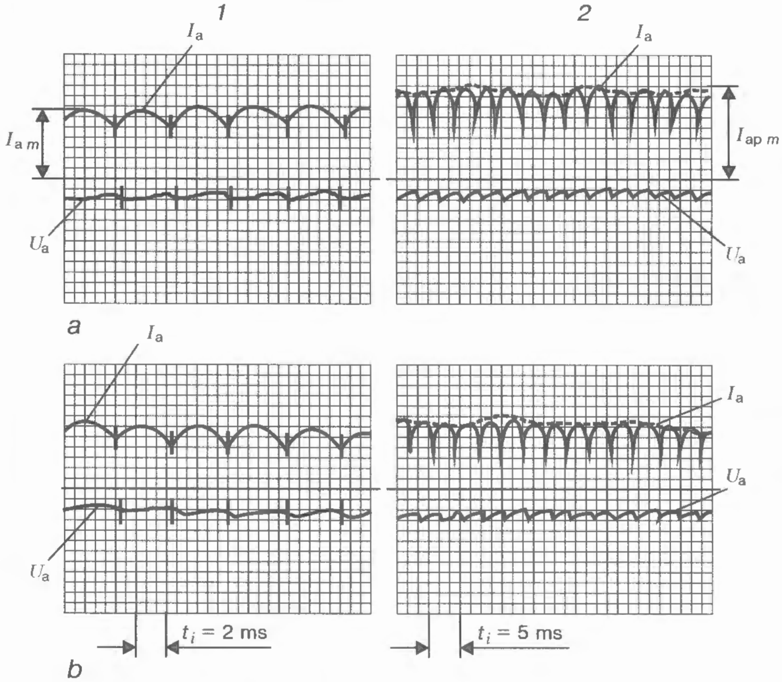

Figure 1. Oscillograms of current (I_a = 200 A) and voltage (U_a = 22 V) in welding aluminium: *1* — undisturbed; *2* — pulsed feed of electrode wire without (*a*) and with (*b*) rings in the flexible guide channel

conductivity of each of the valves of the welding current rectifier, and the current equal to its amplitude value $I_{a\,m}$. For pulsed feed (frequency of 38 Hz, 2.4 mm step), the time was set equal to the period of repetition of the feed pulse, and the current was equal to its amplitude value $I_{ap\,m}$ in the feed pulse. Then the oscillograms were used to perform calculations of the coefficient of current variation ν of the arc process current for the number of realizations $N = 500$ by the following formula:

$$\nu = \sigma/m, \tag{1}$$

where $\sigma = \sqrt{D}$ is the mean root square deviation of current.

Values of variance D and mathematical expectation m can be calculated from the following expressions:

$$m = \sum_{i=0}^{N_{p-1}} t_{c(i)}/N_p, \tag{2}$$

$$D = \sum_{i=0}^{N_{p-1}} (t_{c(i)} - m)/N_p, \tag{3}$$

where N_p is the number of realization samples; t_c is the cycle time.

Table 1

Guide channel bends	Coefficients of variation ν by welding current for motions	
	undisturbed	*disturbed*
None	0.196	0.102
One coil	0.283	0.105

Coefficients of variation for the above processes are given in Table 1. Results were obtained with application of welding process analyzer. Investigations showed that the process of welding with pulsed feed of electrode wire is much more stable than the process of undisturbed motion. Results of technological impact of pulsed wire feed on the process of welding of aluminium and its alloys were described earlier in [6].

In this paper the design of a hose holder was studied (in particular, its flexible guide in the form of a metal spiral or plastic tube through which the electrode wire passes). In [3, 4] some approaches were proposed to solving the problem of lowering the feed resistance of electrode wire of aluminium alloys. In this case a fluoroplastic tube or tube of reinforced polyethylene is recommended to be used as the guide channel. The same solutions are also found in a number of hose holders, which are batch-produced abroad. Experience of operation of holders with plastic guide channels of a relatively small length (1.7–1.8 m) showed that they are justified for feeding wires of different rigidity with a diameter not greater than 2.0 mm. Such an evaluation was conducted by two criteria, namely stability of wire movement (movement without jerks or jamming) and reliability (mean-time-between-failures). In this case a relationship, determined in [7] on the basis of Euler equation, between the electrode wire characteristics, channel material and force of resistance to wire movement is valid. With large wire diameters (3.0 mm and more) this force may be greatly increased, which often leads either to disturbance of the welding process, or crushing of the wire and complete feed failure.

Experimenting with different types of guide channels allowed determination of the mechanism of this phenomenon. Figure 2 shows a section of a flexible

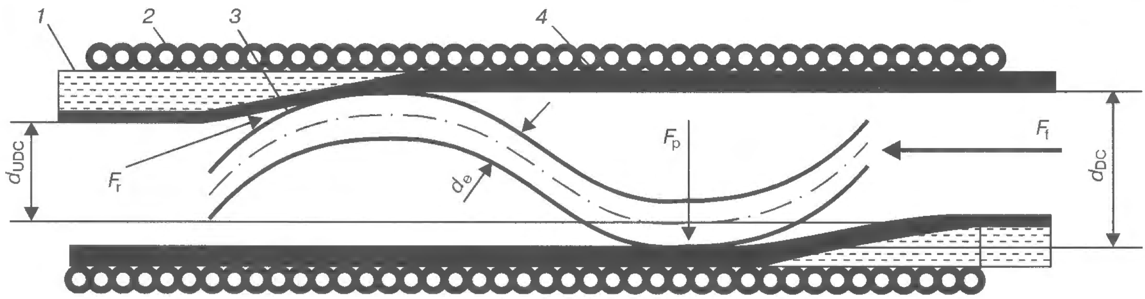

Figure 2. Schematic of section of guide channel, containing the electrode wire: *1* — undeformed guide channel of diameter d_{UDC}; *2* — sheath, enclosing the guide channel; *3* — electrode wire of diameter d_e; *4* — deformed guide channel of diameter d_{DC}

guide channel, holding the electrode wire at high values of feed force F_f characteristic of displacement along the guide channel of aluminium electrode wires of diameters higher than 3.0 mm. Because of the high values of feed resistance force F_r, the wire is trying to take up a position in the channel, close in its shape to a spiral with a great helix angle, which may result in its jamming. This is related to increase of pressure F_p of the wire on the walls of guide channel and deformation of the guide channel in the radial direction, respectively, with formation of an ellipsoidal shape of the inner section of the channel and deformation of the guide channel walls. In both the cases the angle of helix, formed by the electrode wire in the channel, is abruptly decreased, and the angle, at which the wire contacts the guide channel walls, increases.

This may occur by a number of reasons, namely bending of the guide channel, its internal defects and sheath defects (although the latter is usually made of a steel spiral). An abrupt increase of the angle of contact of the wire with the guide channel walls results in its value rising up to the level of the jamming angle. Wire jamming, arc elongation and burning of the nozzle take place, and the feed is completely interrupted.

A possible method of controlling the above phenomenon, when using electrode wires of larger diameters of aluminium alloys, and, therefore, the basis for designing the feed lines and flexible guide channels may consist in synthesis of three conditions, namely a low coefficient of wire friction against the channel walls, radial strength of the guide channel, and absence of the phenomenon of metallization of the internal surface of guide channel with the aluminium alloy (characteristic, when feeding the above wire along spiral channels of steel wire and abruptly increasing the coefficient of wire friction against the channel walls).

A number of technical solutions is known, where a spiral of brass wire is used as the channels. Its use yields a good result in terms of the characteristics of stability of electrode wire movement and reliability indices. Procedures of [8] were used to analyze the causes for such a behaviour of aluminium wire in the guide channel. It was established that in this case not the lowering of the coefficients of friction of the wire against the channel walls, but a significant reduction of channel metallization by the aluminium alloy has a more important role. It is foud, that adhesion of the aluminium wire material to the Cu-containing material of the channel results in that the wire brings to the arcing zone tiniest particles of the channel wall material (guide channels of Cu-containing alloys are quite expensive for a component, the service life of which is 200 h to GOST 18130–79).

In view of the above, a quite simple technical solution is proposed, allowing solving at a much lower cost the problem of development of the guide channel for electrode wires in practically the entire range of their dimensions. This solution consists in that the flexible guide channel is made in the form of a spiral of steel wire, on which a layer of copper is first deposited. In the simplest case, conventional Cu-plated electrode wire (GOST 2246–70) can be used for the channel material. A guide channel, made of Cu-plated electrode wire Sv-08G2S of 1.2 mm diameter, is applied in a number of gun-type holders for semi-automatic machines PSh107VA, developed using the basic PSh107V model along the modular design principle and designed for welding aluminium and its alloys with electrode wires Sv-AK5 of 2.0–3.15 mm diameter. Comparative testing of such semi-automatic machines with different types of channels and determination of coefficients of variation from expressions (2), (3), and arc current oscillograms (by analogy with Figure 1) for welding processes with undisturbed and pulsed motion of electrode wire of Sv-AK5 type of 2.0 mm diameter are presented in Table 2.

Analysis of the results, given in the Table, points to a positive influence of application of a flexible guide channel, made of Cu-plated steel spiral. In this case this effect is more pronounced for pulsed feed (pulsed feed mechanism, given in [9], was used),

Table 2

Guide channel type	*Guide channel bends*	*Coefficients of variation ν by welding current for motions*	
		undis turbed	*dis turbed*
Plastic tube	None	0.196	0.102
Cu-plated steel spiral	Same	0.154	0.085
Plastic tube	One coil	0.283	0.105
Cu-plated steel spiral	Same	0.172	0.071

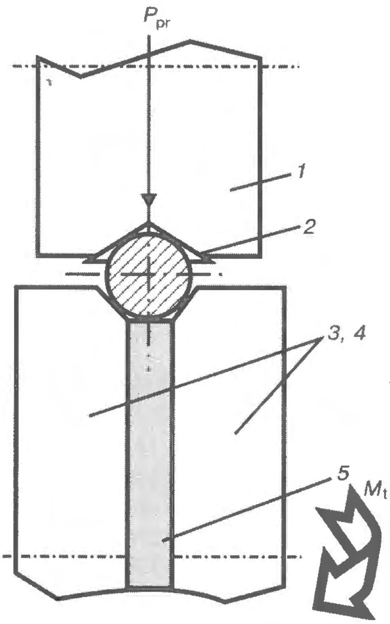

Figure 3. Schematic of a feed roller with a combination of materials: *1* — press-down roller; *2* — electrode wire; *3, 4* — steel parts of the roller; *5* — ring of aluminium alloy (P_{pr} — press-down force; M_t — torque)

which is the result of a smaller degree of attenuation of the amplitude of the motion pulse of electrode wire of aluminium alloys in the flexible guide channel [10]. Another feature of feeding through a Cu-plated steel spiral consists in that at considerable external disturbances, simulated by coils of the guide channel, no interruption or even any significant change of the speed of motion of greater diameter wire is noted (unlike the cases of feed failure, when plastic guide channels were used). The requirements of GOST 18130–79 as to reliability indices (mean-time-between-failures) can be met with appropriate use and maintenance of the guide channel of the above spiral (its periodic cleaning, change of the position of sections, undergoing the most intensive wear by axial turning of the channel or changing its position with a change of the start and end).

It is known that the roller feed mechanism, which is used both for undisturbed and pulsed feed, is the most important element, determining the quality of electrode wire feed [9]. Various technical solutions, based on the design of the rollers proper and the clamping mechanisms, are used to provide a reliable feed of aluminium wires.

As a rule, feed mechanisms with two pairs of steel rollers with a special profiling of grooves are used, which provides a lowering of specific pressure applied by the rollers on the wire and increase of their drag force. In semi-automatic machines of modular design for welding aluminium and its alloys a number of effective proposals are implemented, where the ideas of lowering the specific pressure and increasing the drag force are realized in original solutions [3, 11]. However, looking for solutions for further improvement of the drag force of roller feed mechanisms, including increase of the length of the hose holder (according to GOST 18130–79 the minimum length of the hose holder for aluminium wire is 1.5 m) necessitates increasing the friction between the above rollers and the wire. A solution has been proposed and technically implemented, in which part of the roller, contacting the wire, is made of aluminium alloys (Figure 3). Coefficients of friction of steel over aluminium (non-friction pair) and aluminium over aluminium (friction pair) according to [12] differ 1.5 to 2.5 times. The roller consists of three rings, fixed on one axle. Electrode wire *2* interacts with ring *5* (third point of contact on the feed roller), which is made of an aluminium alloy. Roller testing showed that at other conditions being equal, the drag forces are increased 1.2–1.7 times, compared to steel rollers.

Thus, application of new materials for the components of the wire feed system in combination with certain design solutions is one of the promising trends in improvement of the roller feed mechanisms.

1. Paton, B.E., Lobanov, L.M., Grigorenko, G.M. et al. (2001) Energy- and resources-saving technologies and equipment in welding of aluminium busbars for graphite carbon production. *Svarochn. Proizvodstvo*, **1**, 31–35.
2. Ishchenko, A.Ya., Dovbishchenko, I.V., Budnik, V.P. et al. (1994) Current methods of aluminium alloy arc welding (Review). *Avtomatich. Svarka*, **5/6**, 35–37.
3. Lebedev, V.A., Pichak, V.G., Rogatkin, A.A. et al. (1997) Semi-automatic machine for consumable electrode arc welding of aluminium and its alloys. *Ibid.*, **11**, 51–56.
4. Lebedev, V.A., Pichak, V.G., Rogatkin, A.A. et al. *Semi-automatic welding machine for aluminium and its alloys*. Pat. 24384 A Ukraine. Int. Cl. B 23 K 9/12. Publ. 17.07.98.
5. Lebedev, V.A., Kaveshnikov, S.P., Svetnikov, B.G. et al. (1989) Real possibilities of gearless mechanism of electrode wire pulsed feed. In: *Problems of nuclear science and engineering*. Series Nuclear Engineering and Technology. Issue 4.
6. Voropaj, N.M. (1996) Parameters of conditions and operational possibilities of arc welding with pulsed feed of electrode and filler wire. *Avtomatich. Svarka*, **10**, 3–9.
7. Lebedev, V.A., Svetnikov, B.G. (1984) Assessment of influence of bends of guide channel and current supply nozzle on resistance to electrode wire movement (Statistical analysis elements). *Ibid.*, **9**, 35–37.
8. Kashcheev, V.N. (1978) *Processes in friction zone contact of metals*. Moscow: Mashinostroenie.
9. Lebedev, V.A., Pichak, V.G., Smolyarko, V.B. (2001) Pulsed wire feed mechanism with pulse parameter control. *The Paton Welding J.*, **5**, 27–33.
10. Lebedev, V.A. (1999) Influence of guide channel of semi-automatic machine on parameters of pulsed electrode wire feed. *Avtomatich. Svarka*, **2**, 45–48.
11. Lebedev, V.A., Pichak, V.G. (2000) A new approach to design of the electrode wire feed mechanism. *The Paton Welding J.*, **4**, 33–36.
12. (1978) *Friction, wear, lubrication*. Ed. by I.V. Kragelsky, V.V. Alisin. Moscow: Mashinostroenie.

EFFECT OF EXTERNAL ELECTROMAGNETIC ACTION ON HYDROGEN CONTENT IN WELD METAL IN WET UNDERWATER WELDING

S.Yu. MAKSIMOV[1], **E.A. PRILIPKO**[1], **R.N. RYZHOV**[2] and **V.A. KOZHUKHAR**[2]
[1]E.O. Paton Electric Welding Institute, NASU, Kyiv, Ukraine
[2]National Technical University of Ukraine «KPI», Kyiv, Ukraine

It was established that application of electromagnetic action is an effective method of degassing welds. The presence of extremum in experimental curves will make it possible to optimize the parameters of controlling magnetic field.

Keywords: *underwater arc welding, low-carbon steels, electromagnetic stirring, diffusion and residual hydrogen, heat-affected zone, structural transformations*

High content of hydrogen dissolved in weld pool melt is the main cause of occurrence of pores and cold cracks in welded joints in wet underwater welding [1]. Most methods of decreasing the amount of the mentioned defects is based on adding gas-forming elements, reducing a partial pressure of hydrogen in a vapour-gas bubble, and elements, binding the hydrogen into compounds insoluble in weld metal, to the composition of electrode coatings and charge of flux-cored wires [2, 3]. It is possible to improve the quality of welds in underwater welding by a combined use of the above-mentioned chemical methods with external physical actions allowing us to control the hydrodynamic pool and transfer of the electrode metal.

Thus, in air welding with consumable electrode in mixture of shielding gases the use of high-speed rotation of the electrode could reduce the amount of hydrogen in welds by 25 % due to metal pool stirring and refining of electrode metal drops [4]. Taking into account the technical difficulties in realization of this technological procedure in the conditions of water medium, the application of electromagnetic stirring (EMS) of the weld pool metal seems to be more promising, as its use can reduce significantly the hydrogen amount in the weld metal [5]. In addition, there are no mechanical rotating elements in the zone of welding, and the three-dimensional force action on melt is created in interaction of natural electrical field of the weld pool with external axial controlling magnetic field (CMF). Analysis of literature sources showed that today there is no experience in use of this action in underwater welding, therefore, the aim of the present work was to evaluate the feasibility of decreasing hydrogen content in weld metal in wet underwater welding by the use of electromagnetic action on the weld pool.

Automatic welding of St.3 samples was made by flux-cored wire PPS-AN2 at 0.3 m depth at current of straight and reverse polarity using the following condition: I_w = 180–200 A; U_a = 36 V; v_w = 10 m/h. Axial CMF in the zone of welding was generated using an electromagnet, mounted over the weld pool coaxially to a nozzle and consisting of a ferromagnetic core and four-layer coil. Parameters of electromagnetic action were controlled using unit F-91 [6]. Total amount of hydrogen in welds was considered equal to the sum of its diffusive and residual components: $[H]_\Sigma = [H]_{diff} + [H]_{res}$. Content of $[H]_{diff}$ was determined by chromotographic method using recommendations of [7], $[H]_{res}$ was determined by the method of melting in a flow of gas carriers (instrument RH-2).

It was established that dependences of hydrogen content in welds on induction of CMF have a form of curves with extremum, reached at B = 10 mT (Figure 1). At this condition the most noticeable reduction in $[H]_\Sigma$ in welds was recorded in welding at current of straight polarity, i.e. 2.2 times, while at reverse polarity it was 2.5 times. At all the conditions of EMS the reduction in $[H]_\Sigma$ was mainly due to the decrease in $[H]_{diff}$ value. Under the conditions of experiment both in welding at conventional technology and also using electromagnetic action the change in polarity of welding current from straight to reverse polarity led to the decrease in $[H]_{diff}$ by 10–12 %. Here, the content of $[H]_{res}$ in samples welded by the conventional technology decreased by 14 %, and with use of EMS it decreased by 50 %.

Nature of experimental curves can be explained as follows. During underwater welding a large part of dissolved gases has no time to escape from the pool melt due to high rates of crystallization. Specifics of welding with EMS is the fact that the flows of molten metal formed at its top part are stirred periodically along the lateral edges of the pool, that accelerates the detachment and removal of gas bubbles forming as a result of thermodiffusion at the crystallization front. In addition, during metal pool stirring both averaging of temperature [8] and also significant decrease in chemical inhomogeneity of melt are occurred [5]. These factors promote levelling of concentration of dissolved hydrogen in the pool volume. In combination with typical increase in area of pool surface [8] it has a favourable effect on weld degassing. Re-

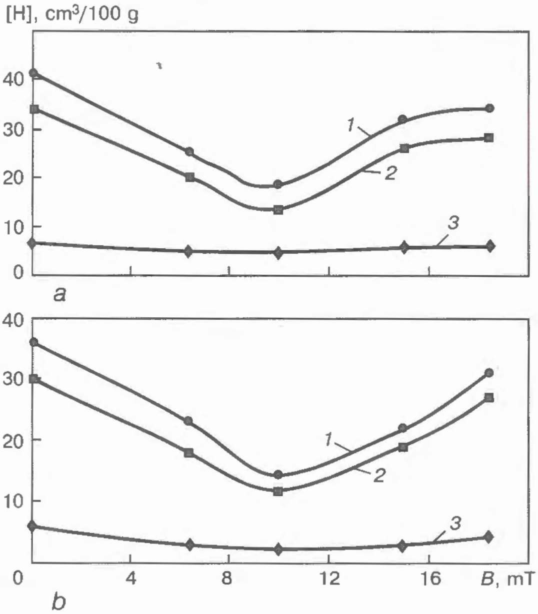

Figure 1. Effect of induction of axial CMF on hydrogen content in welds in welding at current of straight (*a*) and reverse (*b*) polarity: *1* — $[H]_{\Sigma}$; *2* — $[H]_{diff}$; *3* — $[H]_{res}$

duction in $[H]_{\Sigma}$, recorded during experiment (Figure 1), can be explained by increase both in intensity of EMS and in induction of CMF.

In the field of welding the value of CMF induction is directly proportional to the magnetizing current and inversely proportional to the distance to the electromagnet edge. It was established in measurement of CMF parameters that the magnetic field induction at the axis of electrode wire in the region of formation of drops is approximately 2 times higher than that in pool mirror plane, and with changes in magnetizing current in the range of 1–3 A it is 12–35 mT. It follows from the relationship given in [9] that in conventional welding the frequency of transfer of drops is 10–15 Hz, while with use of electromagnetic actions the induction of longitudinal CMF is increased from 10 to 35 mT with increase in frequency of transfer from 35 to 45 Hz. Taking into account that during experiments the parameters of welding and wire diameter were not greatly differed from those given in [9], it can be assumed that time of metal duration in overheated state at the drop stage decreased from 0.1 to 0.026 s. It is shown in [10] that saturation of drops with hydrogen occurs for 0.1 s. Consequently, in the conditions of experiments the drops of metal had no time to be completely saturated with hydrogen that, finally, could influence positively the degassing of welds. It is known that the change in polarity of welding current does not influence greatly the effectiveness of EMS, however, in welding at current of reverse polarity the process of electrode wire melting is intensified. This circumstance promotes also the reduction in $[H]_{\Sigma}$ in welds.

It is known that excessive increase in induction of CMF leads to the increase in spattering, that deteriorates the processes of formation of welds [5]. Similar effect was observed also in conductance of the present experiments that can explain the increase in $[H]_{\Sigma}$ in welds during welding with EMS under the conditions at which the induction of CMF in mirror plane exceeds 10 mT, and in the field of formation of drops it exceeds 20 mT. Analysis of kinetics of evolution of $[H]_{diff}$ from samples shows that in welding using conventional technology the change in polarity of welding current does not influence the rate of degassing (Figure 2, *a*). These relationships differ by amount of $[H]_{diff}$, evolved during first 10 min. In welding with EMS (B = 10 mT) the maximum evolution occurs a little later that can be explained by a lower concentration of hydrogen and due to intensive stirring of melt by its levelling in the entire volume of the weld. Samples welded at current of reverse polarity are characterized by higher rate and intensity of evolution of $[H]_{diff}$ (Figure 2, *b*).

The underwater welding is used in erection and repair of structures, in which the welds are located in all spatial positions, and often in hard-to-reach places. Taking into account the specifics of surrounding medium this causes a wide application of manual methods of welding. In this case the effectiveness of application of electromagnetic actions can be decreased due to instability of induction values in the zone of welding, caused by changing the distance from pool surface to magnetic core edge. Nature of experimental relationships, given in Figure 1, shows that in welding at current of reverse polarity the zone of optimum values of CMF induction is a little wider than at current of straight polarity. Consequently, technological disturbances typical of manual methods of welding will influence the degree of degassing of welds to a less extent.

Thus, the use of external electromagnetic actions in the process of wet underwater welding on hydro-

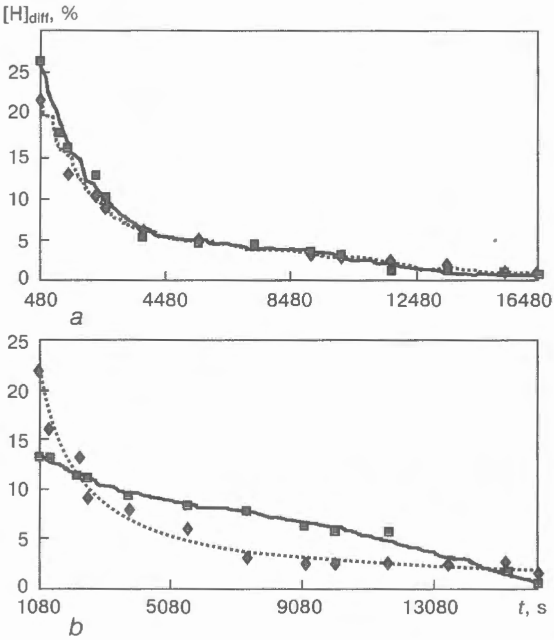

Figure 2. Kinetics of evolution $[H]_{diff}$ from samples in welding using conventional technology (*a*) and EMS (*b*) (solid curve — welding at straight polarity; dotted line — at current of reverse polarity)

dynamics of weld pool melt and electrode metal transfer made it possible to 2.2–2.5 times decrease the hydrogen content in weld metal. The highest effect is attained in welding at current of reverse polarity with CMF induction in the 8–12 mT range. It can be expected that the use of EMS as a result of changing induction and polarity of welding current will enable us to control the hydrogen diffusion in HAZ metal with allowances for structural transformations, proceeding in it, that is very important from the point of view of prevention of cold crack formation.

1. Ibarra, S., Grubbs, C.E., Liu, S. (1994) State-of-the-art and practice of underwater wet welding of steel. In: *Proc. of Int. Workshop on Underwater Welding of Marine Structures*, New Orleans, Dec. 7–9, 1994.
2. Gretsky, Yu.Ya., Maksimov, S.Yu., Kravchenko, N.V. (1993) Influence of marble in rutile electrode coating on hydrogen content in weld metal during underwater welding. *Avtomatich. Svarka*, **7**, 51–52.
3. Gretsky, Yu.Ya., Maksimov, S.Yu., Kravchenko, N.V. (1993) Influence of fluorite in rutile electrode coating on hydrogen content in weld metal during underwater welding. *Ibid.*, **8**, 54.
4. Gordonny, V.G., Gajvoronsky, A.A., Sarzhevsky, V.A. (1993) Influence of high-speed electrode rotation on structure and properties of 12GN2MFAYu high-strength steel welded joints. *Ibid.*, **5**, 28–31.
5. Chernysh, V.P., Kuznetsov, V.D., Briskman, A.N. et al. (1983) *Welding with electromagnetic stirring*. Kyiv: Tekhnika.
6. Korab, N.G., Skachkov, I.O., Matyash, V.I. (1993) System of control by electromagnetic effects during welding. *Avtomatich. Svarka*, **11**, 52–53.
7. Pokhodnya, I.K., Paltsevich, A.P. (1980) Chromatographic method of determination of diffusive hydrogen in welds. *Ibid.*, **1**, 37–39.
8. Chernych, V.P., Kuznetsov, V.D., Turyk, E.V. (1976) Variation of temperature state of welding pool in electromagnetic stirring. *Ibid.*, **7**, 5–8.
9. Boldyrev, A.M., Birzhev, V.A., Chernykh, A.V. (1991) Peculiarities of electrode metal fusion in external longitudinal magnetic field welding. *Svarochn. Proizvodstvo*, **5**, 28–30.
10. Pokhodnya, I.K., Shvachko, V.I., Portnov, O.M. (2000) Mathematical modelling of absorption of gases by metal during welding. *The Paton Welding J.*, **7**, 11–16.